Development of Alkaline Metal Stabilized Nitrogen Rich Alpha Sialons using Nano Precursors and Spark Plasma Sintering

BY

Bilal Anjum Ahmed

A Dissertation Presented to the

DEANSHIP OF GRADUATE STUDIES

KING FAHD UNIVERSITY OF PETROLEUM & MINERALS

DHAHRAN, SAUDI ARABIA

In Partial Fulfillment of the
Requirements for the Degree of

DOCTOR OF PHILOSOPHY

In

MECHANICAL ENGINEERING

April 2018

KING FAHD UNIVERSITY OF PETROLEUM & MINERALS

DHAHRAN- 31261, SAUDI ARABIA

DEANSHIP OF GRADUATE STUDIES

This thesis, written by Bilal Anjum Ahmed under the direction of his thesis advisor and approved by his thesis committee, has been presented and accepted by the Dean of Graduate Studies, in partial fulfillment of the requirements for the degree of **DOCTOR OF PHILOSOPHY IN MECHANICAL ENGINEERING.**

Dr. Tahar Laoui
(Advisor)

Dr. Zuhair Mattoug Gasem
Department Chairman

Dr. Abbas Saeed Hakeem
(Co-Advisor)

Dr. Salam A. Zummo
Dean of Graduate Studies

Dr. Nasser Al-Aqeeli
(Member)

11 / 7 / 2018
Date

Dr. Saheb Nouari
(Member)

Dr. Syed Fida Hassan
(Member)

Dedicated

To

My Grandparents

For their love and memories I will cherish forever

My Parents

For scarifying their comfort in an effort to shape up my life.

For their love and prayers which have clung to me all my life

And for never being able to thank you enough

Aiman

For her patience, her love and her faith

As she always understood

For being the glow that lights up my life

And for not being able to thank you for your part in my life

Basir Ahmed, Saleha Basir, Sadyyah Aqil, Durria Fawad, Sammar Sajid and Darakhshan Anjum

For being a wonderful, loving family and for supporting me all the way

Munir Ahmed, Uzma Munir, Umer Munir and Asfa Munir

For all the prayers, love and support

Asiyah, Taaha, Hadiyah, Safwah and Ibrahim

For, if nephews and nieces were jewels, I would have the most precious gems ever

ACKNOWLEDGMENTS

And my success is not but through Allah. Upon him I have relied, and to Him I return (Al-Quran 11:88).

First and foremost, I would like to thank Allah SWT, for the countless blessings that I was unable to thank for. Ya Allah, thank you for all the blessings and for being there with me, always.

I offer my sincerest gratitude to my supervisor, Dr. Tahar Laoui, who has guided and supported me throughout my thesis with his patience and knowledge whilst allowing me with the room to work in my own way. As my advisor and mentor, he has taught me more than I could ever give him credit for here.

I would like to thank my Co. advisor, Dr. Abbas Saeed Hakeem, who has guided, motivated and supported me at every stage of my research work and has been there for me anytime and every time I needed his help.

I would like to thank Dr. Nasser Al-Aqeeli, Dr. Saheb Nouari and Dr. Syed Fida Hassan for being part of my PhD thesis committee and for their support whenever I needed it.

I would like thank the mechanical engineering department especially, Dr. Esmail Mokheimer (Graduate Coordinator) and Dr. Zuhair Qasem (Chairman ME Department), for their support whenever I needed it.

I would like to acknowledge and thank for the support provide to me by CENT, especially Dr. Zain Hassan Yamani (Director CENT) and Dr. Nasiruzzaman Shaikh (CENT Lab Manager), in terms of an easy and frequent access to state of the art synthesis and characterization labs.

I would like to acknowledge the support provided by (KACST) for funding this work through project 13-NAN1700-04.

My sincere thanks also goes to Dr. Anwar-Ul-Hamid for providing me access to state of the art equipments of high temperature XRD and TEM and arranging the training sessions on the said equipment.

A very special thanks to Mr. Faheemuddin Patel, Mr. Latif Hashmi, Mr. Ahmed Ghanim and Dr. Ali Ehsan for their continuous support and help.

I am very grateful to all of those with whom I have had the pleasure to work during this and other related projects.

Most importantly, I would like to thank my family, especially, my parents (Dr. Anjum Tauqir and Mrs. Rubina Rathore), whose love and prayers are with me in whatever I pursue. Also, I wish to thank my wife, Aiman, whose support has been a constant source of comfort and motivation for me.

Table of Contents

LIST OF TABLES

LIST OF FIGURES

LIST OF ABBREVIATIONS

HP	:	Hot Pressing
HIP	:	Hot Isostatic Pressing
GSP		Gas Pressure Sintering
SPS		Spark Plasma Sintering
HV		Hardness Vickers
FESEM		Field Emission Scanning Electron Microscope
XRD		X-ray Diffraction
EDX		Energy Depersive X-ray
TEM		Transmission electron microscope
cBN		Cubic Boron Nitride
hBN		Hexagonal Boron Nitride
HEBM		High Energy Ball Mill
DLS		Dynamic Light Scattering
RPM		Revolutions per Minute
MCL		Maximum Crack Length
SE		Secondary Electron

BSE	Back Scattered Electron

ABSTRACT

Full Name : [Bilal Anjum Ahmed]

Thesis Title : Development of Alkaline Metal Stabilized Nitrogen Rich Alpha Sialons using Nano Precursors and Spark Plasma Sintering

Major Field : [Mechanical Engineering]

Date of Degree : [April 2018]

Sialon-based ceramics have been widely used as high temperature materials due their superior mechanical and thermal properties. Sialon exists in two major phases, alpha and beta sialon. In alpha sialon, metallic cations are used as additives to bring charge neutrality to the sialon structure. Most of the work reported on synthesis of sialons has utilized conventional sintering techniques (HIP, HP and GPS) and micron sized precursors with temperatures greater than 1700^{o}C. Majority of the study on alpha sialons has focused on utilization of rare-earth metallic cations as the stabilizing additives. However, alpha to beta transformation in rare-earth stabilized alpha sialons in the range of 1350-1600^{o}C as well as their low solubility in alpha sialons have shifted the focus towards utilization of calcium cation as the stabilizing additive for alpha sialons. In the present work relatively low temperature (1500^{o}C) synthesis of nitrogen rich (Ca, Mg) metal stabilized alpha sialons by employing a combination of nano precursors and spark plasma sintering (SPS) technique was carried out.

Calcium stabilized nitrogen rich sialon ceramics having a general formula of $Ca_xSi_{12-2x}Al_{2x}N_{16}$ with x values in the range of 0.2-2.2 for compositions lying along the Si_3N_4-$1/2Ca_3N_2$:3AlN line were selected for the synthesis. The developed sialons were characterized for their microstructure, phase and compositional analysis, physical and

mechanical properties. Furthermore, a correlation was developed between the lattice parameters and the content (x) of alkaline metal cation in the alpha sialon phase. Nitrogen rich calcium alpha sialons were observed to form in the range of $0.15 \leq x \leq 1.83$. Well densified single-phase nitrogen rich alpha sialon ceramic were achieved in the range of $0.6 \leq x \leq 1.4$. Nitrogen rich single phase alpha sialon sample having a hardness (HV_{10}) of 22.4GPa and a fracture toughness of 6.1 $MPa.m^{1/2}$ was developed.

With the aim to investigate the possible existence of Mg-doped single phase alpha sialons (on the Mg-alpha sialon plane), Mg-doped nitrogen rich sialon ceramics were synthesized for the very first time. Despite the fact that a relatively low sintering temperature (1500°C) was utilized, well densified sialons samples were achieved, however the densification of the samples became difficult with high x value ($x>1.6$). Contrary to the expected belief that a single phase Mg-doped sialon might exist along the nitrogen rich line (on Mg-alpha sialon plane), a single phase Mg stabilized alpha sialon region was not observed. This distinctive behavior in magnesium doped sialons was believed to be due to the formation of highly stable Mg-containing aluminum nitride polytype phase which consumed most of the high temperature transient liquid phase. Magnesium doped nitrogen rich sialon sample having the maximum amount of alpha phase depicted a hardness (HV_{10}) of 21.4GPa and a fracture toughness of 3.5 $MPa.m^{1/2}$.

With the aim to enhance further the mechanical properties, sialon/cBN and sialon/SiC composites were prepared at $1500^{o}C$. Significantly improved hardness and fracture toughness values of 24.5 GPa and 11.0 $MPa.m^{1/2}$ for the sialon/30%SiC and 24.0 GPa and 5.67 $MPa.m^{1/2}$ for sialon/30%cBN were measured respectively.

ملخص الرسالة

الاسم الكامل: بلال انجوم احمد

عنوان الرسالة: تطوير سيالونات ألفا القلوية معدنية الإستقرار و الغنية النيتروجين باستخدام نظائر النانو و تلبد شرارة البلازما

التخصص: مهندس ميكانيكى

تاريخ الدرجة العلمية: أبريل 2018

تم استخدام السيراميك الذي أساسه السيالون على نطاق واسع كمواد ذات درجة حرارة عالية بسبب خصائصها الميكانيكية والحرارية الممتازة. يوجد السيالون في طورَي ألفا وبيتا الرئيسيين. في طور الألفا سيالون تستخدم الكاتيونات المعدنية كإضافات لإضفاء الحيادية على هيكل السيالون. إن معظم العمل الذي تم إنجازه في تصنيع السيالون قد أدرج تقنيات التلبيد التقليدية (HIP و HP و GPS) وسلائف بحجم الميكرون مع درجات حرارة أعلى من 1700 درجة مئوية. وقد ركزت غالبية الدراسات عن سيالون الألفا على الاستفادة من الكاتيونات المعدنية الأرضية النادرة كإضافات لتحقيق الاستقرار. ومع ذلك، فإن تحول ألفا إلى بيتا في المدى من 1350-1600 درجة مئوية وكذلك القابلية القليلة للذوبان في سيالونات ألفا قد وجهت التركيز الى استخدام كاتيونات الكالسيوم كإضافة الاستقرار ل سيالونات ألفا. في العمل الحالي، تم إجراء تصنيع في درجة حرارة منخفضة نسبيا (1500 درجة مئوية) سيالونات مستقرة عنية بالنيتروجين (Ca، Mg) من خلال استخدام مزيج من الحبيبات النانوية وتقنية تلبد البلازما (SPS) .

سيراميك السيالون الغني بالنيتروجين المستقر بالكالسيوم الذي لديه صيغة عامة من $Ca_xSi_{12-2x}Al_{2x}N_{16}$ مع قيم x في المدى 0.2-2.2 لتركيبات تقع على خط :Si_3N_4-1 / $2Ca_3N_2$ تم اختياره للتوليف. السايالونات المطورة تم اختبار تفاصيلها المجهرية ، والتحليل الطوري والتركيبي ، والخصائص الفيزيائية والميكانيكية. علاوة على ذلك، تم تطوير علاقة بين معاملات البنية ومحتوى (x) من كاتيون المعادن القلوية في سيالون ألفا. ولوحظ أن سيالونات ألفا كالسيوم الغنية بالنيتروجين تتشكل في نطاق $0.15 \geq \times \geq 1.83$. تم التوصل إلى سيراميك سيالون ألفا أحادي الطور و الغني بالنيتروجين بشكل جيد في نطاق $0.6 \leq x \leq 1.4$. تم تطوير عينات من سيالون ألفا الغني بالنيتروجين ذات صلابة 22.4 GPa ومتانة ضد الكسر $6.1\ MPa.m^{1/2}$ عند تلبد منخفض إلى حد كبير. بهدف استكشاف إمكانية وجود سيالون ألفا أحادية الطور و المنشط بالمغنسيوم (على مستوى سيالون الفا-مغنسيوم)، تم تصنيع سيراميك سيالون الغني

بالنتروجين المنشط بالمغنيسيوم لأول مرة. على الرغم من حقيقة أنه تم تبني درجة حرارة منخفضة نسبيا للتلبيد، فقد تم الحصول على عينات من السيالون بكثافة جيدة ، و مع ذلك تكثيف العينات أصبح صعبًا مع قيمة x عالية (محتوى Mg_3N_2 / AlN عالي). خلافا للاعتقاد المتوقع أنه يمكن وجود سيالون أحادي الطور منشط بالمغنسيوم على الخط الغني بالنيتروجين (على مستوى سيالون الفا-مغنسيوم)، لم يتم العثور على منطقة سيالون ألفا أحادية الطور مستقرة بالمغنسيوم. ويعتقد أن هذا السلوك المميز في السيالونات المنشطة بالمغنيسيوم ينشأ بسبب تشكيل من المغنسيوم عالية الاستقرار التي تحتوي على طور نيتريد الألمنيوم المتعدده والتي استهلكت معظم المرحلة السائلة عند درجة الحرارة العالية. أظهرت عينة السيالون الغني بالنيتروجين المنشط بالمغنيسيوم تحتوي على الكمية القصوى من طور ألفا صلابة (HV_{10}) تبلغ 21.7 GPa ومتانة ضد الكسر تبلغ $3.5\ MPa.m^{1/2}$

تم تنفيذ تلبيد البلازما لمركبات Sialon / cBN و Sialon / SiC في 1500 درجة مئوية بهدف تحسين الخصائص الميكانيكية. تم قياس قيم صلابة وصلابة محسنة بدرجة ملحوظة بلغت 24.5 GPa و $11.0\ MPa.m^{1/2}$ ل Sialon/30%SiC و 24.0 GPa و $5.67\ MPa.m^{1/2}$ لل Sialon/30%cBN على التوالي.

CHAPTER 1

INTRODUCTION

1.1 Introduction

Si_3N_4 ceramics have been shown to sustain severe working conditions due to their remarkable mechanical and thermal properties, namely hot hardness, chemical inertness and thermal shock resistance [1]. However, full densification of Si_3N_4 powder compacts using conventional solid-state sintering technique has proven difficult without applying excess pressure and temperature. This is attributed to strong covalent bonding between Silicon and Nitrogen atoms that inhibits any lattice diffusion at temperatures below 1850°C [2,3]. Thus, the alternative approach adopted is adding metal oxide additives with silicon nitride powder to facilitate liquid phase sintering and hence the densification [1–3]. The use of additives such as MgO, Al_2O_3, Y_2O_3 and Ln_2O_3 as sintering additives not only eased the densification of silicon nitride but also modified the structure [4–12]. The modified structure is known as Sialon ceramic. Along with the said oxides, some metals and their nitrides such as calcium, aluminum, calcium nitride and aluminum nitride have also been tried as the additives [12–15]. The kind and quantity of additive employed for sintering controls the nature and amount of the amorphous grain boundary phase and hence the mechanical properties.

Sialon materials, which are solid solutions of silicon nitride, form primarily two phases, alpha and beta. Alpha-sialons are basically solid solution of alpha-silicon nitride in which part of the Si and N is replaced by Al and O, respectively, in a simultaneous process to maintain charge neutrality [10–12]. In particular, alpha-sialons have attracted much attention in the past two decades due high hardness of alpha-sialon [16,17]. Generally, alpha-sialon possesses higher hardness than beta-

sialon, while the latter shows better fracture toughness than the former. The reason behind this variation in the mechanical properties is explained usually through the consideration of the phase morphologies, in which alpha-sialon is formed mainly as equiaxed grains, while beta-sialon grains tend to form elongated hexagonal prisms. However, scientists have successfully developed ceramics with elongated alpha-sialon grains to enhance its fracture toughness [18,19].

Alpha-sialons are based on the alpha-$Si_{12}N_{16}$ unit cell with stoichiometric formula [10]: $M_x Si_{12-(m+n)} Al_{(m+n)} O_n N_{16-n}$ where m is the number of Al-N bonds, n is the number of Al-O bonds, M represents the added cation such as the rare earth or alkaline earth elements, where v indicates the valence of the added cation. Alpha-sialon is developed from the reaction of silicon nitride with precursors such as aluminum nitride, silicon oxide and the oxide or nitride of a suitable cation M (Y_2O_3, CaO, Ca_3N_2 etc.) such that the precursors satisfy the above mentioned general formula of alpha-sialon. The densification occurs by formation of oxy-nitride liquid phase. The reaction sequence is such that at high temperature these additives react to form oxy-nitride liquid phase and the silicon nitride dissolves in that liquid phase. The dissolution of silicon nitride is followed by the re-precipitation of alpha-sialon. The quantity of liquid reduces slowly until, precipitation of alpha solid solution completes, theoretically. In practice, large amount of oxide additives are required to facilitate the densification process, however, this usually results in large amount of the liquid phase [10–12,16,20,21]. However, studies have also proved that a adding a small amount of oxide into sialon material would adversely affect the high temperature behavior of the material [22,23].

Synthesis of alpha-sialons using the above referred additives by employing conventional sintering techniques such as Hot Pressing (HP), Hot Isostatic Pressing (HIP), Gas Pressure Sintering (GSP)

normally require temperatures greater than 1700°C [24–29]. Rare earth sintering additives, such as oxides of Neodymium (Nd), Lanthanum (La), Yttrium (Y) and Ytterbium (Yb), have predominately been the major research interest in the last few decades [24,30,31]. However, because of the relatively high cost in addition to crystal defects of these rare earths [32], the research focus has shifted to other additives, such as alkaline earth elements, namely Barium (Ba), Magnesium (Mg) and Calcium (Ca). Not only this but alpha to beta transformation in rare-earth stabilized alpha sialons in between 1350-1600°C in contrast to much stable calcium based alpha sialons has been also a factor towards this shift [33]. Calcium also seems to be the promising candidate to replace many of the rare-earth additives as it can be incorporated easily into the alpha-sialon structure with a wider solubility range [28,29]. Further, it can be easily formed from fly ash, which explains the relative low price of Calcium compounds compared with other alternatives [34].

Over the last few years, researchers have utilized spark plasma sintering (SPS) as sintering method for various powder mixtures to form ceramics. Compared to other sintering techniques, due to the high heating rate and pulsed nature of the current, SPS has confirmed its benefits of rapidly densifying compacted powders at relatively low energy input [35–38].

1.2 Thesis Aim and Objectives

In this study, it was proposed to develop low temperature (1500°C) nitrogen rich alkaline metal (calcium and magnesium) stabilized alpha sialons by employing a combination of nano precursors and spark plasma sintering (SPS) technique. The compositions satisfying the general formula of $Ca_x/Mg_xSi_{12-x}Al_{2x}N_{16,}$ covering the range of $0.2<x<2.2$ were to be synthesized. Solubility limits of

these alkaline earth stabilizers along the nitrogen rich line were investigated. The aim called for a deep understanding of sialon based system, leading to the following objectives:

1. To synthesize dense nitrogen rich alkaline metal stabilized alpha sialons, incorporating calcium and magnesium metal cations.
2. To prepare sialon ceramics at relatively low temperatures (1500^{o}C) and holding time of 30 minutes by utilizing nano starting precursors and SPS.
3. To investigate the solubility limits of calcium and magnesium metal precursors along the nitrogen rich line.
4. To study the effect of varying the composition from $0.2 < x < 2.2$ on formation of single phase alpha sialon region along the nitrogen rich line.
5. To characterize the developed sialons for their microstructure, phase and compositional analysis and physical and mechanical properties.
6. To correlate the phases developed, lattice parameters and mechanical properties with the achieved content of alkaline metal cation in the alpha sialon and the microstructures evolved.

Moreover, synthesis of Sialon/cBN and Sialon/SiC composites and the influence of the amount of reinforcements on the physical, structural and mechanical characteristics of the composites was to be studied.

1.3 Thesis Overview

In the present work, chapter 2 presents the in-depth literature review on sialon materials, phase stability regimes of rare-earth stabilized alpha sialons, limitations of rare-earth stabilized alpha sialons and the research reported on the synthesis and characterization of alkaline earth stabilized sialons. Chapter 3 provides general information related to the classification of starting powder

precursors, sample preparation method/s and details of characterization techniques. Chapter 4 highlights the importance of SPS technique and the effect of size of staring powder precursors on the low temperature synthesis of Sialon materials. Chapter 5 and Chapter 6 presents the work done on synthesis and characterization of calcium and magnesium stabilized nitrogen rich alpha sialons. Chapter 7 and 8 reports the work on synthesis and characterization of Sialon/cBN and Sialon/SiC composites. Finally Chapter 9, summarize the main findings of the research work, contribution to the already existing knowledge and future directions to pursue.

CHAPTER 2

LITERATURE REVIEW

2.1 Silicon Nitride and Sialons

Silicon Nitride material may possess two different crystal structures: alpha silicon nitride and beta silicon nitride. Alpha silicon nitride has trigonal crystal structure belonging to P31c space group with the lattice parameters of a = 7.7541 Å and c = 5.6217 Å. Beta silicon nitride has a hexagonal crystal structure belonging to P63/m space group with the lattice parameters of a = 7.6044 Å and c = 2.9075 Å.

Sialon materials are solid solutions of silicon nitride and metal oxides and nitrides (such as CaO, Y_2O_3, AlN, SiO_2, Al_2O_3 and many others). Sialon form primarily two phases, alpha and beta. Beta-Sialon was the phase that was first discovered in 1970's [11,12]. Beta sialon is formed by concurrent equal replacement of silicon and nitrogen for aluminum and oxygen and its chemical formula has been generally defined as $Si_{6-z}Al_zO_zN_{8-z}$ where the value of z varies from 0~4.2 for the samples synthesized at 1760^{o}C [20,39]. The behavioral diagram of Si-Al-O-N system at 1730^{o}C is depicted in **Figure 1** [17,20]. The region belonging to beta-sialon phase has been of interest for many years as materials belonging to this region have demonstrated good sinterability as well as good mechanical properties such as moderate hardness with impressive fracture toughness.

The change in the lattice parameter of beta-sialon which results due to the substitution of (Si-N) bonds by (Al-O) bonds is very small. The reason for this small alteration is due the fact that the bond lengths of Al-O (1.75 Å) and Si-N (1.74 Å) are very close to each other. However empirical

relationship developed to account for this small change in lattice parameter, with reasonable accuracy, is as follows:

Beta Sialon: [40]

$z_a = (a-7.603)/0.0297$ Å

$z_c = (c-2.907)/0.0255$ Å

$z = (z_a + z_c)/2$ Å

Alpha-Sialon phase was discovered later. The chemical formula of the alpha-sialon crystallographic unit cell, which includes four units of Si_3N_4, is generally described by $M_x^vSi_{12-(m+n)}Al_{m+n}O_nN_{16-n}$ where $x < 2$, $m = xv$. The value v represents the valance of metallic cation M whereas m (Al-N) bonds and n (Al-O) replace (m+n) (Si-N) bonds [10–12,41]. Importance of metallic oxides comes from the fact that the metallic cation brings charge balance to the alpha sialon in accordance with the above specified general formula. Metallic cation occupies the two large interstitial sites within the alpha sialon unit cell and hence the value x is limited to maximum of two as per the general formula. The value of x is also governed by the valency v of the cation occupying the interstitial sites within an alpha sialon unit cell. The cationic size of M is also important in the sense that it will determine the solubility range of a specific cation in alpha sialon. The extent of solubility of metallic cation in alpha sialon would thereby determine the changes in the lattice parameters due to the modification in structure.

The change in the lattice parameter of alpha-sialon is however more considerable as the difference in the bond length of Al-N (1.87 Å) and Si-N (1.74 Å) is more prominent. In case of most of the

rare-earth cation doped alpha-sialons the modified lattice parameters may be defined by the following relationship, with reasonable accuracy.

Alpha-Sialon: [10, 42]

$$a = 7.706 + 0.0117m + 0.0824r_m + 0.055x \quad Å$$

$$c = 5.578 + 0.0259m + 0.0774r_m + 0.0171n \quad Å$$

Where r_m is defined as the radius of ion M.

2.2 Phase Relations in Rare Earth Stabilized Alpha Sialons

Understanding of phase relationships is very important in order to synthesize alpha sialons. However, while phase diagrams are used to represent nitride and oxide based materials, there are considerations to be taken into account. Firstly, it is essential to appreciate that most phase diagrams of nitride and oxide systems represents phase relationships that are not necessarily in thermodynamic equilibrium. Secondly, amorphous grain boundary phase, which is always present in these systems due low diffusivity in oxynitride systems is not accounted in the phase diagrams. Also, only major solid phases are represented, while the existence and effect of vapor phases as well as that of surface contaminations are usually disregarded. Furthermore a precise calculation of the composition is challenging due to the light elements such as oxygen and nitrogen.

The earliest appearance of the phase diagram containing alpha sialon region is of the Si_3N_4-A1N-Y_2O_3 system [25]. Later on, a 2D alpha sialon plane was proposed (see **Figure 2**). As of today, the most comprehensive alpha sialon system is of Y-Si-AI-O-N. The general formula of Yttrium stabilized-alpha-sialons is $Y_xSi_{12-(m+n)}Al_{(m+n)}O_nN_{16-n}$ where x = m/3, and m and n have been defined earlier in the text. First detailed study on the alpha sialons was done on Si_3N_4-AlN-Y_2O_3 for which

the phase diagram is shown in **Figure 3** [25]. In this study a sloid solution of alpha-silicon nitride was observed along the Y_2O_3:9A1N line. The limits of solubility of Yttrium cation (represented by x in the general formula) extends from values of 0.33 to 0.67. The diagram also represents the formation of Si_3N_4-Y_2O_3 and $Si_2N_2O.2Y_2O_3$ compounds as a result of reaction between silicon nitride and Y_2O_3. However, $Si_2N_2O.2Y_2O_3$ does not lie on the plane of Si_3N_4-AlN-Y_2O_3. Regions containing yttrium stabilized alpha-sialon are being characterized in the following five triangles. Alpha'sialon-Si_3N_4- $Si_3N_4.Y_2O_3$, Alpha'sialon - $Si_3N_4.Y_2O_3$, Alpha'sialon - $Si_3N_4.Y_2O_3$-A1N, Alpha'sialon –AlN, Alpha'sialon -AlN- Si_3N_4.

A section ($Si_{12}N_{16}$-$Y_4Al_{12}N_{16}$-$Si_4Al_8O_8N_8$) of the proposed Y-alpha sialon plane (shown in **figure 2**) was selected for detailed study of the phases existing on the plane (see **figure 4**). The studies were conducted at 1700^{o}C. A more comprehensive work on developing the phase diagram of the proposed Y-alpha sialon plane at 1700^{o}C was also performed as shown in **figure 5** [42–44].

The rare earth (Gd, Dy, Er, and Yb) stabilized alpha sialons have the same diagrams as that of Si_3N_4-AlN-Y_2O_3. [45]. However, Sm or Nd stabilized alpha sialon phase sections are a little different from the aforementioned systems such that AlN reacts with Nd_2O_3 and Sm_2O_3 to form Nd_2AlO_3N and Sm_2A1O_3N, respectively (as shown in **figure 6**). Solubility limits of rare-earth stabilized alpha sialons are depicted in **figure 7** [45]. Lower limit of solubility is the same for all the rare-earth stabilizing cations, while the upper limit increases with a decrease in the size of stabilizing cation.

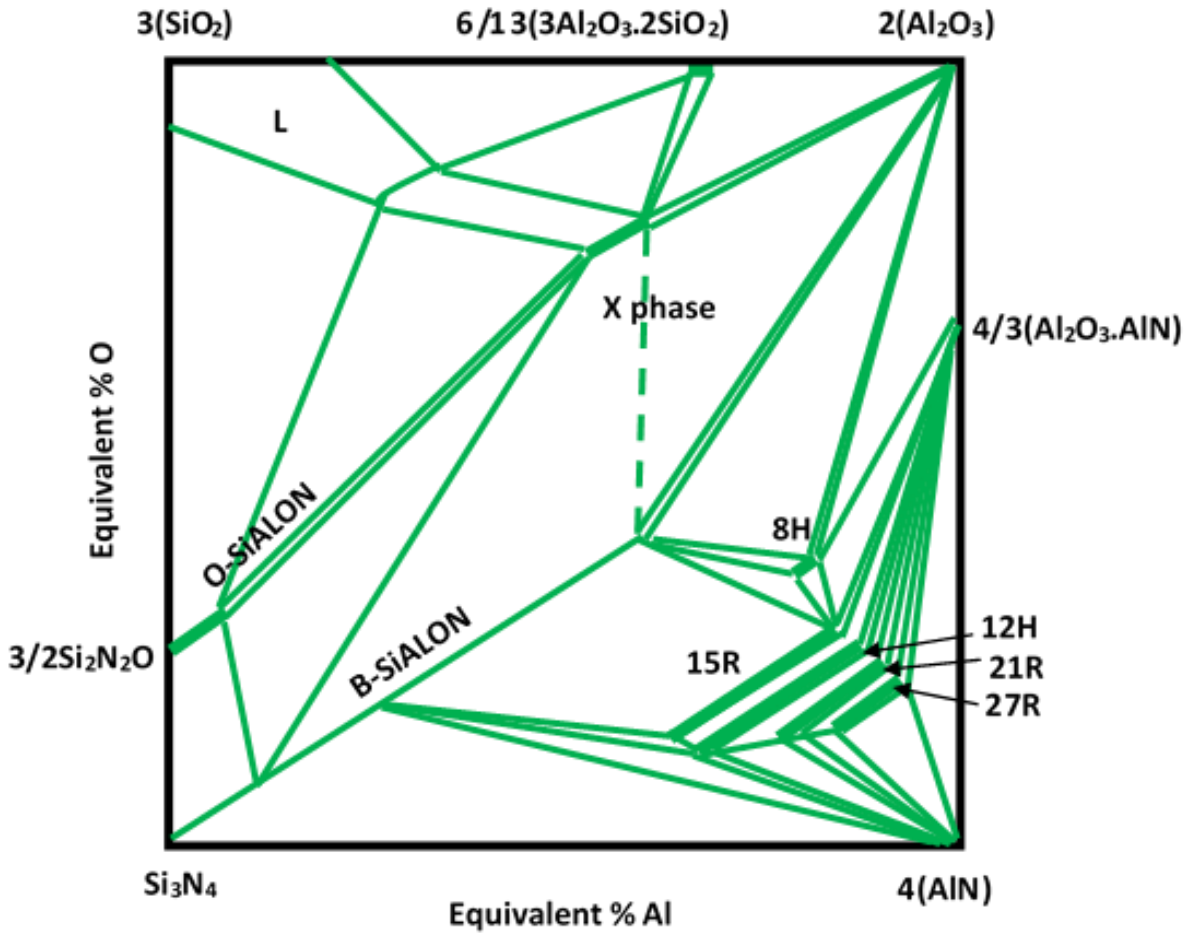

Figure 1 Redrawn phase diagram of Sialon at temperature of 1730^{o}C [17,20].

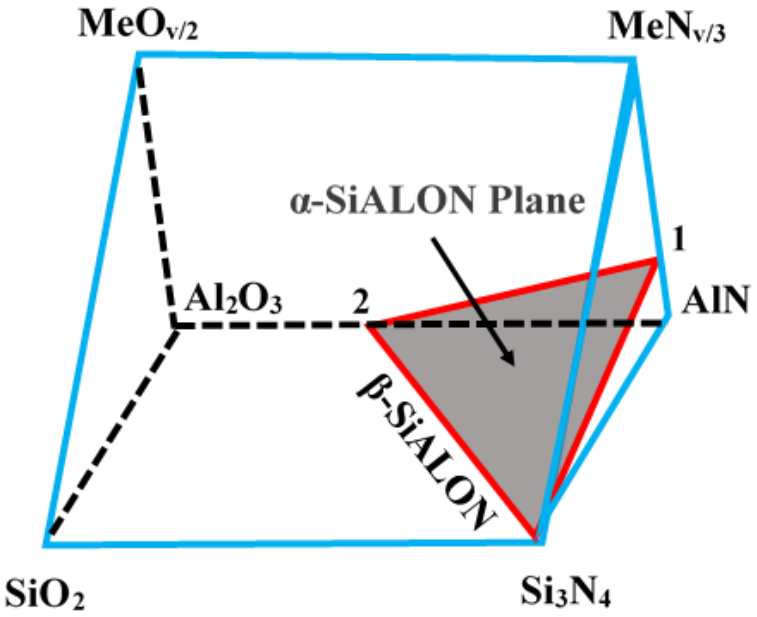

Figure 2 Redrawn schematic of Janecke prism containing alpha sialon plane. Me represents metallic cation having valence of v. (1) represents MeN:3AlN point and (2) represents a point on Al_2O_3-AlN line [25].

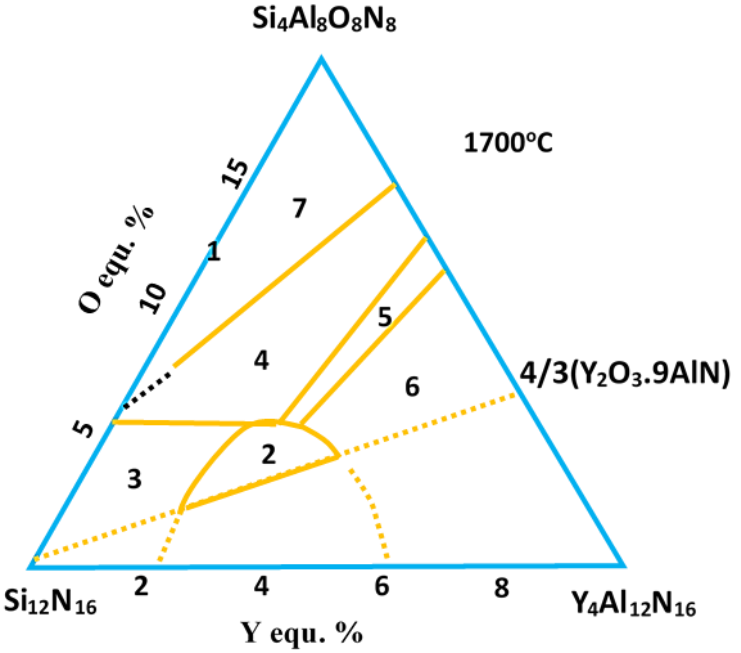

Figure 3 Redrawn Si_3N_4-AlN-Y_2O_3 system (Sub-solidus diagram) where the line α' s-s represents single phase alpha sialon regime [25].

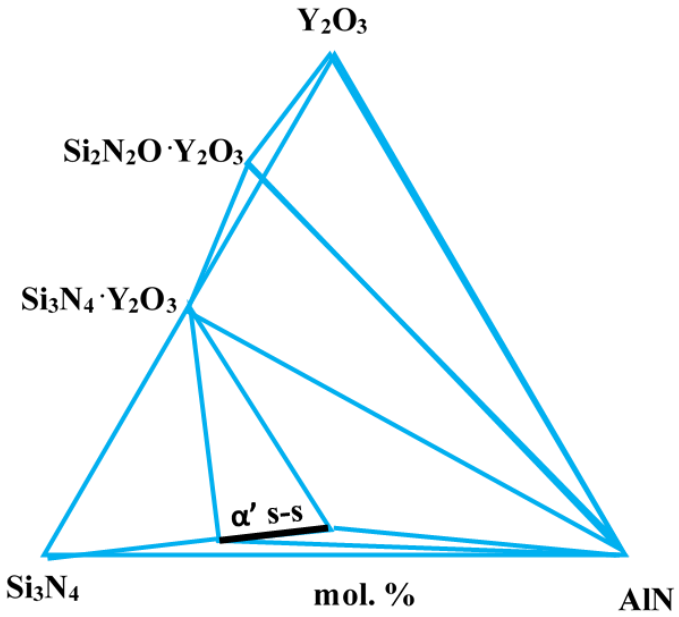

Figure 4 Phase relations in the $Si_{12}N_{16}$-$Y_4Al_{12}N_{16}$-$Si_4Al_8O_8N_8$ at 1700°C: (1) Beta-Sialon; (2) Alpha –Sialon; (3) Alpha + Beta Sialon; (4) Alpha + Beta Sialon + AlN polytype (12H); (5) Alpha Sialon + AlN polytype (12H); (6) Alpha Sialon + AlN polytype (21R); (7) Beta Sialon + AlN polytype (12H) [44–46].

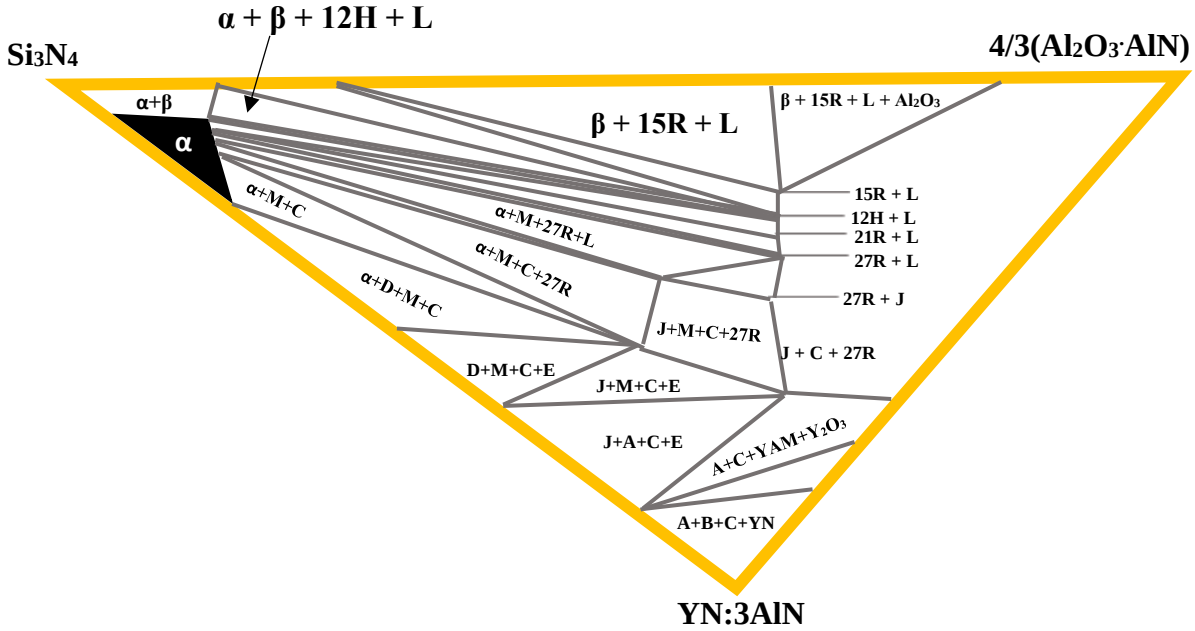

Figure 5 Yttrium-alpha sialon plane at 1705°C: (A) $Y_6Si_3N_{10}$; (C) AlN; (D) YSi_3N_5; (E) $Y_2Si_3N_6$; (J) $Y_4Si_2ON_2$-$Y_4Al_2O_9$; (L) liquid; (M) $Y_2Si_3O_3N_4$. Region highlighted in black represents single phase alpha sialon region. [42–44]

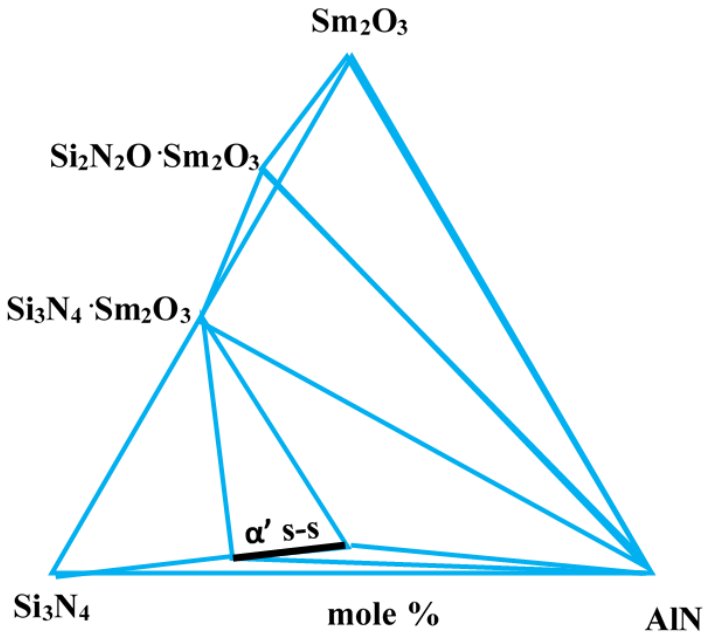

Figure 6 Si_3N_4-AlN- Sm_2O_3 system (Sub-solidus diagram) where the line α' s-s represents single phase alpha sialon regime [25].

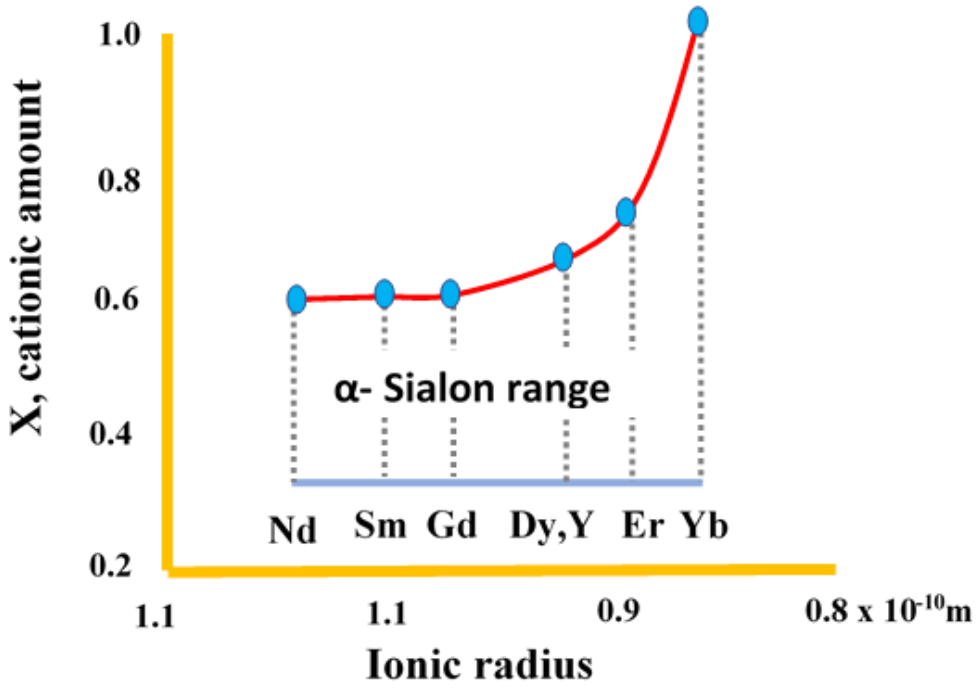

Figure 7 Solubility limits of rare-earth cations in alpha-sialon. The solubility of cation in the alpha sialon unit cell increases with the cation radius [45].

2.3 Reaction Sequence in Yttrium Stabilized Alpha Sialons

Since the Y-sialon is the most studied alpha sialon system a reaction mechanism involving the formation of alpha sialon has been elaborated in **figure 8** [25,42,43,46]. It shows the reaction order when a powder mixture of aluminum nitride, silicon nitride and yttria is fired at high temperature. The initial powder mixture was selected to achieve Y-alpha-sialon having a final composition of $Y_{0.5}Si_{9.75}Al_{2.25}O_{0.75}N_{15.25}$. The presence of oxygen-rich 1ayer on the surface of nitride particles suggests that an oxide subsystem of SiO_2-$A1_2O_3$-Y_2O_3 [47–49] is present during the reaction. With the increases in temperature surface oxides react to form a eutectic liquid at about 1350^{o}C [50,51]. Furthermore, this eutectic temperature of liquid formation may decrease a little in the presence of some other impurities and nitrogen [52,53]. Consequently, the presence of this liquid phase is witnessed at temperatures which are less than 1350^{o}C.

Studies suggest that the formation of the oxide liquid phase is followed by the starting of the dissolution of silicon nitride to form an oxynitride liquid phase at about 1380^{o}C, and the precipitation of alpha-sialon follows immediately [53]. This process of dissolution and precipitation continues with the increase in temperature and it gets completed at about 1800^{o}C. During the reaction an intermediate compound Si_3N_4-Y_2O_3 precipitates but after 1500^{o}C it re-dissolves into the liquid. It has been observed that precipitation of this intermediate compound does not affect the precipitation of alpha sialon.

2.4 Limitations of Rare-Earth Stabilized Alpha Sialons

The alpha phase stability filed of rare-earth doped sialons is seen to be dependent upon the atomic mass of the stabilizing cation as well as upon temperature. The alpha stability region increases with increase in atomic mass or decrease in cationic size (see **figure 9**) [54].

Another important aspect in rare-earth doped sialons is alpha to beta transformation. The alpha to beta phase transformation requires breaking of Silicon-Nitrogen bond [55–58]. The mechanism suggested is such that the alpha sialon dissolves in the liquid phase while at high temperatures beta precipitates from the liquid [59–63]. This transformation initiates in the presence of a liquid phase at about 1400^{o}C and finishes at temperatures close to 1800^{o}C.

Studies on various rare earth sialon systems proved that residual grain boundary liquid phase is one of the most influencing feature effecting the conversion. The degree of conversion is observed to be relying on the quantity and thickness of the intergranular liquid phase [64].

In rare-earth doped alpha sialons another characteristic to be considered is the tendency of alpha to beta phase transformation. Several rare-earth doped (Nd, Sm, Gd, Dy, Y, Er and Yb) alpha sialons synthesized at 1950^{o}C were subsequently annealed at 1500^{o}C for 240 hrs.to analyze this phase transformation [54]. It was observed that transformation was more extensive in case of Nd and it decreased progressively as the size of stabilizing cation decreases (see **figure 10**).

2.5 Alkaline Earth Metal Stabilized Alpha Sialons

In contrast to the rare-earth stabilized alpha-sialons, studies on calcium (belonging to alkaline earth series) stabilized alpha-sialons have displayed a much better thermal stability when used as a sole sintering additive or even when used in a combined form with other densifying agents such as Nd and Sr. Not Only this but calcium stabilized alpha sialons may be synthesized using a wide range of starting precursors. Studies conducted by Hewitt, C. L., Cheng, Y.-B. show that Ca-alpha-Sialons not only exhibit a large stability field on the alpha sialon plane as compared to rare-earth stabilizers but also far more resilient towards an alpha to beta transformation in sialons [65].

Hasan Mandala and Derek P. Thompson studied the high temperature stability of alpha-sialon with starting compositions belonging to pure alpha and mixed alpha-beta regions of phase diagram[66].

Sintered samples via hot pressing were heat treated at 1450^{o}C for a period of month to access the effect of stabilizing agents including CaO, SrO, Nd_2O_3 and mixed Ca/Nd and Ca/Sr oxides. It was observed that in case of Sr cations no alpha phase, in case of Nd cations 97% of alpha and in case of Ca cations pure alpha was formed. On the contrary Nd and Sr cations when used in combination of with Ca, stable pure alpha phase was achieved. This effect of Calcium on alpha phase could be better explained on the lower valence of Calcium i.e. +2.

The phase stability regime of Si_3N_4, A1N and CaO system at 1800^{o}C, is shown in **figure 11** [26]. The phase regime follows the same pattern as that of Si_3N_4, A1N and Y_2O_3 system. Alpha sialon is formed along Si_3N_4-CaO:3AlN line. Single phase alpha sialon range is defined by 0.3 to 1.4 calcium atoms per unit cell of alpha-sialon. Higher solubility limit of Ca cation (0.3 to 1.4) along the tie line Si_3N_4-CaO: 3AlN [26,27] has been reported as compared to solubility limit of (0.33 to 1.0) along the tie line Si_3N_4-RE_2O_3: 9AlN [25] for rare-earth cations. The higher solubility of calcium ion as well as its relative stability have recently made it a preferred additive [24,27–29,34]. Moreover, the greater availability of Ca-based compounds, and hence their lower costs, make them advantageous as sintering aids [34]. Calcium stabilized silaon follows the same reaction sequence as that in Y-Sialons. Normally a eutectic oxynitirde liquid is observed in the temperature range of 1170-1350^{o}C. Solution-precipitation reuslting in the formation of alpha sialon starts at about 1450^{o}C and completes at temperatures greater than equal to 1700^{o}C [67] .

The Si_3N_4-A1N-MgO system has also been studied [68]. But, in this study pure magnesium-alpha-sialon phase was not observed along the Si_3N_4-MgO:3AlN line. As we move from Si_3N_4 towards MgO:3AlN a combination of more than one phase namely beta + alpha sialon, alpha sialon + A1N polytypoid (12H), and alpha sialon + A1N polytypoid + AlN, respectively were observed. It is also expected that a small region of single phase magnesium-alpha-sialon may be found along the

nitrogen rich line [68]. Therefore single-phase magnesium-alpha-sialon may be synthesized by employing Mg_3N_2 as the starting precursor.

2.6 Mechanical Properties of Alpha and Beta Sialons

The properties of silicon nitride and sialons are dependent upon the phase/s, their composition and microstructure. The literature data on mechanical properties is widely scattered. This is due to the difference in compositions as well as microstructures. **Figures 12** and **13** gives the comparison of Vickers hardness (HV) and fracture toughness (K_{1c}) of yttrium stabilized alpha and beta sialon ceramics, respectively [69,70]. It is observed that yttrium stabilized alpha sialon ceramics have higher hardness and fracture toughness as compared to beta sialons.

A study by H.X. Li reported that gas pressure sintering of Y-alpha-sialon at 1800 °C, resulted in hardness (Vickers) of 18GPa and fracture toughness (K_{1c}) of 3.4 MPa.$m^{1/2}$ [71]. Pressure less sintering of Y-Sialon at 1850^{o}C, conducted by C.R. Zhou resulted in elongated alpha-sialon grains. For the $Y_{0.667}Si_{8.5}Al_{3.5}O_{1.5}N_{14.5}$ composition sintered at 1850 °C a hardness value of 17.6 GPa and fracture toughness value of 6.2 MPa.$m^{1/2}$ was reported [72].

P.L. Wang et al studied the mechanical properties of calcium and (calcium and magnesium) stabilized alpha sialons at 1750^{o}C prepared via hot pressing. The nominal compositions used in the synthesis were located on the join between Si_3N_4-MO:3AlN (M=Ca or 0.5 Ca,0.5 Mg) with formula $M_xSi_{12-3x}Al_{3x}O_xN_{16-x}$ (x=0.3, 0.6, 1.0 and 1.4), where m=2n, x=m/2=n [28]. The results of mechanical properties indicated that for solely Calacium stabilized alpha silaons hardness varied in the range of 16-19 GPa whereas the fracture toughness remained in the range of 3-6 MPa.$m^{1/2}$. In case of calcium/magnesium stabilized alpha sialons hardness varied from 18.3-19.6 GPa while fracture toughness varied from 4.9-5.6 MPa.$m^{1/2}$.

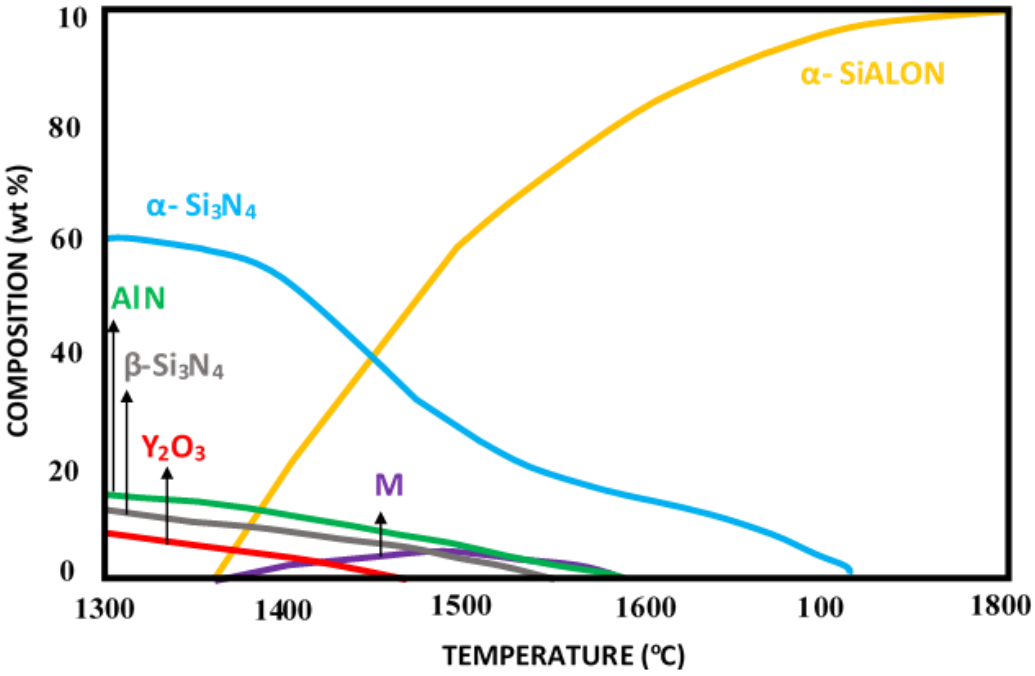

Figure 8 Progress of the reaction which results in precipitation of alpha-sialon; M represents Si_3N_4-Y_2O_3 [53].

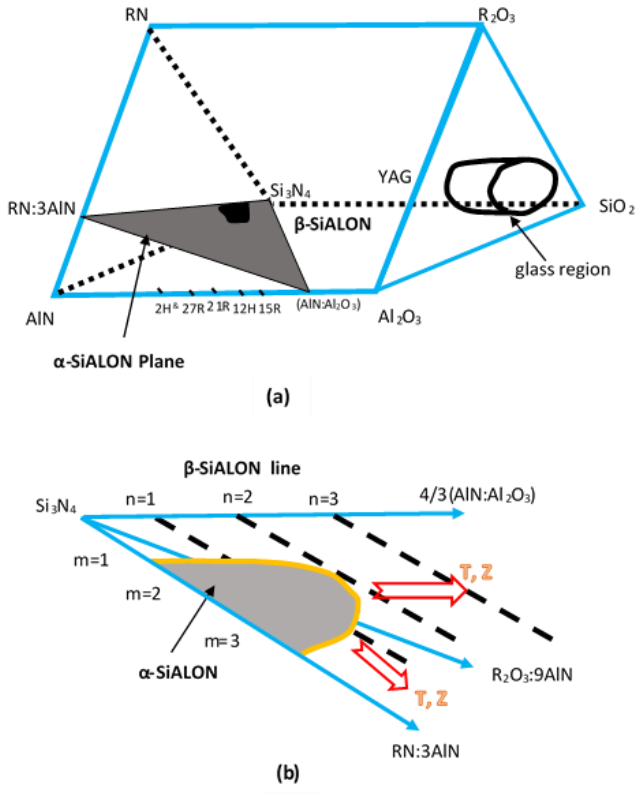

Figure 9 (a) Janecke prism containing alpha sialon plane, (b) Alpha-sialon plane showing single phase alpha region expanding with temperature (T) and atomic mass (Z) [54].

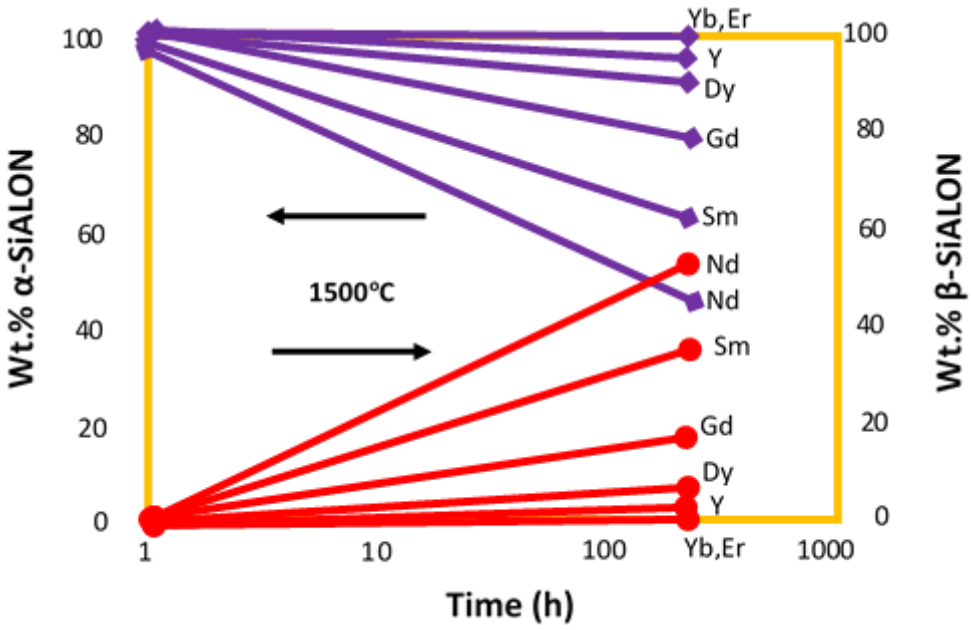

Figure 10 Alpha to beta transformation rates for rare earth dope alpha sialons at 1500ºC [54].

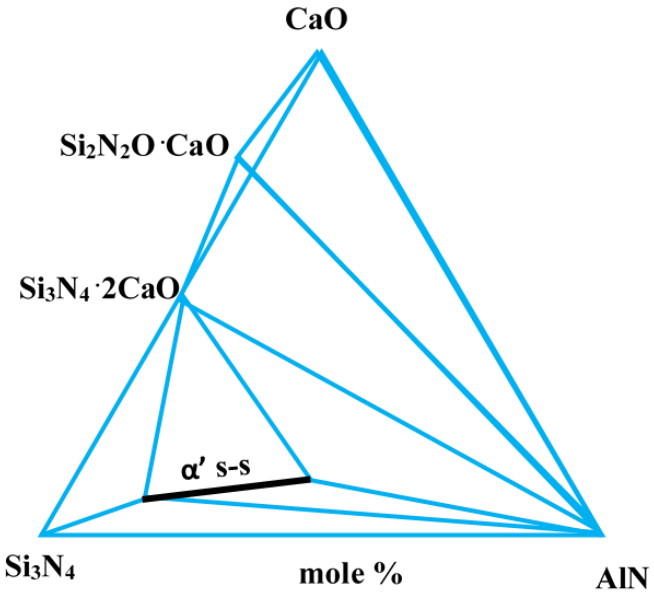

Figure 11 Si_3N_4-AlN-CaO system (Sub-solidus diagram) where the line α' s-s represents single phase alpha sialon regime [26].

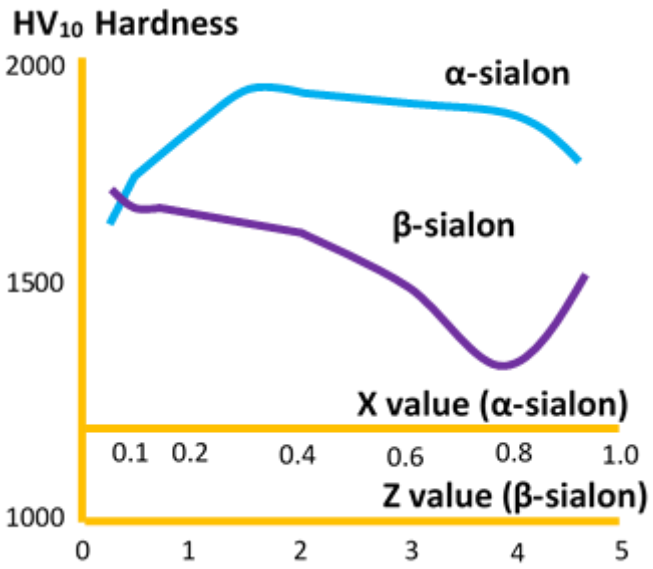

Figure 12 Vickers hardness (HV_{10}) for alpha and beta sialon samples with different compositions [70].

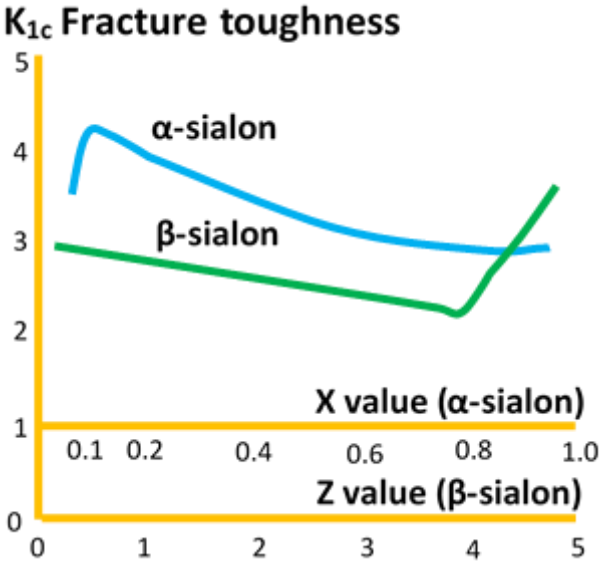

Figure 13 Fracture Toughness (K_{1c}) for alpha and beta sialon samples with different compositions [69]

In a recent study of Ca-alpha-sialon, where nitrogen rich liquid phase sintering was performed at 1800^{o}C using hot pressing technique a combination of high hardness ranging from 21-22 GPa and moderate fracture toughness in the range of 4.8-5.8 MPa $m^{1/2}$ was reported [73].

A summarized list of mechanical properties representative of silicon nitride and silicon nitride based sialons is summarized in **Table 1**. A unique combination of properties such as high hardness and toughness along with good wear resistance makes silicon nitride based materials an ideal choice for wide range of applications. A summary of the applications and their requirements is presented in **Table 2** [74,75].

Table 1 Properties of silicon nitride based materials [1,17,28,69–73,76–78].

Material	**HV_{10} (GPa)**	**K_{1c} (MPa.$m^{1/2}$)**
α-Si_3N_4	<20	~3
β-Si_3N_4	<16	4-7
Y-α-Sialon	17.6-20	3.5-6.2
Ca-α-Sialon	16-19	3-6.0
Ca/Mg-α-Sialon	18.3-20.5	4.9-5.6
Ca-α-Sialon (Nitrogen Rich)	20.8-22	4.8-5.8
Commercial β-Sialon (Int.Syalon101)	14.7	7.7
Commercial α/β Sialon (Int. Syalon 050)	19.81	6.5

Table 2 Applications and properties for silicon nitride based materials [74,75].

Applications	**Important Properties**
Cutting tools	Hardness, toughness, thermal conductivity, chemical stability, thermal shock resistance
Wear components	Hardness, toughness, coefficient of friction
Thermal Applications	Chemical resistance, creep resistance
Bearings	Toughness, hardness, strength, wide range of operating temperatures

The most extensively used cutting tool materials are based on alumina (pure and composites), cemented carbides and silicon nitride based (α/β Sialons and β Sialons). A list of common

properties of these materials is summarized in **Table 3**. A combination of high hardness, toughness and thermal conductivity of silicon nitride based materials present them a suitable candidate for interrupted cutting machining operations.

Table 3 Properties of silicon nitride based materials and other materials for cutting tool application [28,69–73,77–81]

Tool Material	Hardness HV_{10} (GPa)	Fracture Toughness K_{1c} ($MPa.m^{1/2}$)	Thermal Conductivity κ W/m/K	Coefficient of thermal Expansion α $10^{-6}K^{-1}$
Y-α-Sialon	17.6-22	3.5-6.5	-	-
Ca-α-Sialon	16-19	3-6.0	-	-
Ca/Mg-α-Sialon	18.3-20.5	4.9-5.6	-	-
Ca-α-Sialon (Nitrogen Rich)	20.8-22	4.8-5.8	-	-
WC-Co 6wt%	7.5	10	-	5.4
Alumina	17	3-5	-	8.7
SiC	25	3	-	4.3
Commercial β-Sialon (Syalon 101)	14.71	7.7	28	3
Commercial Alumina (Aluminon 96)	15.71	3.5	20	7
Commercial Alumina (Aluminon 999)	17.65	4.5	30	8.5
Commercial α/β Sialon (Syalon 050)	19.81	6.5	20	3.2

2.7 Summary

In the last few decades quite a lot of work has been done on the synthesis and characterization of alpha and beta sialons. Firstly, most of the work done on sialons has incorporated conventional sintering techniques [24–29]. Secondly, more of the above referred work has focused upon the utilization of rare-earth stabilized alpha sialons[25,42,43,45,46]. Alpha to beta transformation in rare-earth stabilized alpha sialons in between 1350-1600^{o}C in contrast to much stable calcium

based alpha sialons has resulted in calcium cation as much preferred additive for alpha sialons [33]. Calcium also seems to be the promising candidate to replace many of the rare-earth additives as it can be incorporated easily into the alpha-sialon structure with a wider solubility range [28,29]. Studies have been done on Ca-Sialon, where solubility limits, phase formation regions and mechanical properties have been investigated along the (oxygen rich) Si_3N_4-CaO:3AlN line [26,27]. There is only one study where systematic exploration of the solubility limits, phase formation region and properties of nitrogen rich Calcium-alpha sialon has been worked upon using conventional sintering technique at a temperature of 1800^{o}C [73]. The Si_3N_4-A1N-MgO system has also been studied [68]. However, in this system single-phase Magnesium-alpha-sialon has not been obtained on the line (oxygen rich) Si_3N_4-MgO:3AlN. Thus study of nitrogen rich calcium and magnesium-alpha-sialon using non-conventional sintering technique needs exploration.

In the initial part of the thesis size effect of aluminum nitride precursor (1 μm and 50nm) on the phase analysis, microstructural and mechanical characteristics of the calcium doped sialon was studied. Calcium stabilized alpha-sialon ceramic was synthesized using spark plasma sintering (SPS). The development of alpha phase was found to be strongly dependent on the particle size of the aluminum nitride (AlN) precursor. Interestingly, this novel approach of changing particle size from micro to nano level combined with the SPS process resulted in the formation of alpha-sialon ceramic at much lower than previously reported sintering temperature i.e. 1500^{o}C as compared to 1700/1800^{o}C.

Moreover synthesis of alkaline earth (Ca and Mg) nitrogen rich alpha sialons was carried out using non-conventional sintering technique i.e. SPS. With a combination of nano precursors and spark plasma sintering technique nitrogen rich alpha sialons were synthesized at relatively low temperatures of 1500^{o}C. Well densified sialon ceramic materials having the general formula of

$Ca_x/Mg_xSi_{12-x}Al_{2x}N_{16}$ with the compositions in the range of $0.2<x<2.2$, were developed. Moreover, relatively refined microstructures achieved at relatively low sintering temperature resulted in remarkable mechanical properties.

The last part of the thesis deals with synthesis of Sialon/cBN and Sialon/SiC composites. The influence of the amount of reinforcements on the physical, structural and mechanical characteristics of the composites were studied.

CHAPTER 3

MATERIALS AND METHOD

3.1 Introduction

This chapter provides the general information related to the classification of starting powder precursors, chemical compositions, powder mixing techniques, sintering conditions and details of characterization techniques, employed for the preparation and analysis of the synthesized sialon and sialon based composite ceramic materials.

3.2 Raw Materials and Chemical Compositions

The whole work is based on the general formula of alpha sialon, that is $M_x^vSi_{12-(m+n)}Al_{m+n}O_nN_{16-n}$, where M stands for calcium or magnesium cation. The specific oxygen rich alpha sialon composition having the chemical formula $Ca_{0.8}Si_{9.2}Al_{2.8}O_{1.2}N_{14.8}$ was selected for the study on effect of AlN particle size on the kinetics of formation of alpha sialon (details of the study is provided in chapter 4). This formula corresponds to m value of 1.6 and n value of 1.2 in the chemical formula of alpha sialons indicated above. The above referred composition was also used to prepare sialon/cBN and sialon/SiC composites details of which are provided in chapter 7 and 8 respectively. Nitrogen rich calcium or magnesium stabilized alpha sialon ceramics (free of oxygen) are generally defined by the chemical formula of $Mg_xSi_{12-m}Al_mN_{16}$ (where x= m/2). In order to synthesis nitrogen rich sialon ceramics (chapter 5 and 6) compositions represented by the x values in the range of 0.2-2.2 were selected for the synthesis.

Starting powder precursors employed for the synthesis included alpha-silicon nitride, silicon oxide, aluminum nitride, calcium oxide, calcium nitride, magnesium nitride, cubic boron nitride and

silicon carbide. Classification of these powder precursors based on their particle sizes is summarized in **Table 4**.

Table 4 Classification of starting powder precursors.

S/No.	Powder	Company	Particle Size
1	α-Si_3N_4	Ube Industries, Japan	~300nm
2	SiO_2	Sigma Aldrich, Germany	20nm
3	AlN	Sigma Aldrich, Germany	50nm
4	AlN	Sigma Aldrich, Germany	1µm
5	CaO	Sigma Aldrich, Germany	~160nm
6	Ca_3N_2	Sigma Aldrich, Germany	~200 mesh
7	Mg_3N_2	Sigma Aldrich, Germany	~325 mesh
8	cBN (ABN800)	Element Six, USA	20 µm
9	SiC	Buehler	~ 11 µm

3.3 Mixing the Powder Mixtures

The masses of the various precursors were chosen to satisfy the stoichiometry of a specific alpha sialon composition and for every sample a total mass of 5 g was weighed. These weighed out precursors were homogenously mixed for 30 min, using ethanol as a sonicating medium in an ultrasonic probe-sonicator (Model VC 750, Sonics, Connecticut, USA). Furthermore, the sonicated powder mixture was desiccated at 80^{o}C for 24 hrs. to remove ethanol.

In order to prepare the HEBM sialon/cBN composites (chapter 7) initial powder precursors (without cBN) were high energy ball milled for one hour followed by a 30 min probe sonication of the HEBM mixture along with cBN particles (details are mentioned in chapter 7). High-energy

ball milling was carried out in Union Process model HDMM using 625 micron zirconium dioxide (ZrO_2) balls. The HEBM process was performed in ethanol media in air where the machine was operated at 3000 rpm for one hour with powder to balls ratio of 1:20.

Moreover, in order to prepare sialon/SiC composites (chapter 8), as-received SiC powder with an average particle size of 11 μm was milled using a high-energy ball mill (Union Process HD01/HDDM) for 3 hours at 1000 revolutions per minute (RPM) with ethanol as a mixing medium. The powder to balls ratio was 1:20. ZrO_2 balls were utilized, with an average size of 625 μm. The particle size after milling was estimated to be 2 μm on average based on five measurements using a Microtrac particle size analyzer (Model S3500/Turbotrac). The weighted powder mixture of alpha sialon precursors and HEBM SiC particles (details mentioned in chapter 8) was then homogenized using an ultrasonic probe sonicator (Model VC 50, Sonics, USA) for 30 min, utilizing ethanol as a mixing medium. Sonicated powder mixtures of samples were then dried in a furnace at 80°C for 12 h to remove the ethanol.

3.4 Characterization Techniques

Sintered samples were firstly cleaned carefully from graphite to measure their densities. Afterwards, samples were mounted (Evolution, IPA 40 Remet, Bologna, Italy) in transparent polymeric powder to help handling the sample for subsequent processing. Diamond grinding wheels were utilized in automatic grinder (Automet 300 Buehler grinding machine), following the standard sequence; 74, 40, 20 and 10μm particle size. Later, polishing wheel was used with a series of diamond polishing suspensions, starting by 9 μm and ending up with 0.25 μm, passing through 6, 3 and 1μm diamond suspensions. To reveal the microstructure, several etchants were adopted, including concentrated and diluted HF and molten NaOH at 400^{o}C. For SEM examination, samples

were gold-coated, either by the sputter coater (Model Q150T, Quorum Technologies, UK) or by the metal evaporation coating machine.

3.4.1 Archimedes Method for Density Measurement

Density measurement plays an essential role in qualifying the sintered samples. A typical way to evaluate the density is to use the role of mixture to evaluate the theoretical density, and thereafter the densification. However, individual densities are not often available, and hence calculating the theoretical densities is not practically possible. To overcome this issue, we evaluated the density of the sintered samples though the well-known Archimedes' principle and compared it to the density values of similar compositions reported in literature. **T**he general formula to calculate the density for the sintered samples is shown below.

$$\rho = \frac{A}{A-B}(\rho_0 - \rho_L) + \rho_L$$

$$\rho_L = 0,0012\ g/cm^3$$
$$\rho_0 = 1\ g/cm^3$$

A and B represent the weight of sample in air and liquid, respectively. ρ_o is the liquid density which is water in our case, while ρ_L stands for air density. Units of weights should be kept in grams and densities in g/cm^3.

3.4.2 Phase Analysis

To identify the phases present in the synthesized samples, a Rigaku MiniFlex (Japan) X-ray diffractometer (XRD) was used with Cu $K_{\alpha 1}$ radiation (γ = 0.15416 nm), a tube current of 10 mA, and an accelerating voltage of 30 kV. Step size of 0.02 degrees and a scan speed of 2°/min was

adopted for XRD analysis. The software UnitCellWin was used to calculate the lattice parameters. The amount of alpha and beta phases was calculated using the following equation [82]:

$$\frac{I_\beta}{I_\alpha + I_\beta} = \frac{1}{1 + K[(1/W_\beta) - 1]}$$

Where I_α represent observed intensities of (102) and (210) peaks belonging to alpha phase while I_β represent observed intensities of (101) and (210) peaks belonging to beta phase. W_β represents fraction of beta phase while K is the proportionality constant (0.518 for β (101) and α(102) peaks while 0.544 for β(210) and α (210) peaks) [82]. The high-temperature X-ray diffractometer (XRD) analysis was conducted by using a Rigaku Ultima IV (Japan) having a scintillation counter with an HT 1500 high-temperature attachment. Constant flow of high purity argon gas (99.999%) was maintained during the entire experiment. To fit the patterns to the formed phases, PDXL program was used with very large and up-to-date database. Phase analysis of cBN and SiC particles was performed using DXR2 Raman microscope. The 532-nm-wavelength laser line was used as the excitation wavelength, and the laser power used was 2.5 mW. The spectra were acquired at 25 °C between 100 and 3000 cm^{-1}.

3.4.3 Microstructural Analysis

Filed-emission scanning electron microscope (FESEM, Lyra 3, Tescan, Czech Republic) was used to study the resultant morphologies of the sintered samples. The electron gun voltage was varied between 20-30 KeV to get the best possible contrast. Both secondary and backscattered imaging modes were utilized in this study, as per the need. An accompanied energy dispersive spectrometer (EDS, Oxford Inc., UK) was of great help in linking the XRD phases with their corresponding morphologies. Phoenix focused ion beam (Helios G4 UX DualBeam, FEI) was used to prepare the transmission electron microscope (TEM) lamellas. High resolution imaging and selected area

diffraction patterns were acquired using FEI's Titan transmission electron microscope equipped with EDX detector.

3.4.4 Mechanical Testing

Sintered samples were mechanically tested for their hardness and fracture toughness. Vickers hardness of 98 N force was followed in this study to keep up with the literature convention. A universal hardness tester (Zwick-Roell, ZHU250, Germany) with diamond pyramid indenter was used to get the depression diagonals of the polished samples. Hardness can be calculated in GPa using the following equation where which d represents the average of the two diagonal lengths in mm.

$$HV_{10} = \frac{1.854}{d^2} \ (9.81\times10^{-3})$$

Fracture toughness testing shows wide variation in the field of hard materials. Single-Edge Notched Beam (SENB) and Single-edge V-Edge Notched Beam (SEVNB) are two leading techniques to evaluate fracture toughness, however none of these has been commercially standardized. One issue arises when applying these techniques is that samples should be relieved from residual stresses prior to testing [83]. Another limitation in these techniques is the difficulty of initiating a pre-crack with the specified size. Furthermore, in the field of sialon materials indentation method (IM) has widely been adopted. Hence, we used indentation method to compare our results with the values obtained from literature. Several formulations have been introduced in the field of hard ceramics to evaluate fracture toughness using indentation hardness, however, Evan's equation [84] is one of the most frequently used relation in the field of sialon materials.

Evan's equation is shown below where MCL stands for the maximum crack length initiated from the indentation and d is the average diagonal.

$$K_{IC} = 0.48\left(\frac{MCL}{d/2}\right)^{-1.5}\left(\frac{HV_{10}\sqrt{d/2}}{3}\right)$$

CHAPTER 4

LOW-TEMPERATURE SPARK PLASMA SINTERING OF CALCIUM STABILIZED ALPHA SIALON USING NANO-SIZE ALUMINUM NITRIDE PRECURSOR

Summary

Calcium stabilized alpha-sialon ceramic was synthesized using spark plasma sintering (SPS). The size effect of aluminum nitride precursor (1 μm and 50nm) on the phase analysis, microstructural and mechanical characteristics of the processed sialon was studied. Alongside the size of AlN precursor, holding time and sintering temperature were also varied in orde88888r to assess the degree of densification, phase transformation and its subsequent effect on the mechanical properties of these materials. The development of alpha phase was found to be strongly dependent on the particle size of the aluminum nitride (AlN) precursor. Interestingly, this novel approach of changing particle size from micro to nano level combined with the SPS process resulted in the formation of alpha-sialon ceramic at much lower than previously reported sintering temperature i.e. 1500ºC as compared to 1700/1800ºC. Surface oxide layer associated with AlN particles resulted in the formation of additional beta phase along with major alpha phase in the final product. The sialon product synthesized from micron-size AlN particles (1μm) at a sintering temperature of 1500ºC exhibited Vickers hardness value $HV_{10,}$ of 18 GPa and moderate fracture toughness of 5.6 MPa√m. However, sialon materials synthesized from nano-size AlN particles (50nm) showed a hardness value of 14 GPa while displaying an improved fracture toughness of 7 MPa√m. Increase in holding time resulted in a slight increase in densification of these materials, however its

influence on mechanical properties was less significant as compared to the effect of particle size of aluminum nitride staring powder precursor.

4.1 Introduction

Ceramics have been long known as ideal materials that can withstand extreme operating conditions such as high temperature, loads and wear. Silicon nitride is an example of a ceramic that exhibits exceptional thermal and mechanical properties [1]. However, the strong covalent nature of its bonds, makes it difficult to achieve completely densified silicon nitride materials. While very high temperatures have been used to help achieve completely densified silicon nitride materials [2], performing operations at such high temperatures and carrying out sintering for necessarily long periods of time present practical complexities. In order to avoid these problems and to synthesize completely dense silicon nitride materials at lower temperatures, metal oxide additives have been used as densifying agents [1,2,85]. This modification resulted in the formation of sialon materials [10–12].

Sialon materials, which are solid solutions of silicon nitride, form generally two main phases, alpha sialon and beta sialon, which have different microstructure and crystal structure and thermo-mechanical characteristics. Beta sialon is formed by concurrent identical replacement of silicon by aluminum and nitrogen by oxygen. Its chemical formula has been commonly defined as $Si_{6-z}Al_zO_zN_{8-z}$. The chemical formula of the alpha-sialon, which embraces four units of Si_3N_4, is generally described by $M_x^vSi_{12-(m+n)}Al_{m+n}O_nN_{16-n}$ where $x < 2$, $x = mv$, and m (Al-N) bonds and n (Al-O) replace (m+n) (Si-N) bonds [10,11,20,41]. Alpha and beta sialon have been intensely investigated in the course of the last couple of decades because of their outstanding mechanical

properties, explicitly the better fracture toughness due to elongated morphology of beta phase and the high hardness of alpha phase [16,17].

Higher hardness as well as better sinterability of sialon materials in comparison to silicon nitride make them a desirable candidate material for cutting tools[86–88]. Company named CeramTec provides special tool materials composed of alpha/beta sialons specifically for boring, turning and milling of cast iron in interrupted along with uninterrupted machining mode [89].

Although rare-earth metallic ions have been used as stabilizers in the synthesis of sialons for decades, the higher solubility of calcium oxide as well as its relative stability have recently made it a preferred additive [24,28–31,90]. Moreover, the greater availability of Ca-based compounds, and hence their lower costs, make them advantageous as sintering aids[34,91]. A study by Wang et al. on phase formation of calcium alpha-sialons at 1750^{o}C using hot pressing technique concluded that maximum calcium content in alpha-sialons is about 70% of x value in M_x[27]. Conventional sintering techniques in combination with micron sized precursors require long sintering duration as well as a temperature greater than 1700^{o}C for the synthesis of well densified Ca-sialons. [67,73,92]. SPS is a powder sintering process, which has gained focus in the consolidation of powder materials due to its novel pulsed-current-based heating allowing higher heating rate and short synthesis duration. [93,94].

This chapter presents the work in which we have studied the effect of AlN precursor powder size (1μm versus 50nm), on the formation of calcium alpha-sialon phase at a low sintering temperature of 1500^{o}C. We used precursors in amounts that typically form Ca-stabilized alpha sialon. We also studied the effect of holding time during sintering on the mechanical properties of the produced sialon ceramics.

The alpha sialon having the chemical formula $Ca_{0.8}Si_{9.2}Al_{2.8}O_{1.2}N_{14.8}$ was selected for the synthesis. Precursors employed for this synthesis included alpha-Si_3N_4, SiO_2, CaO and AlN (details of power precursors are mentioned in chapter 3). These precursors were processed via SPS at sintering temperatures of 1400^{o}C and 1500^{o}C with holding times of 10, 20 and 30 minutes and uniaxial pressure of 50MPa (details pertaining to experimental procedure is mentioned in chapter 3). Classification based upon size of initial powder mixture as well as that on processing conditions is summarized in the **Table 5**. The sample ID used in **Table 5** and the rest of the chapter starts with the numeric digit '5' , which represents the alpha sialon composition dictated by the "m" and "n" values used, followed by the sintering temperature, holding time and aluminum nitride particle size. For instance an alpha sialon sample having the composition of $Ca_{0.8}Si_{9.2}Al_{2.8}O_{1.2}N_{14.8}$ (m = 1.6, n = 1.2) sintered at 1500^{o}C with 30 minutes of holding using 50nm AlN starting powder precursor is named as 5-15003050.

Table 5 Sets of conditions used to synthesize the sialon ceramics. In all cases, a constant cooling rate in the range of 200^{o}C was used.

S/No	***Sample ID***	***Sintering Temp (℃)***	***Holding Time (min)***	***AlN Particle Size***
1	5-15001050	1500	10	50 nm
2	5-15002050	1500	20	50 nm
3	5-15003050	1500	30	50 nm
4	5-1500101	1500	10	1 μm
5	5-1500201	1500	20	1 μm
6	5-1500301	1500	30	1 μm
7	5-14003050	1400	30	50 nm
8	5-1400301	1400	30	1 μm

4.2 Results and Discussion

4.2.1 Powder Mixture and Densification

To prepare a homogenous powder distribution, the starting precursors (Si_3N_4, SiO_2, AlN, CaO) were mixed for 30 min in ethanol using ultrasonic probe-sonicator. The EDX mapping performed on the powder mixture (using elemental mapping for Si, Al, Ca, O, N) did not reveal agglomeration as the elemental distribution was fairly homogenous, as depicted in **figure 14**.

Table 6 shows the density values of the Ca-sialons synthesized from aluminum nitride particle sizes of 1μm and 50nm for various holding times at the relatively lower sintering temperatures of 1400°C and 1500°C. The alpha sialon sample 5-1500301 showed the highest density of 3.15 g/cm^3. The increase in density value was prominent when the holding time was increased from 10 to 20 minutes for the sialon sample synthesized from the aluminum nitride precursor with a particle size of 1 μm. This increase was primarily due to creation of more amount of liquid phase with the increased holding time for the sample having aluminum nitride of larger particle size. The comparatively lower density value for the samples synthesized from aluminum nitride with a particle size of 50 nm was due to the substantial nucleation and growth of beta-sialon crystals at the expense of a significant amount of liquid phase during the synthesis process.

In contrast to the samples sintered at 1500°C, sialon material sintered at 1400°C, from aluminum nitride with particle size of 1 μm (5-1400301), relatively poor densification, with density values of 2.89 g/cm^3 was observed. However, the sample synthesized from aluminum nitride with a particle size of 50 nm (5-14003050) displayed a density of 3.00 g/cm^3, suggestive of the high reactivity of AlN and hence the creation of a sufficient quantity of the oxynitride liquid even at a temperature of 1400°C. This observation is in line with the large surface area associated with a nano-sized powder acting as the driving mechanism for sintering [36].

It was observed that with the increase in sintering temperature from 1400ºC to 1500ºC there was an obvious increase in shrinkage primarily due to dissolution of nitride precursors and formation of oxynitride liquid phase (1298ºC) followed by precipitation (1480ºC) of sialon phase **(figure 15a &b)**. A similar sort of behavior was observed by J. D. Bolton & A. J. Gant for the ceramic reinforced high speed steel metal matrix composites, where the densification was seen to increase as sintering temperature surpassed the solidus temperature [95]. However, in our case the shrinkage rate became independent of time after an approximate holding time of 10 minutes (due to high heating rate). Another aspect worth noting is that the shrinkage rate was higher for the samples synthesized from nano sized AlN, due to the higher reactivity of the nano sized particles. The relatively lesser shrinkage for the micron-sized AlN sample sintered at 1500ºC may well be attributed to the undissolved micron sized AlN at 1500ºC as confirmed by the XRD results.

Table 6 Density values of the Ca-sialons synthesized from aluminum nitride particle sizes of 1µm and 50nm, for various holding times at 1400°C and 1500°C.

S/No	***Sample ID***	**Density g/cm^3**
1	5-15001050	3.01 ± 0.05
2	5-15002050	3.02 ± 0.04
3	5-15003050	3.05 ± 0.06
4	5-1500101	3.08 ± 0.06
5	5-1500201	3.15 ± 0.05
6	5-1500301	3.15 ± 0.03
7	5-14003050	3.00 ± 0.05
8	5-1400301	2.89 ± 0.07

4.2.2 Phase Analysis

Figure 16 displays XRD results of SPS'ed samples sintered at 1400ºC and 1500ºC. In all samples, the formation of alpha-sialon was observed. For the samples sintered with 30 minutes of holding time lattice parameters and the amount of calcium ion in alpha-sialon calculated using empirical

relationship developed by Yanbing [73] are summarized in **Table 7**. The peak shift to lower 2theta increased slightly with an increase in temperature and decrease in AlN particle size. The samples sintered at 1400°C resulted in an unsatisfactory level of densification, with a measured density of 2.89 g/cm^3 and low Ca-content in alpha-sialon. Samples sintered at 1500°C for 30 minutes had density values of 3.05g/cm^3 and 3.15 g/cm^3 for 50nm AlN and 1um AlN, respectively.

Wang et al. reported similar density values of 3.07g/cm^3 and 3.17g/cm^3 at 1700°C and 1750°C, respectively, for dense hot pressed calcium alpha-sialon having a composition of $Ca_{0.5}Si_{10.5}Al_{1.5}O_{0.5}N_{15.5}$ [28]. The increase in temperature enhanced the diffusion of species, thereby increasing the calcium content in alpha-sialon. Interestingly, particle size of AlN revealed to be an important parameter in this transformation process. XRD indicated that nano size AlN had completely disappeared at 1500°C, primarily due to higher reactivity of nanoparticles, yielding formation of alpha-sialon with calcium content closer to initially selected composition. However, incomplete dissolution of micron-sized AlN precursor at 1500°C restricted completion of intended reaction and hence the complete development of alpha-sialon. In contrast to micron size AlN sample, XRD pattern of sample synthesized using 50nm AlN precursor showed the presence of distinct beta- sialon peaks at 1500°C. The observations indicated that higher reactivity of nano AlN as compared to micron size resulted in larger amounts of liquid phase essential for the formation of intended alpha-sialon phase.

Table 7 Lattice parameters and calcium content in alpha-sialons sintered for 30min.

Sample ID	**Designed Ca value 'x'**	**a (Å)**	**c (Å)**	**Calculated 'x'** [73]
5-1400301	0.8	7.7561	5.6208	0.02
5-14003050	0.8	7.7824	5.6422	0.25
5-1500301	0.8	7.7861	5.6452	0.29
5-15003050	0.8	7.8040	5.6578	0.45

4.2.3 Microstructure Analysis

FESEM micrographs of etched samples sintered at 1500^{o}C are shown in **figure 17 (a-f). The s**ample prepared using micron size AlN precursor at 1500^{o}C revealed two distinct regions as shown in **figure 17a**. Higher magnification images of two regions are shown in **Fig. 17 (b & c)**. The micrograph in f**igure 17b** depicts equiaxed morphology representative of alpha-sialon. However, **figure 17c** depicts a mixed region containing large dark pockets of glassy phase and underdeveloped alpha-sialon as well as very small pocket of early stage beta phase. The region indicated that oxy-nitride glassy liquid phase had formed but the reaction involving the complete dissolution of AlN precursor necessary for the complete formation of alpha-sialon was not achieved, as indicated by XRD pattern.

Figure 17 (d) reveals patches of well-developed elongated beta-sialon embedded in alpha-sialon matrix for the sample synthesized using nano-size AlN precursor. Blown-up view of the matrix **(figure 17e)** shows the equiaxed morphology of alpha-sialon. Higher magnification image exhibiting both alpha and beta phases is shown in **figure 17f**. The smaller size of AlN precursor facilitated the formation of alpha-sialon at lower than normally reported temperature, i.e. 1500^{o}C as compared to 1700^{o}C/1800^{o}C [15,17,19]. However, surface oxide layer associated with nano size AlN precursor has promoted the formation of patches of beta-sialon, as indicated by the XRD pattern.

The results revealed that densification of the sialon materials occurred via formation of a liquid phase. Typically, increasing the temperature for the initial reaction between the precursors resulted in the formation of a Ca-containing liquid phase. This liquid phase is believed to form above 1350°C, which is the eutectic temperature for this system [41]. During the early stages, the liquid

phase has been indicated to contribute to the diffusion and rearrangement of the particles and ultimately result in the formation of alpha sialon via a solution re-precipitation mechanism [20]. The crystallographic analysis of the sialon materials sintered at 1500°C for 30 minutes suggest that the materials were synthesized according to the following overall reactions:

(5-1500301)

$$\text{Alpha-}Si_3N_4 + CaO + \textbf{AlN (1µm)} + SiO_2 \xrightarrow{\textbf{1500°C-30min}} Ca_{0.68}Si_{9.96}Al_{2.04}O_{0.68}N_{15.32} + \text{Ca-Si-Al-O-N (liquid phase)} + \text{Beta Sialon (trace amount)}$$

(5-15003050)

$$\text{Alpha-}Si_3N_4 + CaO + \textbf{AlN (50nm)} + SiO_2 \xrightarrow{\textbf{1500°C-30min}} Ca_{0.68}Si_{9.96}Al_{2.04}O_{0.68}N_{15.3} + \text{Ca-Si-Al-O-N (liquid phase)} + Si_5AlON_7\,\text{(Beta Phase)}$$

transformation in the sample produced from 50-nm-sized aluminum nitride particles most likely resulted from the formation of large amounts of high viscosity liquid phase due to the high reactivity of aluminum nitride. Here, it is important to note that the amount of liquid phase present appeared to substantially influence the evolution of the final microstructure [82,96] . In a study of high-temperature stability of alpha sialon with starting compositions belonging to pure alpha Necip Camucu, Derek P. Thompson and Hasan Mandal concluded that "In a-sialon starting compositions prepared within or at the edge of the alpha-sialon phase region, the ease with which transformation proceeds depends mainly on the cation size of the sintering additive, the presence of beta-sialon grains and also the amount and viscosity of liquid phase present" [82].

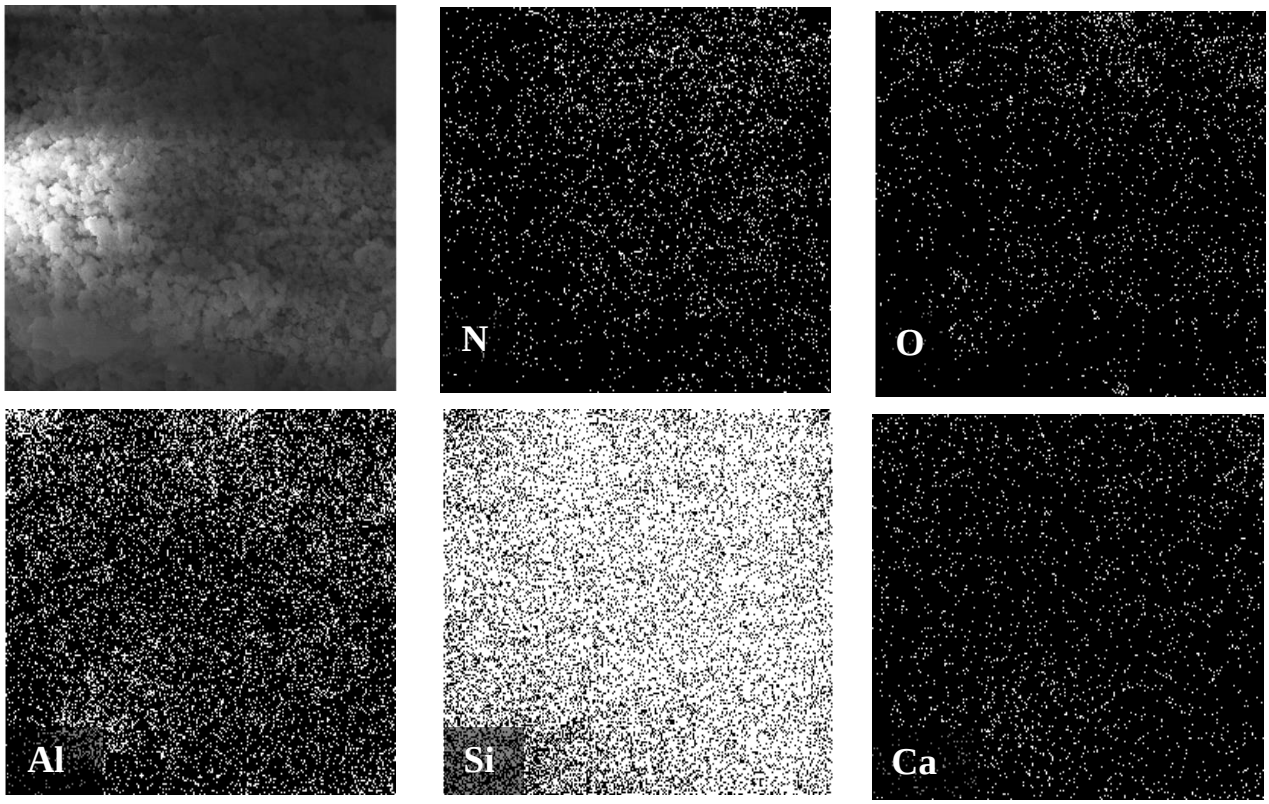

Figure 14 EDX elemental mapping obtained from the probe sonicated powder mixture (containing Si_3N_4, SiO_2, AlN, CaO) revealing a homogenous distribution.

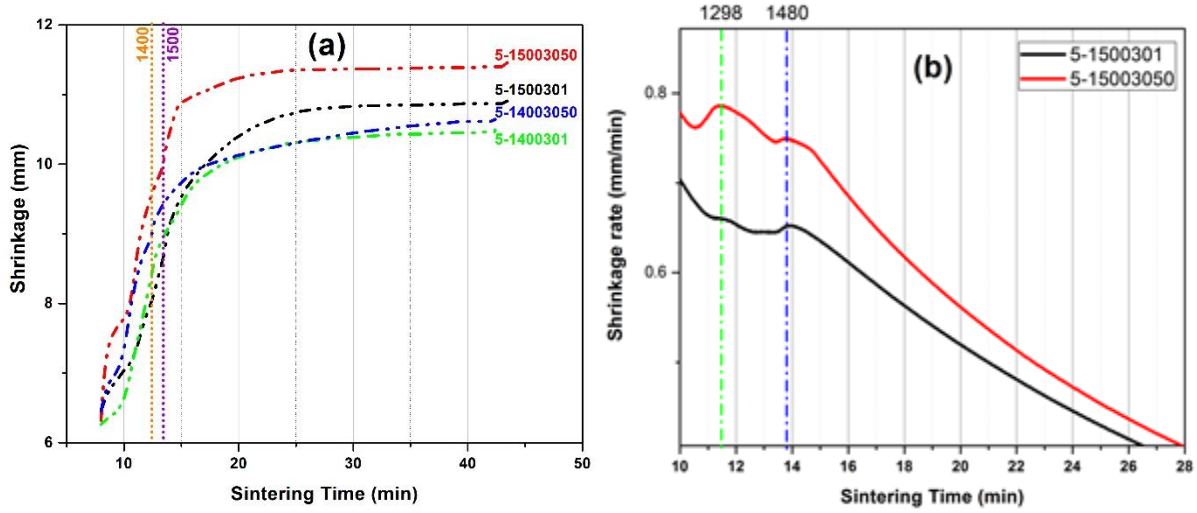

Figure 15 (a) represents shrinkage curves for micro and nano-sized AlN samples sintered at 1400ºC and 1500ºC with 30 minutes holding time where vertical lines marked as 1400 and 1500 represents the initiation of the holding time, **(b)** represents shrinkage rate vs time curves for micro

and nano-sized AlN samples sintered at 1500°C with 30 min holding time. The peak at 1298°C represents the formation of oxynitride eutectic liquid phase and peak at 1480°C is generally attributed to the occurrence of the solution/precipitation mechanism [67].

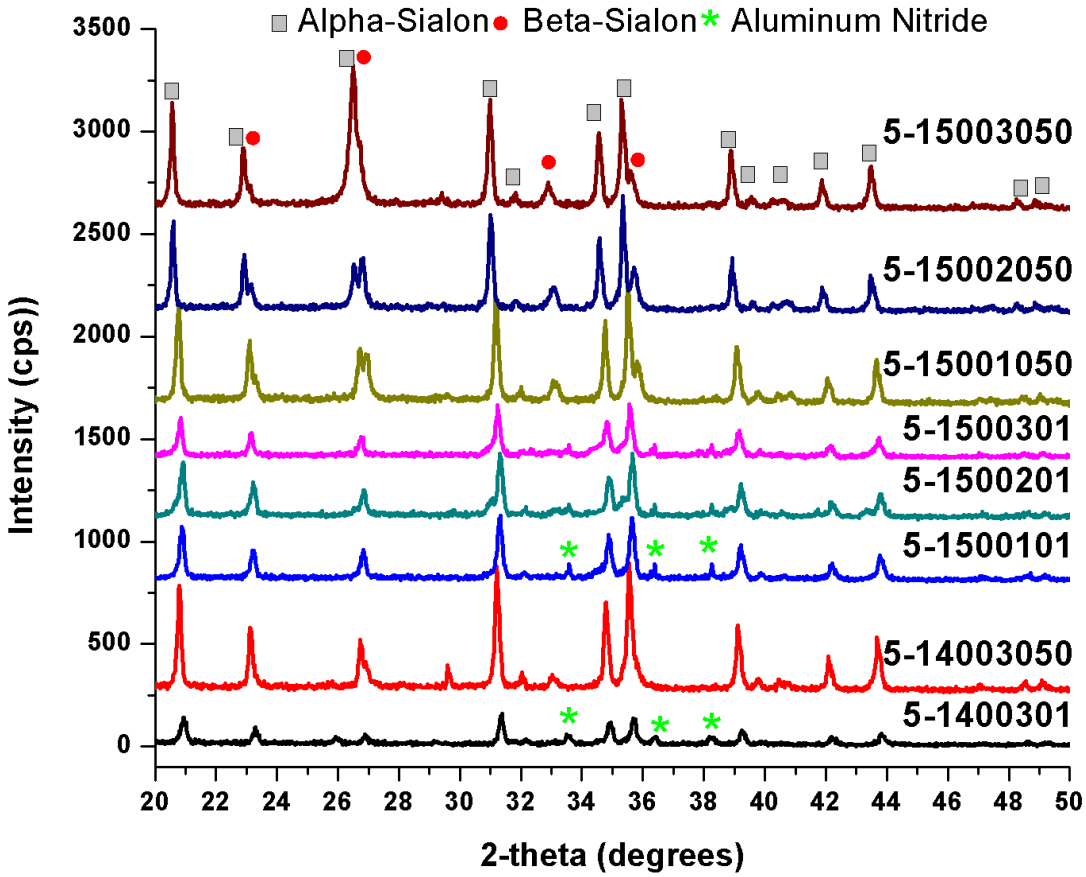

Figure 16 XRD patterns of samples synthesized at 1400°C and 1500°C, 30 minutes.

4.2.4 Mechanical Properties

Figure 18 summarizes the results of mechanical testing of the pure sialon samples synthesized at 1400°C and 1500°C. For the samples synthesized at 1500°C, a marked change in the Vickers hardness was observed as the aluminum nitride precursor particle size was altered between 50 nm to 1 μm. The sample synthesized from the aluminum nitride precursor with a particle size of 1 μm displayed the greatest hardness value, at 18.0 GPa, along with a moderate fracture toughness of

5.5 MPa√m. That from 50-nm-sized aluminum nitride particles showed a maximum hardness value of 13.7 GPa while displaying a fracture toughness of 7.03 MPa√m. This noticeable increase in fracture toughness may well be attributed to the crack deflection, crack bridging effect of the elongated morphology of beta phase embedded in the much finer alpha matrix [97–101]. However, changing the holding time at 1500°C barely affected the hardness values. The slight observed increase in hardness with increasing holding time was primarily due to the increase in the densification of the materials under study.

The samples synthesized at 1400°C showed much lower hardness values than did the samples synthesized at 1500°C. The relatively low strengths of the materials synthesized at 1400°C occurred despite their showing the presence of the hard alpha phase, and were likely due to their incomplete densification at this temperature.

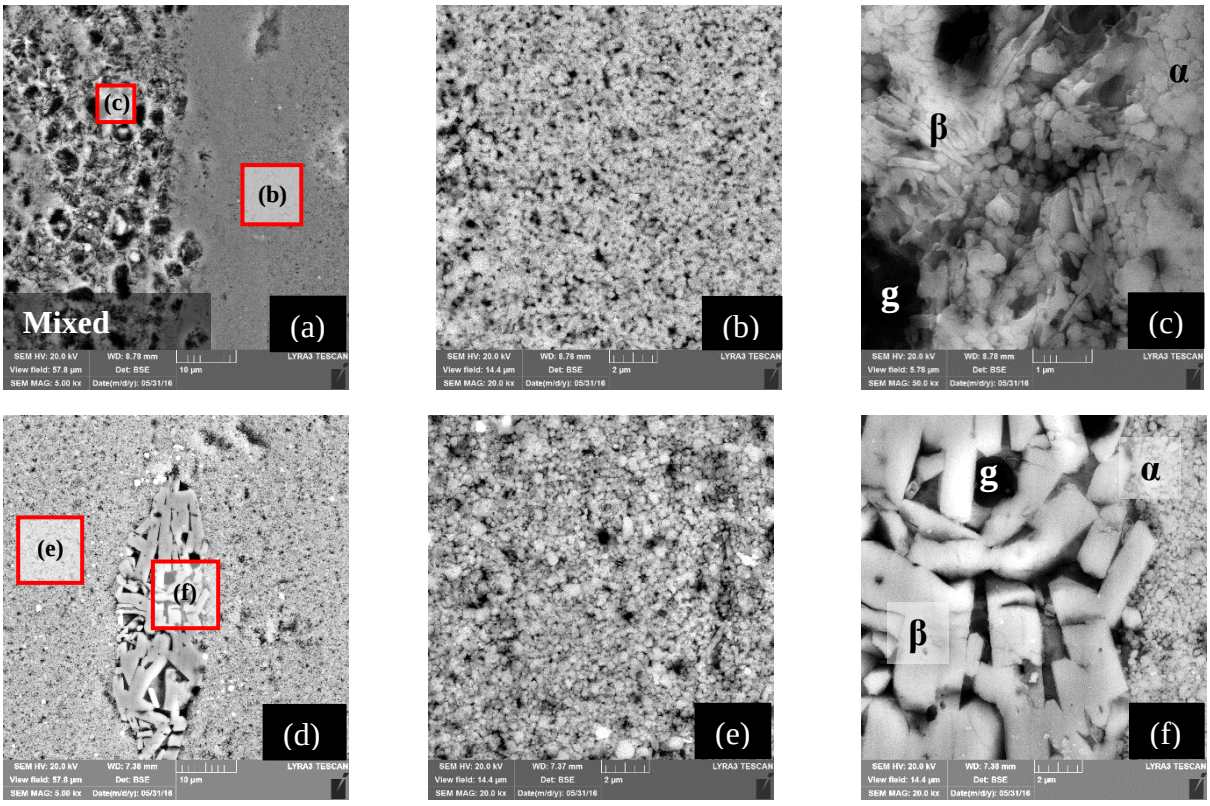

Figure 17 FESEM images of samples sintered at 1500°C, 30 minutes, with AlN precursor particles having sizes of (a-c) 1 µm, (d-f) 50 nm; (α) alpha phase, (β) beta phase and (g) amorphous glassy phase.

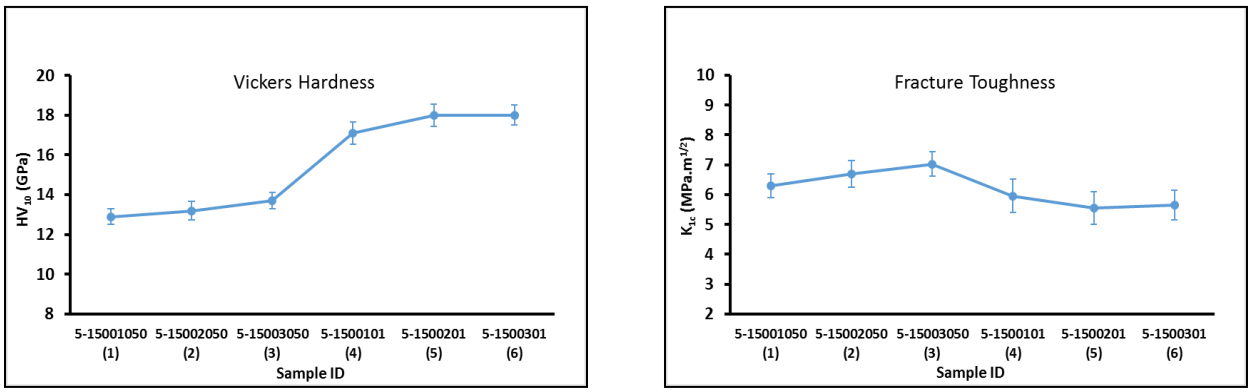

Figure 18 Hardness and fracture toughness of samples synthesized at 1500°C with holding time of 10 to 30 minutes for AlN particles sizes of 50nm and 1um.

4.3 Conclusion

Ca-stabilized alpha sialon samples were synthesized from aluminum nitride precursors of particle size of 50 nm and 1 μm at 1400^{o}C and 1500^{o}C. Probe sonication with ethanol resulted in a satisfactory level of homogeneity in the initial powder mixture of the precursors. Despite the high reactivity of the precursors owing to their nano-size, the samples sintered at 1400^{o}C failed to display satisfactory densification. However, the samples synthesized at 1500^{o}C were thoroughly densified. The factor most worth emphasizing is the effect of the size of the aluminum nitride precursor particle: we found aluminum nitride precursor particles of 50 nm in size to result in the nucleation and growth of the beta-sialon phase for a composition that generally produces only the alpha phase. The reaction time during the earlier stage of synthesis (ca. 1400^{o}C) was sufficient to allow for the melting and/or dissolution of the AlN (50 nm) with the rest of constitutes to form an oxynitride liquid regime. This liquid phase facilitated the growth of the beta-sialon grains. Hardness of the samples synthesized at 1500^{o}C for 30 min. holding time by varying particle size of AlN powder were 13.7 GPa (50nm) and 17.8 GPa (1μm), and their corresponding fracture toughness was 7.03, and 5.66 MPa√m respectively. Increase in fracture toughness from 5.66 to 7.03 MPa√m was observed as the size of aluminum nitride starting powder was decreased from 1μm to 50 nm. The enhancement in the fracture toughness of the samples synthesized from smaller particles may well be attributed to the elongated morphology of beta sialon grains.

CHAPTER 5

DEVELOPMENT OF CALCIUM STABILIZED NITROGEN RICH ALPHA SIALON CERAMICS ALONG THE Si_3N_4-$1/2Ca_3N_2$:3AlN line

Summary

Calcium stabilized nitrogen rich sialon ceramics having a general formula of $Ca_xSi_{12-2x}Al_{2x}N_{16}$ with x value in the range of 0.2-2.2 for compositions lying along the Si_3N_4-$1/2Ca_3N_2$:3AlN line were synthesized, using nano size starting powder precursors and spark plasma sintering technique. The development of calcium stabilized nitrogen rich sialon ceramics at a significantly low sintering temperature of 1500^{o}C (normally reported temperature of 1700^{o}C or greater) remains to be the highlight of the present study. The developed sialons were characterized for their microstructure, phase and compositional analysis, and physical and mechanical properties. Furthermore, a correlation was developed between the lattice parameters and the content (x) of alkaline metal cation in the alpha sialon. Nitrogen rich calcium alpha sialons were observed to form in the range of $0.15 \leq x \leq 1.83$. Well densified single-phase nitrogen rich alpha sialon ceramics were achieved in the range of $0.4 < x < 1.6$. Nitrogen rich alpha sialon samples having a maximum hardness of 22.4 GPa and a maximum fracture toughness of 6.1 MPa.$m^{1/2}$ were developed.

Graphical Abstract

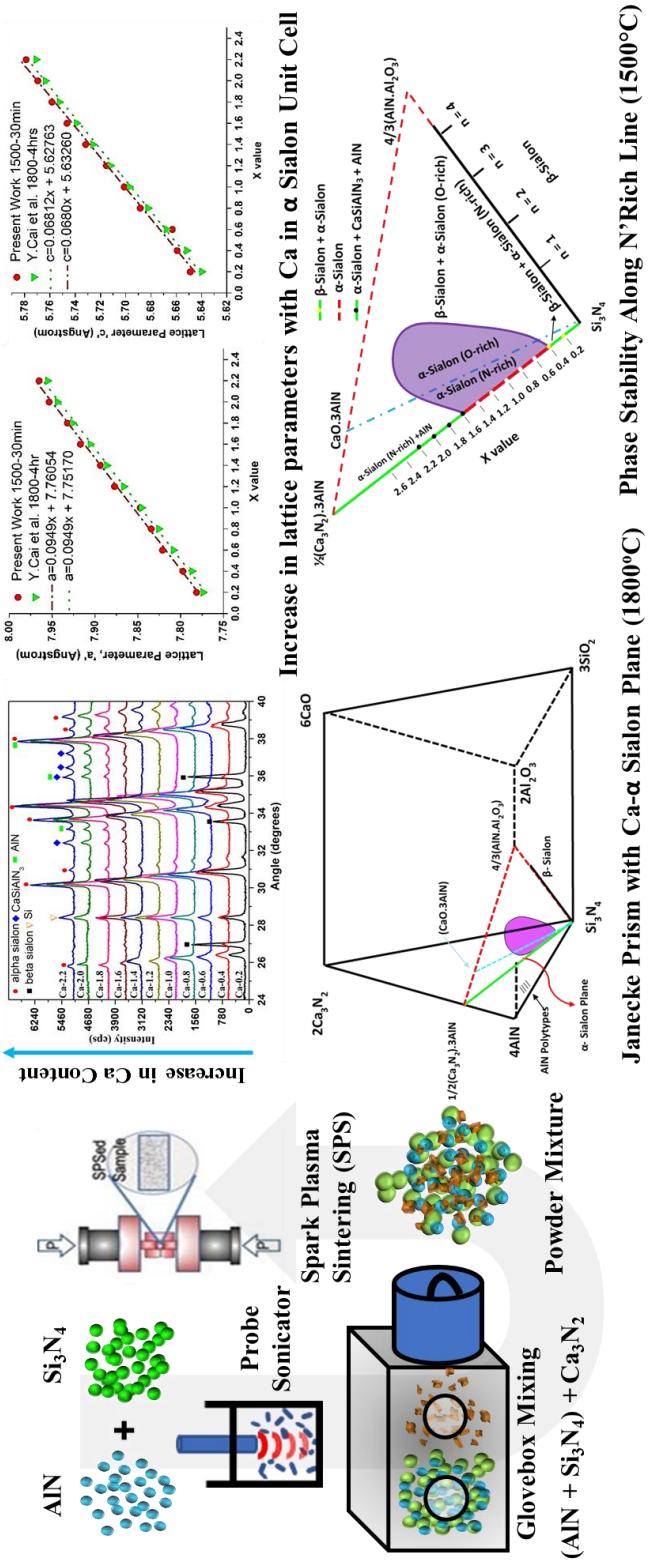

5.1 Introduction

Sialon materials is a class of ceramics that have been thoroughly studied with respect to their phase stability regimes, thermo-mechanical properties, photoluminescence and oxidation behavior [27,67,102–110]. Most of the work on sialon ceramics has been concentrated around the two commonly known phases, namely alpha sialon and beta sialon. As an alloy of silicon nitride, beta-sialon having a general formula of $Si_{6-z}Al_zO_zN_{8-z}$, is formed as a result of chemical replacement of silicon-nitrogen bonds with aluminum-oxygen bonds[1].

Compositions belonging to alpha-sialon phase are generally defined by $M_x^vSi_{12-(m+n)}Al_{m+n}O_nN_{16-n}$ (x and v represents solubility and valence of the cation M in alpha sialon structure, respectively) where $x < 2$, $x = mv$, and m (Al-N) and n (Al-O) replace (m+n) (Si-N) bonds[10]. The substitution of silicon-nitrogen bonds with aluminum-nitrogen and aluminum-oxygen bonds results in a charge imbalance which is neutralized by the incorporation of M^{v+} ions such as Li^+, Ca^{2+}, Mg^{2+}, Y^{3+} and lanthanide ions[25,26,45,111]. Studies have been reported on synthesis and phase stability regime of single phase alpha sialons[25,26,45,111]. Several compositions of yttrium-stabilized alpha sialons along the nitrogen rich line of Si_3N_4–YN:3AlN were synthesized by Sun et al where the solubility limit of yttrium cation in alpha sialon was found out to be $0.43<x<0.8$ [102]. Zhen-Kun et al. studied the formation of oxygen rich yttrium stabilized alpha sialons along the Si_3N_4–Y_2O_3:9AlN and the solubility limit of yttrium cations was reported as $0.33<x<0.67$ [25]. It is well known that synthesis of alpha sialons occurs via solution-reprecipitation mechanism, which involves the formation of an intermediary oxy-nitride liquid phase as a result of reaction between the starting oxide and nitride precursors [17,112].

In contrast to alpha sialons synthesized using yttrium or rare earth stabilizing cations, calcium stabilized alpha sialons have gained considerable attention due to the higher solubility of calcium cation as compared to the former (maximum solubility value x_{max} of 1.6 for Ca^{+2} as compared to x_{max} value of 1.0 for Yb^{+2}) [26,45]. Furthermore, Hassan Mandal, in his study on post sintering heat treatment of alpha sialons, has also reported, that in contrast to rare-earth stabilized alpha sialons calcium stabilized alpha sialons depict complete resistance towards alpha to beta phase transformation in the temperature range of 1450-1500ºC [33]. Higher stability of calcium stabilized alpha sialons has been attributed to the lower valence of calcium cation, since the high temperature stability of alpha sialon increases with increase in the solubility of charge stabilizing cation (x), which in turn increases with decrease in cation valence [113].

Figure 19 shows the Janecke prism and the calcium-alpha sialon plane highlighting the single-phase alpha sialon region (oxygen rich as well as nitrogen rich) along with the neighboring phases at 1800ºC [114]. Several studies conducted on the synthesis of oxygen rich alpha-sialons have reported formation of elongated morphology of alpha sialon as compared to the generally known equiaxed morphology, thus resulting in considerable improvement in the toughness of the these materials [100,115,116]. However, there are very few studies that have been done on the synthesis of nitrogen-rich alpha sialons, mainly due to the fact that they are difficult to densify [73,113]. Studies on the synthesis of calcium stabilized nitrogen rich alpha sialons using all nitride precursors is even more scarce in the literature due to the difficulty in handling and storage of calcium nitride [113].

Xie.et al worked on the synthesis of calcium stabilized nitrogen rich alpha sialons along the Si_3N_4-$1/2Ca_3N_2$:3AlN line at 1700ºC using hot pressing technique [113]. The limits of single phase calcium alpha sialon was reported to be $0.5<x<1.7$. Recently, Yanbing Cai et al. studied the

synthesis of calcium stabilized nitrogen rich alpha sialons using CaH_2 as a starting precursor instead of Ca_3N_2 at 1800°C using hot pressing technique [73]. Single phase alpha sialon ceramics were obtained in the range of 0.50<x<1.38. Raja et al. reported synthesis of oxygen rich calcium alpha sialon ceramics at relatively low temperature of 1500 °C using nano-sized precursors and spark plasma sintering technique [93]. However, to the best of our knowledge, synthesis of nitrogen rich sialons at low temperatures (below 1700°C) has not been reported in the literature.

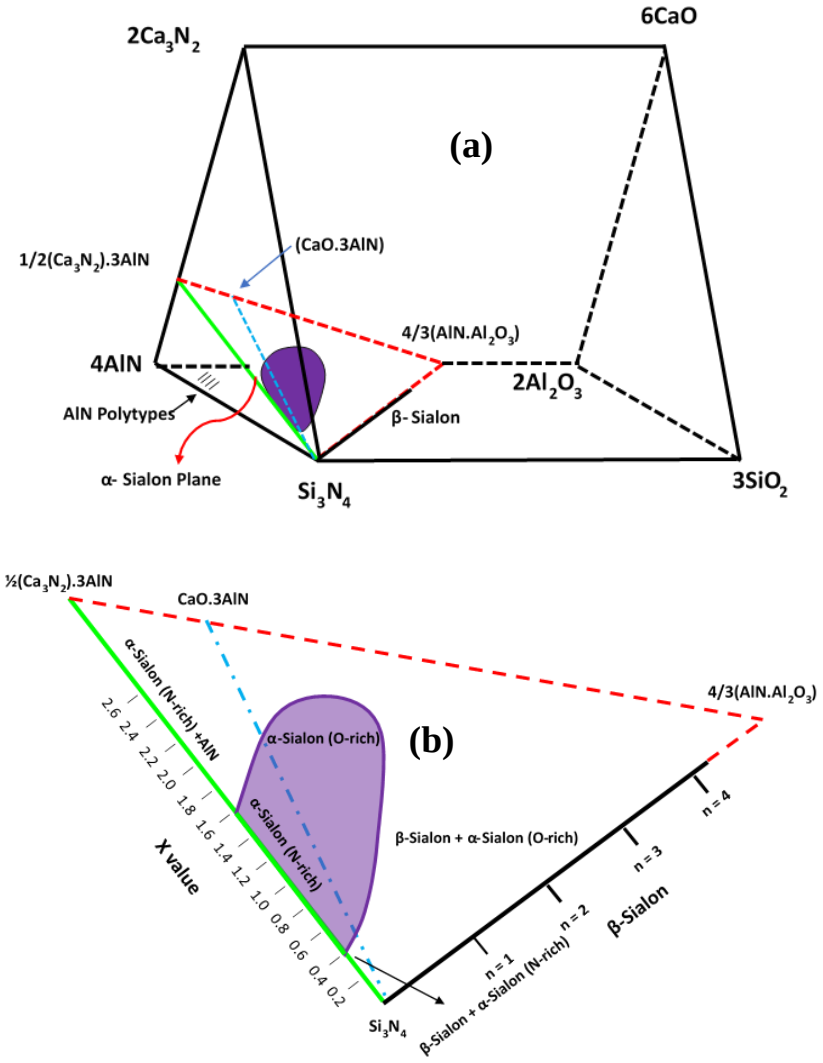

Figure 19 Regenerated schematic representation of **(a)** Jancke Prism of Ca-Sialon System and **(b)** α-plane in Ca-sialon system at 1800°C [114].

The chapter discusses the development of calcium stabilized nitrogen rich alpha sialons along the Si_3N_4-1/2Ca_3N_2:3AlN line at a lower temperature of 1500^oC using spark plasma sintering technique and nano-size starting powder precursors. The developed sialons were characterized for their microstructure, phase and compositional analysis and physical and mechanical properties. Furthermore, a correlation was developed between the lattice parameters and the content of alkaline metal cation (calcium) in the alpha sialon.

Calcium stabilized nitrogen rich alpha sialon compositions having the general formula of $Ca_xSi_{12-m}Al_mN_{16}$ (where x= m/2), along the nitrogen rich line were selected for the synthesis (details of starting powder precursors are mentioned in chapter 3). Alpha sialon samples having the nominal compositions as listed in **Table 8** were synthesized. The sample ID's used in this chapter starts with the letter 'Ca' followed by the nominal value of 'x' selected for the synthesis of a specific composition, for example, sample having the chemical formula of $\mathbf{Ca_{0.2}Si_{11.6}Al_{0.4}N_{16}}$ would be referred to as Ca-0.2.

Table 8 Nominal composition of calcium stabilized nitrogen rich sialons.

Sample ID	Starting Composition	Ca_3N_2 wt.%	Si_3N_4 wt.%	AlN wt.%
Ca-0.2	$Ca_{0.2}Si_{11.6}Al_{0.4}N_{16}$	1.74	95.37	2.89
Ca-0.4	$Ca_{0.4}Si_{11.2}Al_{0.8}N_{16}$	3.43	90.87	5.70
Ca-0.6	$Ca_{0.6}Si_{10.8}Al_{1.2}N_{16}$	5.08	86.48	8.44
Ca-0.8	$Ca_{0.8}Si_{10.4}Al_{1.6}N_{16}$	6.68	82.20	11.11
Ca-1.0	$Ca_{1.0}Si_{10}Al_{2.0}N_{16}$	8.25	78.04	13.71
Ca-1.2	$Ca_{1.2}Si_{9.6}Al_{2.4}N_{16}$	9.78	73.98	16.25
Ca-1.4	$Ca_{1.4}Si_{9.2}Al_{2.8}N_{16}$	11.26	70.02	18.72
Ca-1.6	$Ca_{1.6}Si_{8.8}Al_{3.2}N_{16}$	12.71	66.15	21.13
Ca-1.8	$Ca_{1.8}Si_{8.4}Al_{3.6}N_{16}$	14.13	62.38	23.49

Ca-2.0	$Ca_{2.0}Si_8Al_{4.0}N_{16}$	15.51	58.70	25.79
Ca-2.2	$Ca_{2.2}Si_{7.6}Al_{4.4}N_{16}$	16.86	55.11	28.03

5.2 Results and Discussion

5.2.1 Sintering and Densification Behavior

Sintering behavior of the samples sintered over the range of $0.2<x<2.2$ is shown in **figure 20** (insert shows the complete densification curves), where the ordinate represents the displacement of upper punch of the die in mm, depicting the shrinkage, while the abscissa represents the sintering time. It is observed that with increase in the x value, or denoting the increase in calcium (Ca) content, the shrinkage curve shifts to the left (towards shorter time). Samples having higher x value exhibit larger shrinkage (larger displacement) and subsequently were densified earlier. It is quite known that the densification of silicon nitride based materials involve the formation of a transient liquid phase, where the densification behavior depends on the viscosity; amount and wetting characteristic of the transient liquid phase. In case of the calcium stabilized alpha sialons synthesized using oxide additives, the formation of transient liquid phase takes place as a result of reaction between silicon oxide present on the surface of silicon nitride powder and oxide additives. In our case there are basically two sources of liquid phase. Firstly, due to the eutectic reaction between silicon oxide, aluminum oxide and calcium oxide present on the surfaces of starting nitride precursors and secondly due to the melting of calcium nitride which takes places at about 1195^{o}C (since calcium nitride is not used as a starting precursor in synthesis of oxygen rich calcium alpha sialons) [117]. Furthermore, since the oxide rich eutectic liquid phase is generated as a result of surface oxide layer present on the surface of starting nitride precursors, the amount of oxide rich transient liquid is very small. On the other hand, the amount of nitrogen liquid phase formed

because of melting of calcium nitride increase, with increase in x value (more calcium nitride) and consequently results in easier densification (higher shrinkage within a shorter time) of the samples having high x value. Xie.et al reported a similar trend for the nitrogen rich alpha sialons synthesized using hot pressing technique and micron size precursors at 1700^{o}C and 1 hr. holding time [113]. However, the reported shrinkage rate was much slower due to the slower reaction kinetics as a result of the conventional heating technique (slower heating rate) as well as due to larger size (> 1μm) of the starting powder precursors.

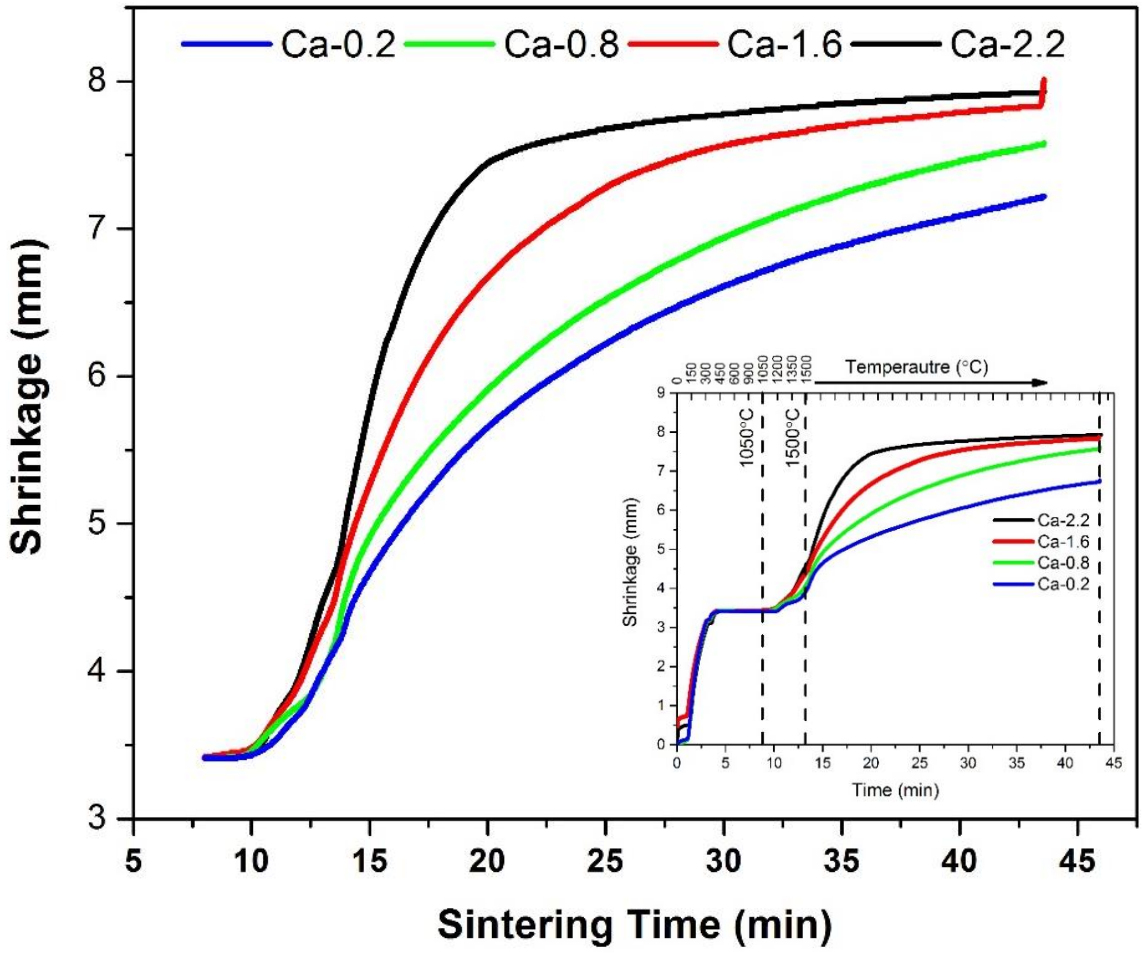

Figure 20 Densification curves of several compositions of calcium stabilized nitrogen rich sialons sintered at 1500^{o}C using spark plasma sintering technique, where Ca content varies between 0.2-

2.2. The insert shows the complete densification curves while the main plot represent the selected high temperature region (heating from 1050°C to 1500°C followed by 30 min holding time).

Table 9 shows the density values of the nitrogen rich calcium stabilized alpha-sialons for compositions having x values in the range of 0.2-2.2, synthesized at relatively low sintering temperature of 1500°C. Density of the samples sintered at 1500°C was measured to be in the range of 2.96-3.21 g/cm^3 and was seen to increase with the increase in x value (increase in Ca_3N_2 content). Xie.et al reported comparable density values (3.10-3.15 g/cm^3) with a similar trend for the nitrogen rich alpha sialons synthesized at 1700°C using hot pressing technique and micron size precursors [113]. Recently, Yanbing Cai et al. worked on the synthesis of calcium stabilized nitrogen rich alpha sialons at 1800°C using hot pressing technique [73]. The observed density values were reported to be in the range of 3.16-3.26 g/cm^3. Furthermore, Wang et al. reported density values of 3.07g/cm^3 and 3.17g/cm^3 at 1700°C and 1750°C, respectively, for dense hot-pressed oxygen rich calcium alpha-sialon having a composition of $Ca_{0.5}Si_{10.5}Al_{1.5}O_{0.5}N_{15.5}$ [28]. Xie.et al communicated a failure to synthesize well densified yttrium stabilized nitrogen rich alpha sialons along the Si_3N_4–YN:3AlN where insufficient amount of liquid phase was referred to as main reason [113]. This suggests that along with nano size starting precursors and novel pulsed based spark plasma sintering technique, low melting temperature (1195°C) of calcium nitride played a pivotal role in achieving well densified samples at 1500°C.

Table 9 Density of calcium stabilized nitrogen rich alpha sialon sintered at 1500°C.

Sample ID	Ca-0.2	Ca-0.4	Ca-0.6	Ca-0.8	Ca-1.0	Ca-1.2	Ca-1.4	Ca-1.6	Ca-1.8	Ca-2.0	Ca-2.2
X	0.2	0.4	0.6	0.8	1	1.2	1.4	1.6	1.8	2	2.2
Density (g/cm^3)	2.96	3.06	3.09	3.14	3.17	3.17	3.18	3.19	3.20	3.20	3.21

5.2.2 Phase Analysis

Figure 21 shows x-ray diffraction patterns of the samples synthesized at 1500°C. Single phase calcium stabilized alpha sialon phase is observed for samples produced in the range of $0.6 \leq x \leq 1.4$ (Ca-0.6 to Ca-1.4). Dual phases (alpha and beta sialon) are observed for samples having $x \leq 0.4$, where the amount of beta sialon phase is seen to decrease as the compositions shifts towards single phase alpha sialon. Beyond the single-phase region, alpha sialon coexists with AlN and $CaSiAlN_3$ in the range of $1.6 \leq x \leq 2.0$. **Figure 22a** shows the regenerated schematic representation of α-plane in Ca-sialon system showing phase stability regime region along the N'Rich line at 1500°C where **figure 22b** represents the same, where the orientation of alpha plane is the one which is most commonly presented in literature. A similar observation is reported by Xie. et al. for the calcium stabilized nitrogen rich samples synthesized at 1700°C using hot pressing technique [113]. Furthermore, Yabaing et. al in their work on the synthesis of nitrogen rich sialons at 1800°C, have also communicated the formation of AlN and $CaSiAlN_3$ phases along with alpha phase for higher values of x ($x>1.6$) and the single phase alpha sialon phase is reported to be in the range of $0.6 \leq x \leq 1.6$ [114].

X-ray diffraction results of the samples synthesized at 1500°C are summarized in **Table 10**. Lattice parameters of alpha sialon are seen to increase with the increase in x value attributed to the fact that more amount of Si-N bonds are replaced by Al-N bonds as well as more amount of calcium ion is being incorporated in the structure. In calcium stabilized alpha sialons, the charge imbalance caused as result of substitution of Si^{+4} for Al^{+3} is brought into balance by addition of Ca^{+2} ions at the interstitial positions. It is established that alpha sialon unit cell contains two interstices per unit cell, the upper solubility limit of calcium ion in alpha sialon having a composition of $Ca_2Si_8Al_2N_{16}$ is ideally believed to be 2. However, due to the unavoidable presence of oxide layer on the surface

of starting precursors, this composition has not been achieved so far. Recently, Yabaing et al. in their work on the synthesis of nitrogen rich sialons at 1800^{o}C, have reported a maximum achieved solubility limit of 1.82 for nominal x value of 2.2 [73]. Similarly, Xie. et al. reported the maximum solubility value of 1.7 for the calcium stabilized nitrogen rich samples synthesized at 1700^{o}C using hot pressing technique [113]. In our case the maximum solubility limit has been determined to be 1.83 for the nominal x value of 2.2.

Table 10 Lattice parameters, mechanical properties and phase assemblage of calcium stabilized nitrogen rich sialons synthesized at 1500^{o}C.

Sample ID	x (Ca)		Lattice Parameters		HV_{10}	K_{1c}	Phase Assemblage
	Nom	EDX	a (Å)	c (Å)	GPa	MPa.m$^{1/2}$	wt.%
Si_3N_4*	0	-	7.7541	5.6217	-	-	-
Ca-0.2	0.2	0.15	7.7814	5.6490	18.5 ± 0.3	4.5 ± 0.4	α (61), β (39)
Ca-0.4	0.4	0.33	7.7971	5.6593	19.4 ± 0.7	5.0 ± 0.4	α (87), β (13)
Ca-0.6	0.6	0.53	7.8210	5.6631	22.2 ± 0.2	5.6 ± 0.3	α (100)
Ca-0.8	0.8	0.73	7.8343	5.6885	22.4 ± 0.5	5.7 ± 0.3	α (100)
Ca-1.0	1.0	0.84	7.8470	5.7011	21.8 ± 0.4	5.7 ± 0.3	α (100)
Ca-1.2	1.2	1.01	7.8770	5.7153	21.6 ± 0.2	5.3 ± 0.2	α (100)
Ca-1.4	1.4	1.27	7.8937	5.7316	21.0 ± 0.3	6.1 ± 0.3	α (100)
Ca-1.6	1.6	1.39	7.9170	5.7464	20.8 ± 0.4	5.8 ± 0.2	α (82), A (10), C (8)
Ca-1.8	1.8	1.54	7.9320	5.7583	20.1 ± 0.7	5.5 ± 0.3	α (82), A (9), C (9)
Ca-2.0	2.0	1.68	7.9534	5.7695	19.3 ± 0.6	5.7 ± 0.2	α (79), A (10), C (11)
Ca-2.2	2.2	1.83	7.9651	5.779	18.7 ± 0.5	5.2 ± 0.3	α (75), A (12), C(13)

*JCPDS 41-0360, (Nom) Nominal, (α) Alpha Sialon, (β) Beta-Sialon, (A) Aluminium Nitride (JCPDS 25-1133), (C) $CaSiAlN_3$ (JCPDS 39-747).

Figure 23 shows the variation of alpha sialon lattice parameters with respect to change in x value. A similar behavior is reported by Yabaing for samples synthesized at 1800^{o}C (**figure 23**) [114]. The dependence of alpha sialon lattice parameters with amount of Ca^{+2} can be well defined by the following empirical relationships:

$$a = 0.0949x + 7.7605 \text{ (Å)} \quad (1)$$

$$c = 0.0680x + 5.6326 \text{ (Å)} \quad (2)$$

Formation of alpha sialon phase for sample having x value as low as 0.2 along with the observation suggesting a linear dependence of alpha sialon unit cell parameters with x value, provide a good reason to believe that calcium stabilized nitrogen rich alpha sialon forms continuously in the range of $0<x<1.83$. Therefore, the previously reported low solubility limit of Ca^{+2} in alpha sialons shall not be attributed to a structural limitation but should rather be ascribed to the fact that formation of single phase alpha sialons near the nitrogen rich corner has not been attained due to the presence of oxide layer contamination leading to the formation of beta-sialon phase.

5.2.3 Microstructure Analysis

Figure 24 (a-c) show the secondary electron FESEM micrographs of the polished surfaces of few of the nitrogen rich samples synthesized at 1500^{o}C. Dual phase sample (Ca-0.2) with the least amount of Ca_3N_2 shows regions highlighting the fact as if full densification has not been achieved. The observation coincides with the fact that slightly lower density value was observed for the sample Ca-0.2. On the other hand, surfaces of samples having higher x ($x>0.4$) values (more Ca_3N_2) were free from any signs of porosity and appeared to be well densified. However very minimal material removal due to the harsh grinding process may be observed at certain sites.

Figure 25 (a-f) depicts the secondary electron FESEM micrographs of the fractured surfaces of samples from the nitrogen rich sialon ceramics sintered at 1500^{o}C. Primarily, classical intergranular fracture was observed in all samples along with some amount of grain pullout. Sample Ca-0.2 containing alpha and beta sialon phases exhibits elongated morphology of beta sialon along with smaller equiaxed grains of alpha sialon (**figure 25a**). Samples with x values

greater than 0.4 (Ca-0.6 to Ca-2.2) composed of single phase or almost single-phase nitrogen rich calcium alpha sialon depicted fine equiaxed grains (a morphology typical of alpha sialon phase). However, with increase in x value (more Ca_3N_2), alpha sialon grains with elongated morphology are also observed. Not only is this but with increase in x value an increase in average grain size of the alpha sialon observed. The grain size distribution for the three samples (Ca-0.6, Ca-1.2 and Ca-2.0) is depicted in **figure 26** where the average grain size is measured to increase from 286+ 98nm to 385$\pm$ 96 nm to 468$\pm$169 nm respectively.

Figure 27 (a-e) shows the low and high resolution TEM images of the microstructures of nitrogen rich calcium alpha sialon samples (having the Id's as Ca-0.6, Ca-1.2 and Ca-2.0). In accordance with observations made on fractured surfaces, sample Ca-0.6 displays an equiaxed morphology of alpha sialon grains with an average grain size of 277 $\pm$ 34.56 nm. For samples Ca-1.2 and Ca-2.0 dual morphology of alpha sialon grains i.e. elongated grains alongside the equiaxed grain are observed. The average size of the grains is measured to be 386 $\pm$ 127nm for Ca-1.2 and 449 $\pm$ 142 nm for Ca-2.0. Alpha-sialon ceramics having an elongated morphology as a result of preferential grain growth during densification process has also been reported in the synthesis of hot-pressed oxygen rich Ca-alpha sialons [28,65,67]. It is known that grain growth of alpha sialon takes place via solution re-precipitation mechanism and that the presence of liquid phase is necessary to promote the grain growth. Therefore, the presence of elongated morphology of alpha sialon grains as well as the grain growth for samples having higher x (more Ca_3N_2) value may well be attributed to the formation of higher amount of transient liquid phase. A. Thorel et al. in their study on high temperature mechanical properties and intergranular structure of sialons (oxygen rich) have reported that intergranular phase (if present) is always amorphous and can exist as reasonably large pockets having a size in the range of 0.1 to 1μm or interfacial glassy film with the minimum

reported thickness of about 60nm [118]. In our study, the high-resolution TEM images of nitrogen rich sialons (**figure 27 b, d, and e**) reveal that there is no sign of a glassy phase present at the grain boundaries nor at the junction of multiple grains. These results suggest that the synthesized nitrogen rich sialons would be more stable at high temperature (1400-1600^{o}C) compared to the oxygen rich sialons containing an amorphous grain boundary phase.

5.2.4 Mechanical Properties

Vickers hardness (HV_{10}) and fracture toughness (K_{1c}) of the calcium stabilized nitrogen rich alpha sialons synthesized at 1500^{o}C are summarized in **Table 10**. The two-phase sample (Ca-0.2), having alpha and beta sialon phases, displays a hardness of 18.5 GPa and fracture toughness of 4.5 MPa.m$^{1/2}$. The Vickers hardness of the single-phase alpha sialon samples (Ca-0.6 – Ca-1.4) are found to be in the range of 21.0-22.4 GPa while the fracture toughness is measured to be in the range of 5.6-6.1 MPa.m$^{1/2}$. For samples having x value greater than 1.6, a gradual decrease in the hardness is observed primarily due the formation of $CaSiAlN_3$ and AlN phases along with the major alpha sialon phase. For a sample having 14 wt. % AlN phase and 86 wt. % $CaSiAlN_3$ phase, Y. Cai have reported a Vickers hardness of 14.4 GPa while Stefan R. Witek have reported a hardness of 12 GPa for hot pressed aluminum nitride ceramics [114,119].

Vickers hardness values in the range of 16-20 GPa and fracture toughness of 3-7 MPa.m$^{1/2}$ has been reported in the literature for the single or multi cation calcium stabilized oxygen rich alpha sialons [28,33,67,120,121]. In our study, relatively higher hardness of samples may well be attributed to nitrogen rich alpha sialons. The observation is line with study performed by František Lofaj et al. which reveals that a 4% increase in N content would result in nearly the same increase in micro-hardness of RE-Si-Mg-O-N systems [122]

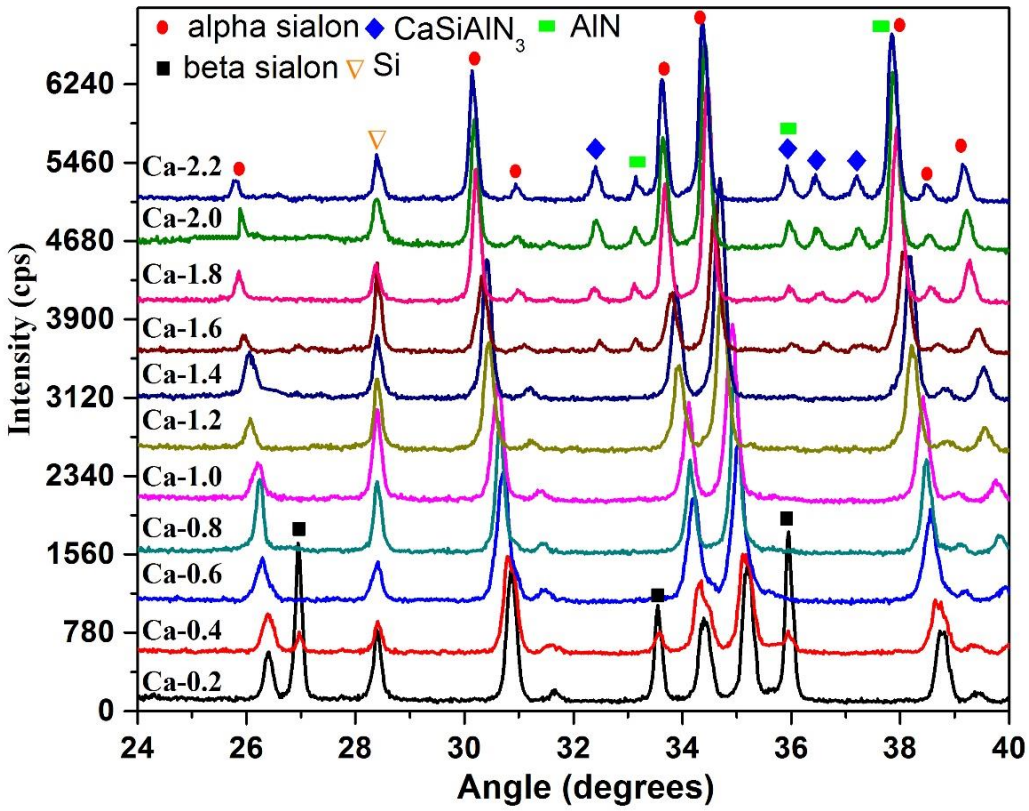

Figure 21 X-ray diffraction patterns of the calcium stabilized nitrogen rich alpha sialon samples synthesized along the Si_3N_4-1/2Ca_3N_2:3AlN line at sintering temperature of 1500^oC.

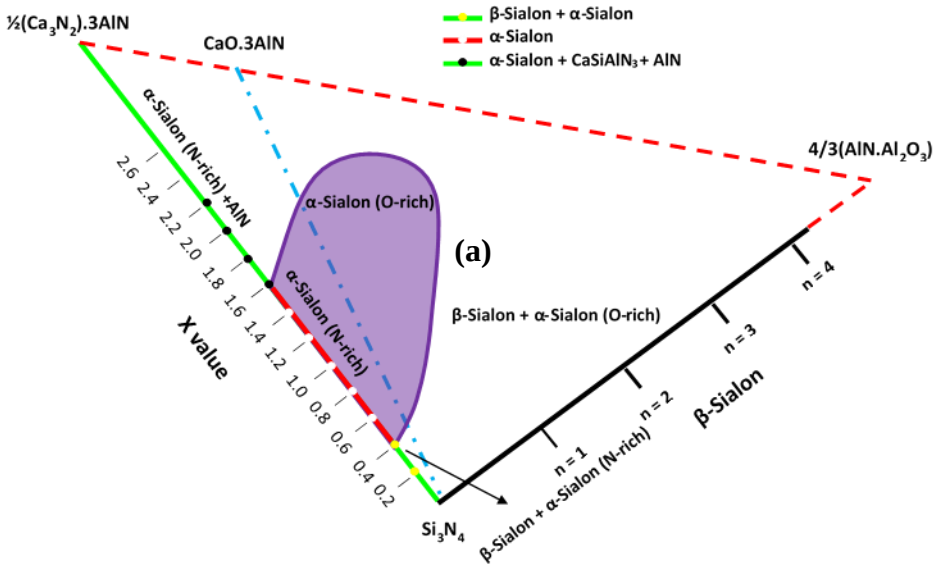

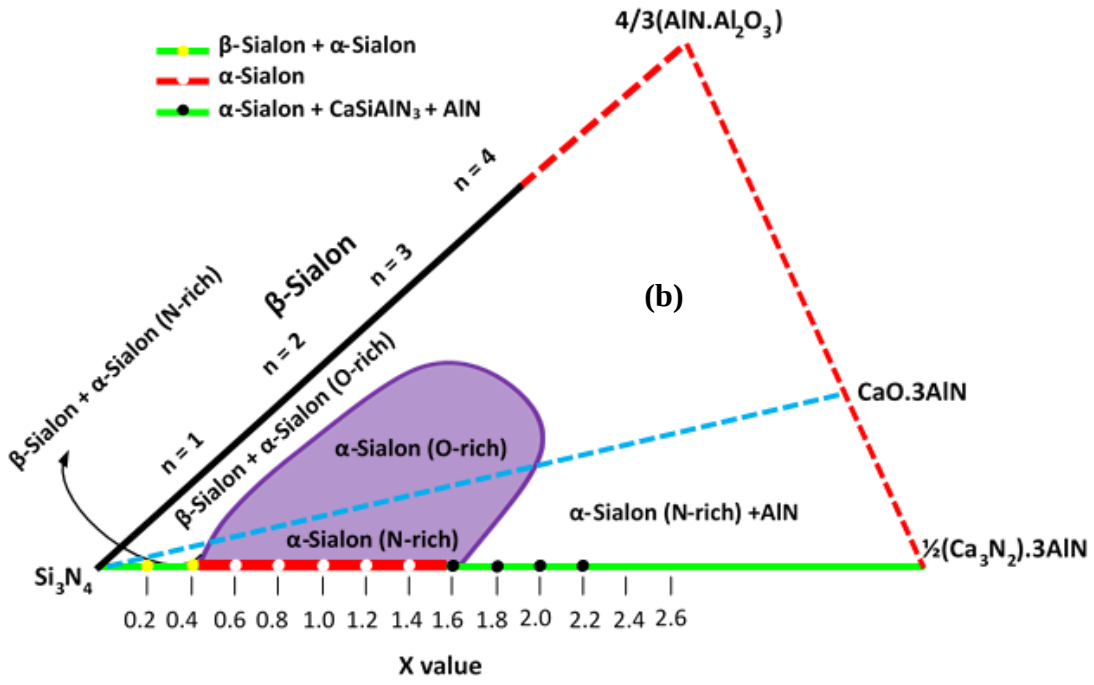

Figure 22 (a) Regenerated schematic representation of α-plane in Ca-sialon system showing phase stability regime along the N'Rich line at 1500°C and **(b)** another representation where the orientation of alpha plane is one which is most commonly reported in literature.

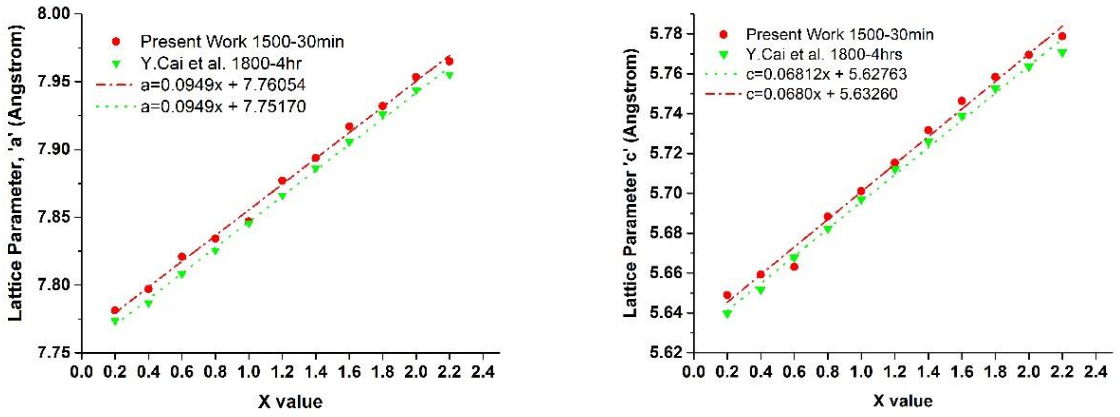

Figure 23 Variation of lattice parameters of calcium stabilized nitrogen rich alpha sialons with x value for samples synthesized at 1500°C using SPS and those reported by Y.Cai et al. at 1800°C using hot press.

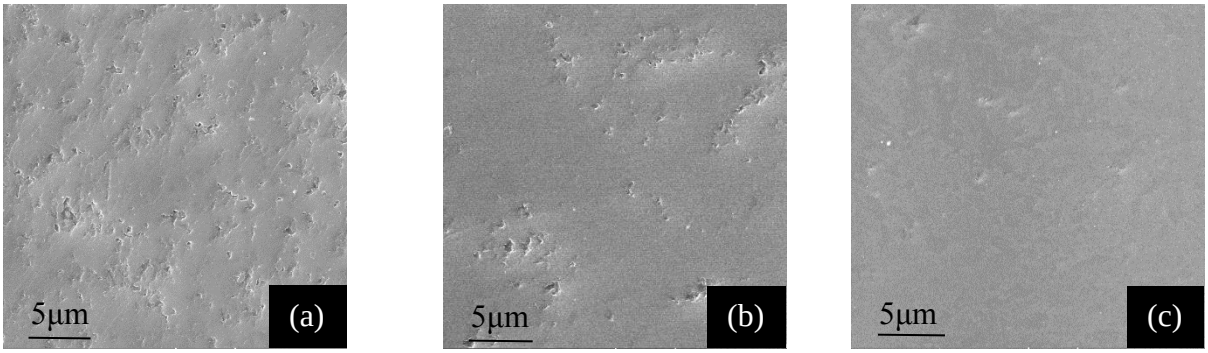

Figure 24 Secondary electron (FESEM) micrographs of the polished surfaces of nitrogen rich samples synthesized at 1500°C using different x values: **(a)** Ca-0.2, **(b)** Ca-0.4, **(c)** Ca-1.2.

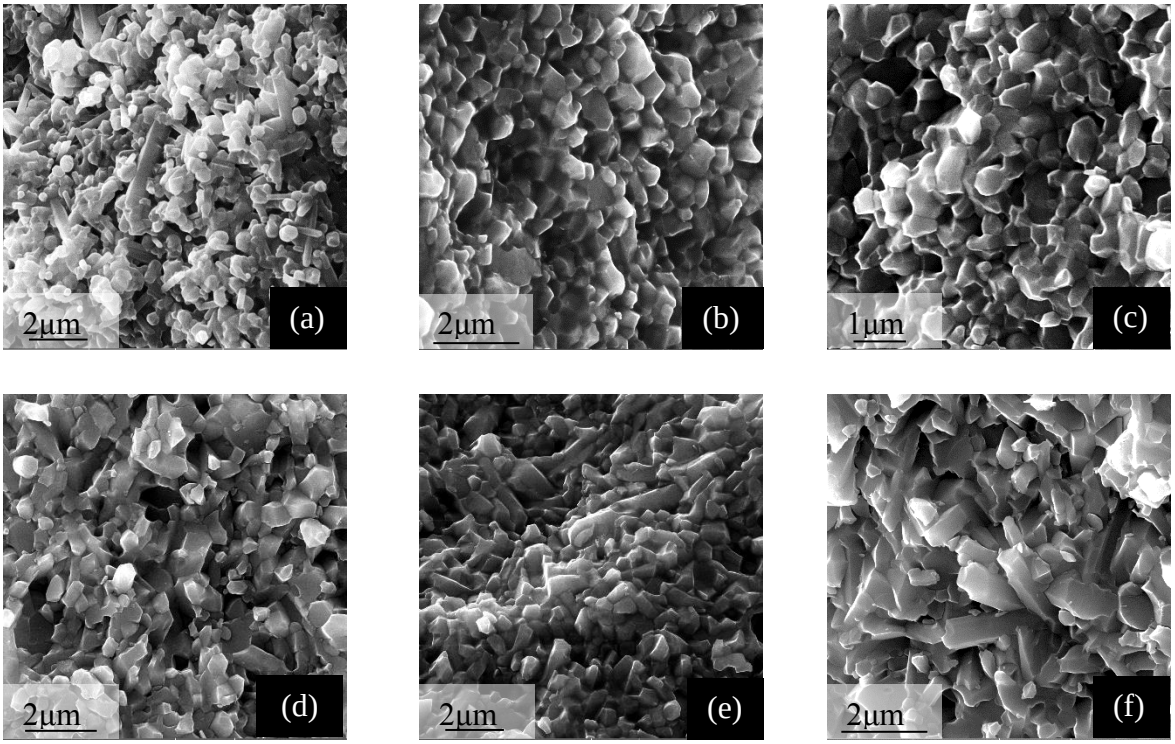

Figure 25 Secondary electron (FESEM) micrographs of the fractured surfaces of nitrogen rich samples synthesized at 1500°C using different x values: **(a)** Ca-0.2, **(b)** Ca-0.6, **(c)** Ca-1.2, **(d)** Ca-1.6, **(e)** Ca-1.8 and **(f)** Ca-2.0.

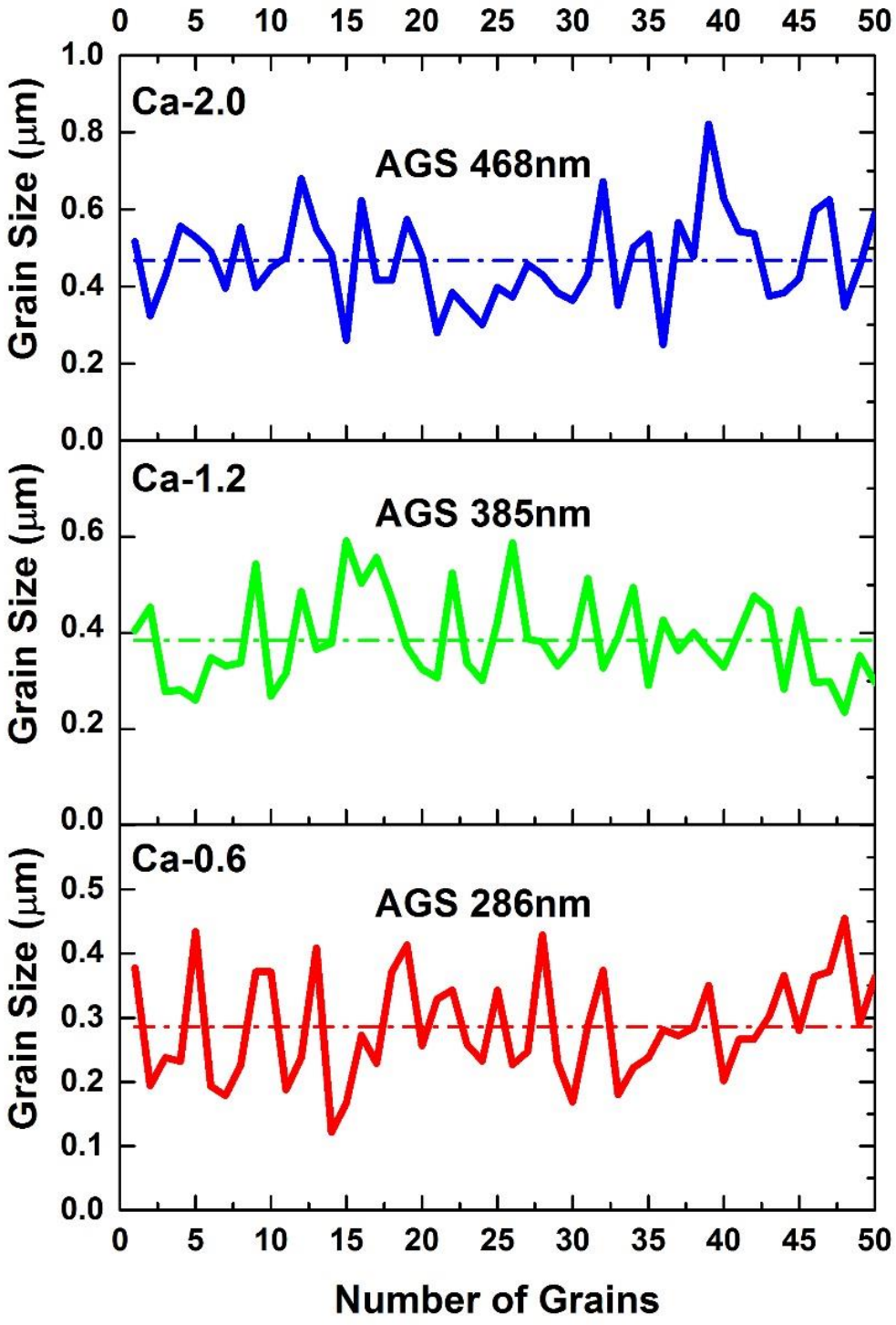

Figure 26 Grain size distribution of nitrogen rich samples synthesized at 1500°C having the sample Id's of Ca-0.6, Ca-1.2 and Ca-2.0.

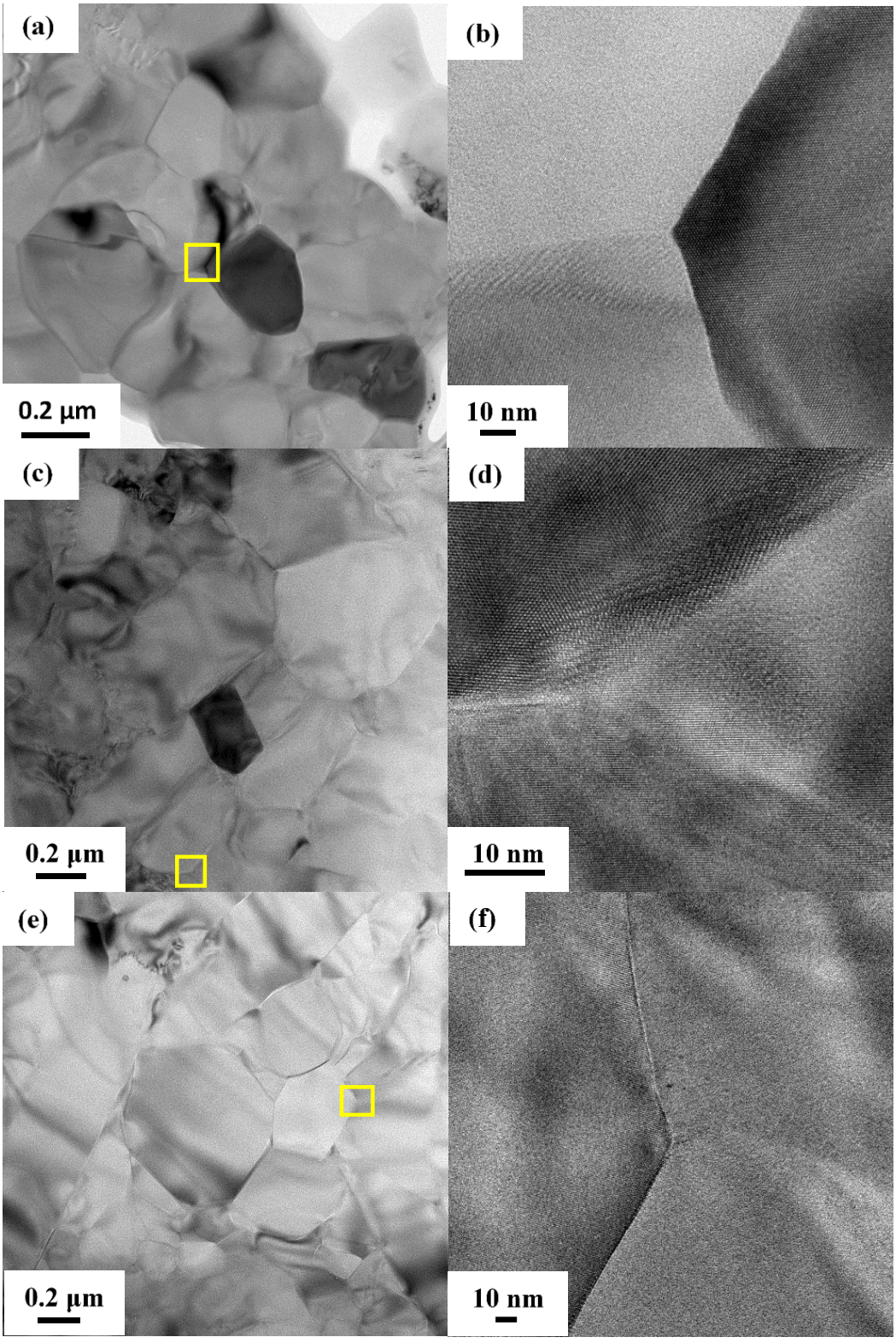

Figure 27 Low and high resolution TEM micrographs of the nitrogen rich samples synthesized at 1500ºC using different x values: **(a & b)** Ca-0.6, **(c & d)** Ca-1.2 and **(e & f)** Ca-2.0.

5.3 Conclusion

Calcium stabilized nitrogen rich sialons having compositions along the Si_3N_4-1/2Ca_3N_2:3AlN line were synthesized at sintering temperature of 1500^{o}C. Enhanced reaction kinetics due to nano size precursors and high heating rates achieved with aid of non-conventional SPS process helped in development of well densified nitrogen rich sialon ceramics at comparatively low temperature (1500°C as compared to 1700°C or 1800°C). Alpha sialon phase for the samples having Ca content (x) in the range of $0.15<x<1.83$ was obtained. Formation of single phase nitrogen rich alpha sialons was achieved for samples having nominal x value in the range of $0.4 < x < 1.6$. Increase in the lattice parameters of alpha sialon unit cell was observed to have a linear relationship with the amount of Ca^{+2} ions incorporated in the alpha structure. Increasing x value resulted in an increase in the average grain size from 286nm to 468nm. Moreover, higher amount of Ca_3N_2 starting powder was observed to facilitate the growth of elongated alpha sialon grains. Calcium stabilized nitrogen rich sialon ceramics having very promising hardness and fracture toughness of 22.4GPa and 6.1 MPa.$m^{1/2}$ were developed. Furthermore, absence of a glassy grain boundary phase in nitrogen rich sialons renders them potentially viable candidates for high temperature application.

CHAPTER 6

DEVELOPMENT OF MAGNESIUM STABILIZED NITROGEN RICH ALPHA SIALON CERAMICS ALONG THE Si_3N_4-$1/2Mg_3N_2$:3AlN LINE USING SPARK PLASMA SINTERING

Summary

With the aim to investigate the possible existence of Mg-doped single phase alpha sialons (on the Mg-alpha sialon plane), the study presents the synthesis and evaluation of Mg-doped nitrogen rich sialon ceramics for the very first time. Magnesium stabilized nitrogen rich sialons having the general formula of $Mg_xSi_{12-2x}Al_{2x}N_{16}$ with x value in the range of 0.2-2.2 for the composition laying along the Si_3N_4-$1/2Mg_3N_2$:3AlN line, were synthesized at 1500^oC, using nano size starting powder precursors and spark plasma sintering technique. Sialon ceramic samples were characterized for their microstructure, phase stability regime and physical and mechanical properties. Despite the fact that a relatively low sintering temperature was adopted, well densified sialons samples were achieved, however the densification of the samples became difficult with higher x value (higher Mg_3N_2/AlN content).Contrary to the expected belief that a single phase Mg-doped sialon may exist near the nitrogen rich line (on Mg-alpha sialon plane), a single phase Mg stabilized alpha sialon region was not found to exist along the nitrogen rich line. Magnesium doped nitrogen rich sialon sample having the maximum amount of alpha phase depicted remarkable hardness (HV_{10}) of 21.4GPa and a fracture toughness of 3.5 MPa.$m^{1/2}$.

Graphical Abstract

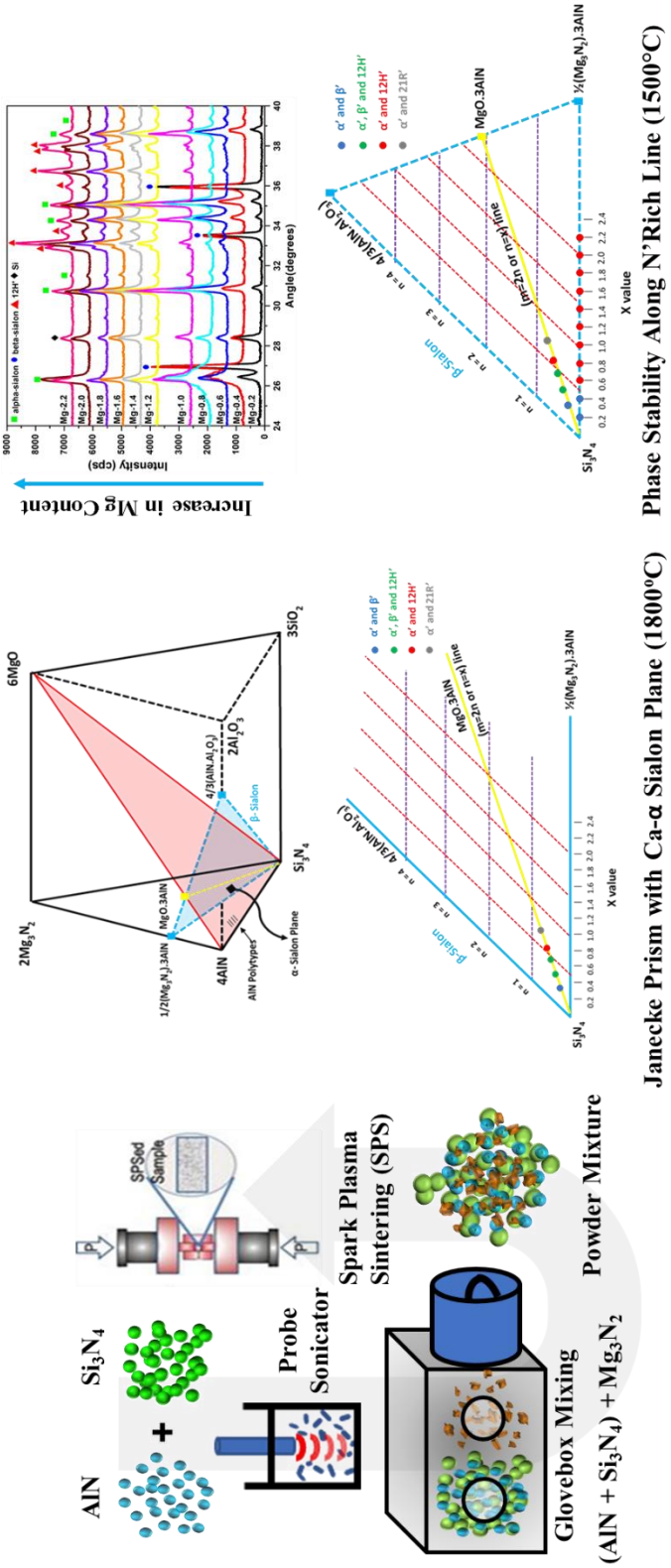

6.1 Introduction

In the past few decades, Sialon ceramics, solid solution of Si_3N_4, have been actively investigated for their thermal, mechanical, chemical and photoluminescence properties as well as work has been done on the development of phase diagrams of these materials [27,67,102–110]. Much of the work done on sialon materials have been focused around the two main polymorphs, alpha sialon and beta sialon, having similar hexagonal crystal structure. In beta-sialon there is an equal amount of replacement of silicon atoms by aluminum and nitrogen atoms by oxygen and is commonly defined by the chemical formula of $Si_{6-z}Al_zO_zN_{8-z}$ [1].

Alpha-sialons are commonly defined by the chemical formula of $M_x^vSi_{12-(m+n)}Al_{m+n}O_nN_{16-n}$, where 'm' represents (Al-N) and 'n' represents (Al-O) bonds substituted for (m+n) (Si-N) bonds. In the general formula of alpha-sialon, the valence and solubility of the cation 'M' is represented by the letters 'v' and 'x', respectively [10]. Formation of aluminum-oxygen and aluminum-nitrogen bonds as a replacement of silicon-nitrogen bonds results in a charge imbalance in the alpha sialon unit cell. This charge imbalance is thus brought into equilibrium by the accommodation of cation 'M' (such as Li^+, Ca^{2+}, Mg^{2+}, Y^{3+} and lanthanide ions) into the two large interstices of alpha-sialon unit cell [25,26,45,111].

In general, alpha-sialon ceramics stabilized by rare-earth doped cations are the ones that have been the studied most. Much of the work reported in literature has been focused on the development of phase diagrams, microstructure evolution and densification mechanism of sialon ceramics [19,21,45] For instance, Sun et al has reported a study on the solubility limit of yttrium cation in alpha sialon unit cell for several compositions along the Si_3N_4–YN:3AlN line where the solubility was found out to be as $0.43<x<0.8$ [102]. Similarly, in another study the solubility of yttrium cation

has been reported as $0.33<x<0.67$ for the oxygen rich compositions lying along the Si_3N_4–Y_2O_3:9AlN line [25]. In light of the in-depth understanding of sialon materials which has developed over years, the microstructure and hence the mechanical properties could be tailored by judicious selection of the staring powder composition, size and the sintering process [19,123,124]. For example, self-reinforced yttrium stabilized sialons having an elongated morphology of alpha grains embedded with in fine equiaxed alpha sialon matrix has been reported [124]. It was found that the amount of elongated grains increased with increasing amount of liquid phase (high amounts of oxynitride additives) [124].

In comparison to rare earth stabilized alpha sialons calcium doped alpha sialons have attained significant attention owing to the greater solubility of calcium cation in the alpha sialon unit cell (maximum solubility value x_{max} of 1.0 for Yb^{+2} as compared to 1.6 for Ca^{+2}) [26,45]. Contrary to rare-earth stabilizers, calcium stabilized alpha sialons have been reported to be completely resistant towards an alpha to beta transformation when subjected to post sintering heat treatment in the range of 1450-1500^oC [33]. Moreover, higher temperature stability of calcium doped alpha sialons is ascribed to the fact that the stability of alpha sialon increases with increase in solubility of charge stabilizer or with decrease in the cationic valence [113].

In contrast to rare-earth or calcium doped alpha sialons, very little work has been reported on magnesium stabilized sialon ceramic materials [68]. A probable reason for the limited work on magnesium doped sialons may be the fact that very little amount of Mg^{+2} ions can be incorporated in the alpha sialon unit cell, as a result of which formation of single phase magnesium stabilized alpha sialon has not been reported in the literature, so far [68,125,126]. Furthermore, the densification of Mg-doped sialons is generally thought of as exceedingly difficult [126]. The very first investigation reported on Mg-sialons has been conducted in the Si_3N_4-A1N-MgO system at

1750ºC [68]. However, in the said study, no information on the density of the Mg-sialons was reported. Menon et al in their study on the synthesis of Mg-stabilized sialon for a composition belonging to m and n value of 1.0 ($Mg_{0.5}Si_{10}Al_1O_1N_{15}$), sintered at 1850ºC using hot pressing technique reported 83% of maximum achievable density [127]. In an study on magnesium doped sialons for the chemical compositions of $Mg_{0.37}Si_{9.99}Al_2O_{1.26}N_{14.74,}$ $Mg_{0.5}Si_{9.74}Al_{2.26}O_{1.26}N_{14.74,}$ and $Mg_{0.75}Si_{9.25}Al_{2.75}O_{1.25}N_{14.75}$ sintered at 1830ºC, S. Kumara et al reported that the densified sialon materials could not be achieved using gas pressure sintering [126].

It was not until the year 2005 R.J Sung et al reported it for the first time that fully dense magnesium doped sialons, having a small amount of magnesium alpha sialons could be synthesized [128]. The sialon materials were reported to have good mechanical and optical properties. Thereafter, various sintering additives (MgO, Y_2O_3) and techniques (hot pressing, spark plasma sintering) have been employed to prepare magnesium doped sialons having improved mechanical and optical properties [129–131]. The most recent work on magnesium sialons was done by Zhangfu Yang et al, where phase formation, microstructure, physical and mechanical properties of several compositions along the Si_3N_4-MgO: 3AlN were studied at 1850ºC using hot pressing technique [125]. Similar to calcium sialon jancke prism a schematic of magnesium sialon jancke prism is shown in **figure 28a**. Most of the work done on magnesium sialons has been focused on the Si_3N_4-A1N-MgO plane **(figure 28b**) for the compositions laying along the Si_3N_4-MgO: 3AlN line [68]. However, unlike the calcium sialon system, formation of a single phase magnesium alpha sialon for the compositions laying along the Si_3N_4-MgO:3AlN line has been not been observed thus far. Nevertheless, it has been expressed in literature that a small region of single phase magnesium-alpha-sialon may exist on magnesium alpha sialon plane (**figure 28c**) along the nitrogen rich line (Si_3N_4-1/2Mg_3N_2.3AlN line) [68,125].

Since, the synthesis of nitrogen rich magnesium sialons has not been reported in the literature, the aim of this study was to develop magnesium stabilized nitrogen rich sialons for the composition laying along the Si_3N_4-1/2Mg_3N_2:3AlN line at a temperature of 1500^oC using spark plasma sintering technique. The developed sialons were characterized for their densification behavior, phases evolved, microstructure, compositional analysis and thermo-mechanical properties.

Nitrogen rich magnesium alpha sialon ceramics along the Si_3N_4-1/2Mg_3N_2:3AlN line on a magnesium alpha sialon plane (**figure 28c**) are generally defined by the chemical formula of $Mg_xSi_{12-m}Al_mN_{16}$ (where x= m/2). In the present study x values in the range of 0.2-2.2 represent the compositions selected for the synthesis. The Id's of the synthesized samples along with their corresponding nominal compositions are summarized is **Table 11**. In this chpater the sample Id's are defined such that the first two letters 'Mg' signify the charge stabilizing cation which is then followed by the x value representative of a specific alpha sialon composition. For instance, the Id Mg-0.2 symbolizes the sample having the general formula of $\mathbf{Mg_{0.2}Si_{11.6}Al_{0.4}N_{16}}$.

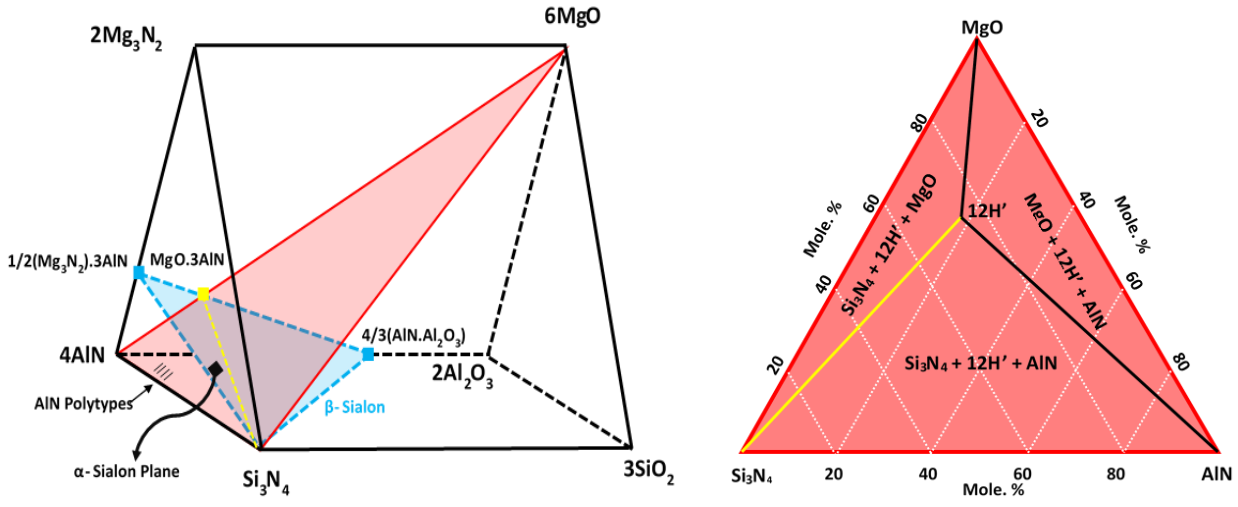

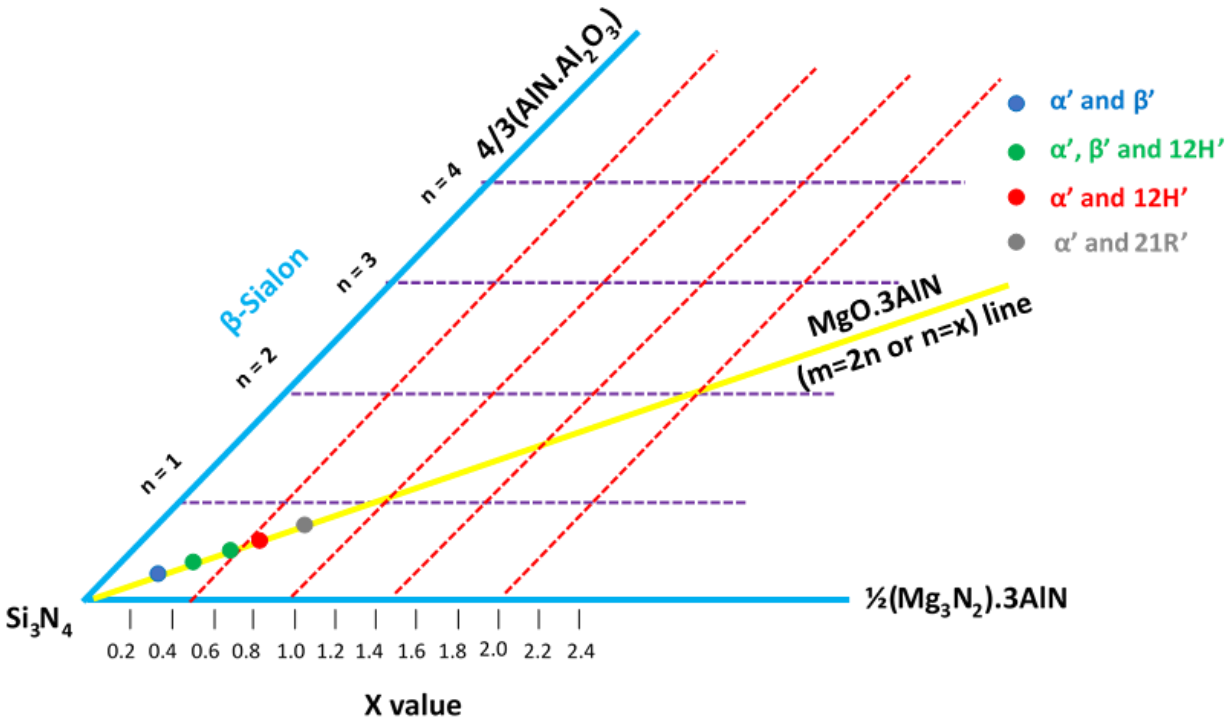

Figure 28 Schematic representation of (a) Janecke Prism of Mg-Sialon System (b) Si_3N_4-A1N-MgO plane in Mg-sialon system at 1750^{o}C showing stability regimes of various phases [68] and (c) α-plane in Mg-sialon system showing stable phases along the Si_3N_4-MgO: 3AlN line for compositions studied at 1850^{o}C using hot pressing technique and the Si_3N_4-1/2Mg_3N_2.3AlN line, compositions along which, has not yet been explored [125].

Table 11 Nominal composition of magnesium stabilized nitrogen rich sialons.

Sample ID	Starting Composition	Mg_3N_2 (wt. %)	Si_3N_4 (wt. %)	AlN (wt. %)
Mg-0.2	$Mg_{0.2}Si_{11.6}Al_{0.4}N_{16}$	1.18	95.91	2.91
Mg-0.4	$Mg_{0.4}Si_{11.2}Al_{0.8}N_{16}$	2.34	91.89	5.77
Mg-0.6	$Mg_{0.6}Si_{10.8}Al_{1.2}N_{16}$	3.49	87.93	8.58
Mg-0.8	$Mg_{0.8}Si_{10.4}Al_{1.6}N_{16}$	4.62	84.03	11.36
Mg-1.0	$Mg_{1.0}Si_{10}Al_{2.0}N_{16}$	5.73	80.18	14.09
Mg-1.2	$Mg_{1.2}Si_{9.6}Al_{2.4}N_{16}$	6.82	76.40	16.78
Mg-1.4	$Mg_{1.4}Si_{9.2}Al_{2.8}N_{16}$	7.90	72.67	19.43

Mg-1.6	$Mg_{1.6}Si_{8.8}Al_{3.2}N_{16}$	8.96	69.00	22.04
Mg-1.8	$Mg_{1.8}Si_{8.4}Al_{3.6}N_{16}$	10.01	65.38	24.62
Mg-2.0	$Mg_{2.0}Si_{8}Al_{4.0}N_{16}$	11.04	61.81	27.15
Mg-2.2	$Mg_{2.2}Si_{7.6}Al_{4.4}N_{16}$	12.05	58.29	29.65

6.2 Results and Discussion

6.2.1 Sintering and densification behavior

Sintering behavior curves of the nitrogen rich magnesium stabilized sialon samples for the compositions covering the range of $0.2<x<2.2$ are shown in **figure 29** (complete densification curves are shown as an insert). In **figure 29**, abscissa represents the sintering time while ordinate representing the shrinkage refers to the displacement of the upper punch of the die in mm. It is seen that with increase in the x value (increase in Mg_3N_2 and AlN content) the curves shifts to the left denoting a higher shrinkage rate. Relatively higher shrinkage rate for samples having higher x values (more additives) is due to the formation of large amount of transient liquid phase. It has been well known that in the synthesis of sialon ceramics the amount of high temperature eutectic liquid increases with increase in the cation and oxygen i.e. m (which is equal to 2x in our case) and n content [27,124]. Also, in our previous study on calcium stabilized nitrogen rich sialons (Chapter 5), we have seen a similar trend where the shrinkage rate was seen to increase with the increase in x value due to the formation of large amount of high temperature transient liquid phase. In the synthesis of silicon nitride based materials it is quite known that the densification process involves the formation of a transient liquid and large amount of transient liquid facilitates the densification of these materials. Nevertheless, the shrinkage behavior curves of magnesium stabilized sialons are observed to contradict this general understanding. It can be seen in **figure 29**

that samples having higher x value exhibit lower shrinkage (smaller displacement), thus making it difficult to achieve well densified ceramics. A similar observation has been reported by Z.Yang et al. where the densification of magnesium doped oxygen rich sialons become difficult for compositions represented by higher m (which is equal to 2x in our case) and n values [125]. The reason for this opposite trend as compared to other sialon systems will be addressed in section 5.3.4.

Density values of the magnesium doped nitrogen rich sialon ceramics for compositions represented by x values in the range of 0.2-2.2, sintered at 1500^{o}C are tabulated in **Table 12**. Densities of the samples are measured to be in the range of 2.82-3.17g/cm^{3}. Since, the accurate determination of secondary phases and the theoretical density is challenging, the calculation of relative density is difficult, however in light of the reported density values in the literature, most of the samples (having the values higher than 3.0g/cm^{3}) are believed to be well densified [128,130,131]. As reported in literature, it is observed that for samples having compositions belonging to higher x values (x= m/2), the density of the samples tends to decrease. In a recent study on the gas pressure sintering of magnesium doped alpha sialons, Z.Yang et al has reported that the composition having higher m value (composition represented by m=2 or x=1, n=1) could not be densified fully at 1800^{o}C [125]. This suggests that in contrast to conventional sintering techniques, novel pulsed based spark plasma sintering technique along with nano-size starting precursors helps achieve well densified magnesium doped sialons for a wider range of compositions (compositions represented by higher x or m/2 values) at relatively lower temperature of 1500^{o}C.

Table 12 Density of magnesium doped nitrogen rich sialons sintered at 1500°C.

Sample ID	**Mg-0.2**	**Mg-0.4**	**Mg-0.6**	**Mg-0.8**	**Mg-1.0**	**Mg-1.2**	**Mg-1.4**	**Mg-1.6**	**Mg-1.8**	**Mg-2.0**	**Mg-2.2**
X	0.2	0.4	0.6	0.8	1	1.2	1.4	1.6	1.8	2	2.2
Density (g/cm^3)	3.17	3.17	3.15	3.16	3.12	3.11	3.08	3.06	2.96	2.90	2.92

6.2.2 Phase analysis

The phase assemblage data of the magnesium doped sialons synthesized at 1500°C-30 min holding time is shown in **figure 30**. S.F.Kuang et al. in his study on the synthesis of magnesium sialons along the Si_3N_4-MgO:3AlN line, suggested that a small region of single phase magnesium alpha sialon may be found close to the nitrogen rich line [68]. However, a single phase magnesium alpha sialon region, as proposed in the previous studies, could not be found for the compositions laying along the nitrogen rich line, which is in good agreement with the already published work on magnesium doped sialons [68,125,126,131]. It is seen that alpha and beta sialon co-exist for the compositions represented by x values in the range of 0.2-0.4 and that beta sialon disappears for the composition represented by x value of 0.6. Furthermore, the amount of alpha sialon phase is seen to decrease gradually with increase in the x value (more Mg_3N_2 and AlN). The presence of AlN polytype phase is first observed for the composition represented by the x value of 0.6 and with increase in x value (more Mg_3N_2 and AlN) the amount of the polytype phase increases continuously until it becomes the dominant phase for the composition represented by the maximum value of x=2.2. The AlN polytype phase identified as 12H' remains unchanged with the change in composition (x value). Phases observed in the present study are in good accordance with the results

reported by S.F.Kuang et al for the composition laying along on the Si_3N_4-MgO:3AlN line on the MgO-Si_3N_4-AlN ternary section obtained at 1750°C **(see figure 28b)** [68].

X-ray diffraction results of the samples synthesized at 1500°C are summarized in **Table 13**. An increase in the lattice parameters of alpha sialon unit cell is observed for values up till x=1.6. However, with further increase in x (more Mg_3N_2 and AlN), lattice parameters becomes almost invariant for the samples having the compositions represented by x values in the range of 1.6-2.2. An initial increase in the lattice parameter may fairly be attributed to the fact that more amount of silicon-nitrogen bonds are being replaced by aluminum-nitrogen bonds as well as more amount of magnesium cation is being incorporated in the alpha sialon unit cell. However, it is observed that as the amount of AlN polytype phases increases, the increases in the lattice parameters of alpha sialon unit cell gets restricted and becomes almost constant. Thus, it can be inferred that for compositions which are rich in AlN (higher x), magnesium cation gets absorbed into the unit cell of AlN polytype. In a recent study by Z.Yang et al. on the synthesis of magnesium doped alpha sialons, a similar trend has been reported where the amount of magnesium cation in the alpha sialon unit cell is seen to decrease from 85% to about 50% (of the initial x value) with the increase in m (m=2x) value [125].

Table 13 Lattice parameters, mechanical properties and phase assemblage of magnesium stabilized nitrogen rich sialons synthesized at 1500°C.

Sample ID	**x (Ca)**		**Lattice Parameters**		**HV_{10}**	**K_{1c}**	**Phase Assemblage**
	Nom	**EDX**	**a (Å)**	**c (Å)**	**GPa**	**$MPa.m^{1/2}$**	**wt.%**
Si_3N_4*	0	-	7.7541	5.6217	-	-	-
Mg-0.2	0.2	0.19	7.7819	5.6445	18.8 ± 0.7	5.4 ± 0.4	α (12), β (88)

Mg-0.4	0.4	0.36	7.7867	5.6490	19.3± 0.5	4.3 ± 0.4	α (28), β (72)
Mg-0.6	0.6	0.48	7.7967	5.6554	21.4 ± 0.2	3.5 ± 0.3	α (86), 12H'(14)
Mg-0.8	0.8	0.7	7.8101	5.6581	21.0 ± 0.2	4.6 ± 0.3	α (85), 12H'(15)
Mg-1.0	1.0	0.79	7.8135	5.6599	20.8± 0.3	4.3 ± 0.3	α (83.7), 12H'(16.3)
Mg-1.2	1.2	0.84	7.8137	5.6624	20.5± 0.2	3.1 ± 0.2	α (71.3), 12H'(28.7)
Mg-1.4	1.4	0.91	7.8141	5.6631	20.5 ± 0.3	3.6 ± 0.3	α (65.8) 12H'(34.2)
Mg-1.6	1.6	1.08	7.8146	5.6639	20.6 ± 0.4	3.1 ± 0.2	α (65.9), 12H' (34.1)
Mg-1.8	1.8	1.05	7.8144	5.6636	19.6± 0.7	2.6 ± 0.4	α (46.4), 12H' (53.6)
Mg-2.0	2.0	1.01	7.8142	5.6633	19.3 ± 0.6	2.5 ± 0.5	α (36.6), 12H' (63.4)
Mg-2.2	2.2	1.03	7.8143	5.6635	18.3± 0.7	2.9 ± 0.5	α (29.5), 12H' (70.5)

* JCPDS 41-0360, (α) Alpha Sialon, (β) Beta-Sialon, (12H') Aluminum Nitride Polytype,

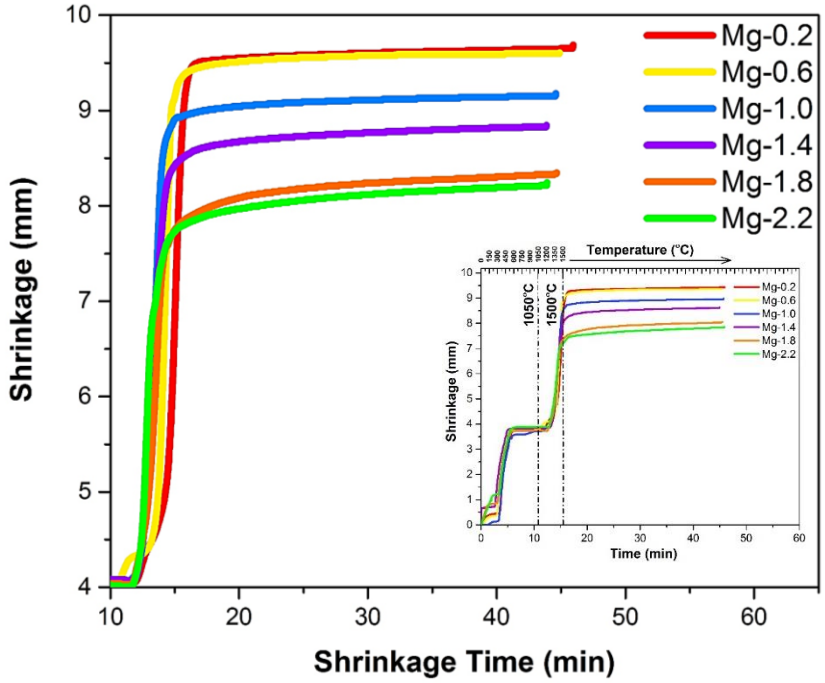

Figure 29 Densification curves of several compositions of magnesium stabilized nitrogen rich sialons sintered at 1500°C using spark plasma sintering technique, where Mg content varies

between 0.2-2.2. The insert shows the complete densification curves while the main plot represent the selected high temperature region (heating from 1050°C to 1500°C followed by 30 min holding time).

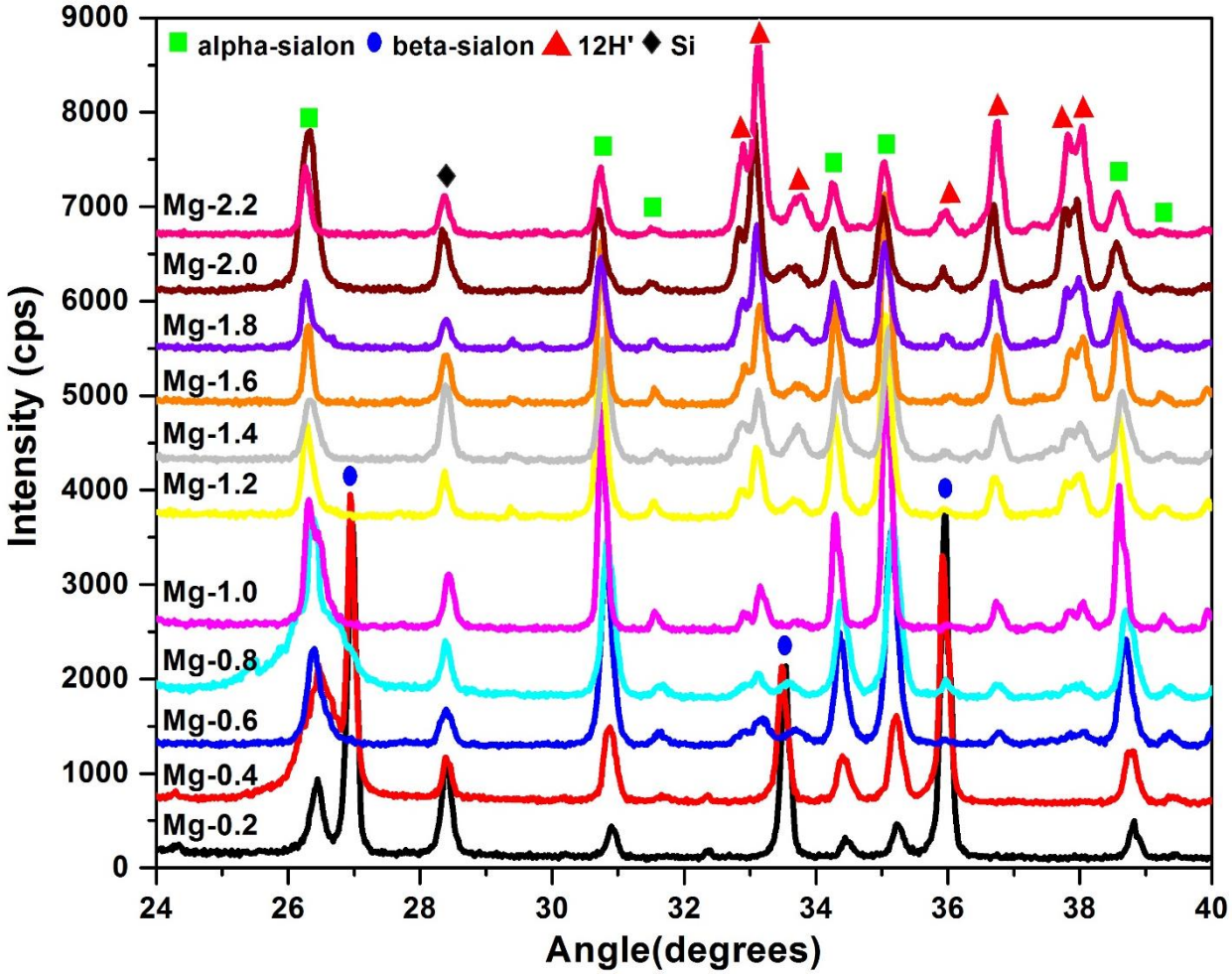

Figure 30 X-ray diffraction patterns of the magnesium stabilized nitrogen rich alpha sialon samples synthesized along the Si_3N_4-1/2Mg_3N_2:3AlN line at sintering temperature of 1500^{o}C.

6.2.3 Microstructure evaluation

Figure 31 (a-l) depicts the secondary electron FESEM micrographs of the fractured and etched surfaces of few of the selected samples from the magnesium doped nitrogen rich series synthesized at 1500^{o}C. **Figure 31 a&b** represents the low and high magnification micrographs acquired from

the fractured surface of sample Mg-0.4. In line with the x-ray diffraction results, elongated morphology characteristic of beta-sialon phase along with the equiaxed grains representative of alpha phase are clearly observed. The average aspect ratio for the elongated beta sialon grains is calculated to be ~3.6. In a recent work on magnesium doped alpha sialons synthesized at 1800^{o}C, Z.Yang et al. has reported that for a similar magnesium sialon composition, the aspect ratio of beta-sialon remained in the range of 2-4. In the past few year several studies (computer simulations as well as experimental work) have been performed in order to understand the mechanism responsible for the anisotropic growth of beta-sialon phase and the presence of large amounts of high temperature eutectic liquid has been reported as the common factor responsible for highly anisotropic growth of beta-sialon grains [132–136]. Moreover, T. Ekstrom in his work on the synthesis of beta-sialon ceramics via hot isostatic pressing technique has reported that in the absence of sintering additives elongated morphology of beta sialon grains couldn't be achieved [137]. Similarly, a low aspect ratio of beta-sialon grains (for an alpha/beta sialon ceramic) as result of limited amount of high temperature liquid phase has also been reported by T.S Sheu [138]. Therefore, for the sample Mg-0.4, synthesized using very minor amount of nitride additives (Mg_3N_2 and AlN), a low aspect ratio of beta-sialon grains could be fairly attributed to creation of small amount of high temperature eutectic liquid phase.

Figure 31 (c-f) represents the low and high magnification micrographs of the fracture surface of samples Mg-0.6 and Mg-1.0. Classical intergranular fracture showing equiaxed alpha sialon grains with no signs of beta-sialon grains having elongated morphology could be seen. The observation made on fracture surfaces is in good agreement with the XRD results, according to which, any evidence pertaining to the presence of beta phase couldn't be found for samples having x value of greater than 0.4. On the basis of an average of 50 readings the average grain size of alpha sialon is

seen to increase from 380nm to 495nm as the x value (representative of sample's composition) is increased from 0.6 (sample Id Mg-0.6) to 1.0 (sample Id Mg-1.0). The increase in average grain size could thus fairly be attributed to the formation of more amount of high temperature liquid phase as a consequence of more amount of nitride additives (more Mg_3N_2 and AlN for sample Mg-1.0 as compared to Mg-0.6) in initial powder mixture. For magnesium stabilized alpha sialons, an increase in average grainsize with increase in amount of oxnitride additives has also been reported by Z.Yang et al [125].

Figures 31 (g-h) represents low and high magnification micrographs of the fracture surface of sample Mg-1.4 synthesized at 1500^{o}C. Most of the fracture surface show equiaxed morphology of alpha grains, however at certain locations a relatively flat fracture showing non-equiaxed features with lath like appearance can be observed (highlighted with red circles in the image). Result of compositional analysis confirmed lath like appearance to be representative of AlN polytype phase. Moreover, polished surface of the sample Mg-1.4 was being subjected to etching using molten NaOH (at 320^{o}C). **Figure 31 (i-j)** represent low and high magnification micrographs of the etched surface of sample Mg-1.4. Well-developed lath/fibrous like morphology of AlN polytype phase could be much clearly observed in the etched sample as compared to the fractured surface. H. Peng and Z. Yeng have reported that Li-sialons with high amounts of intergranular glassy phase gets easily attacked by molten NaOH, causing more grains to fall and resulting in a fracture like morphology of the etched sample [139,140]. Thereby, in our case a fracture like morphology of etched sample (Mg-1.4) is believed to be an indicator of formation of relatively high amount of eutectic liquid phase. Interestingly, the average grain size of alpha sialon for the sample Mg-1.4 is seen to decrease to 401nm as compared to 495nm for the sample Mg-1.0. The grain size distribution for the three samples (Mg-0.6, Ca-1.0 and Ca-1.4) acquired from a total of 50 alpha

sialon grains is depicted in **Figure 32.** It is observed that initially with an increase in x value (0.6 to 1.0) the average grain size increases from 380nm to 596 nm while further increase in x value (1.0 to 1.4) results in a decrease in grain size from 596nm to 401 nm. The observation indicates that with increase in x value (from 1.0 to 1.4) an increase in the formation of high temperature liquid promotes the formation of AlN polytype phase (more than double an increase in the formation of AlN polytype phase for the sample 1.4 as compared to Mg-1.0).

Figure 31 (k-l) represents the fracture surface images acquired from the sample Mg-2.0 sintered at 1500^{o}C. A relatively disjointed yet equiaxed morphology of alpha sialon grains (**Figure 31k**) provides a visual evidence to the fact that densification of magnesium doped sialons gets difficult with an increase in the amount of additives i.e. increase in x value. Moreover, presence of well-developed AlN polytype phase in the form of relatively flat fracture having a morphological appearance of interlocking laths/fibers (**Figure 31l**) is in good agreement with the XRD results.

Figure 33 (a-j) shows the low and high resolution TEM images of the microstructures of magnesium doped nitrogen rich sialon samples (having the Id's as Mg-0.4, Ca-1.0 and Ca-1.4), along with selected area electron diffraction patterns (SAED) acquired from the grains of the different phases present. In line with the results of XRD and FESEM, presence of alpha and beta phases for the sample Mg-0.4 was confirmed by SAED patterns acquired from the grains of respective phases (**figure 33a&c**). As discussed earlier, a relatively low aspect ratio for the beta-sialon phase is believed to be associated with low amount of additives (low x value), which in turn limits the formation of high temperature transient liquid (an essential requirement for anisotropic grain growth). **Figure 33e** shows the low magnification TEM image acquired from the sample Mg-1.0 along with the SEAD pattern which confirms the presence of magnesium stabilized alpha sialon phase. In accordance with the XRD and FESEM results, TEM micrographs for the sample

Mg-1.4, as shown in **figure 33 g&i**, confirm the presence of equiaxed morphology representing alpha sialon phase and the lath like morphology of AlN polytype (12H') phase. Generally, it is believed that the synthesis of sialon materials is accompanied with the formation of an intergranular glassy phase. In a study on the intergranular structure of alpha/beta oxygen rich sialons, A. Thorel have reported that the intergranular phase which is always amorphous, can be found at the junction of multiple grains in the form of large pockets with a size in the range of 0.1 to 1μm or as an vitreous film with a minimum thickness of about 60nm [118]. However, in the present study, high resolution images of samples Mg-0.4, Mg-1.0 and Mg-1.4 (**figure 33b, d, f, h, j**) reveal that there isn't any intergranular glassy phase present in the samples. The results signify that the magnesium doped nitrogen rich sialons synthesized in the present study would be more stable at high temperature (1400-1600^{o}C) as compared to the oxygen rich sialons containing glassy grain boundary phase

6.2.4 Effect of magnesium-rich aluminum nitride polytype

It is widely known that the densification and grain growth of sialon ceramics gets significantly enhanced with the increase in amount of high temperature eutectic liquid [21,27]. Thereby, it is a general understanding that sialon ceramics having compositions which are rich in cation and/or oxygen content (i.e. compositions represented by higher x and/or n values) gets densified with much ease since higher amount of cations and/or oxygen content results in more amount of high temperature eutectic liquid [27]. However, in the present study, magnesium stabilized sialons depict a completely opposite yet an interesting trend, where the densification of the Mg-doped sialons gets difficult with the increases in x value. Furthermore, it is seen that for compositions having higher x value the grain growth of alpha sialon also gets restricted with a simultaneous increase in AlN polytype phase. In light of the above mentioned results, it can be fairly stated that

the exceptional behavior of magnesium stabilized sialons is due to the formation and growth of Mg-containing polytype phase (for compositions having higher x value) at the expense of high temperature eutectic liquid which otherwise is essential for densification and grain growth of alpha-sialons.

In case of sialon compositions rich in AlN starting powder, development and crystal structure of polytypes, which normally occur as minor phase with a major alpha sialon, have been thoroughly worked upon in the literature [21,27,141,142]. It is being reported that in the AlN polytypoid crystal structure, tetrahedral and octahedral sites can easily accommodate cations with small ionic radius (such as Mg^{+2}, Li^{+} and Sc^{+3}) [28,142,143]. Furthermore, it has also been reported that the formation of magnesium doped AlN polytypoid starts to take place at about 1400^{o}C which is slightly greater than the MgSiALON eutectic temperature [125]. Thus, in the present study, formation of high amounts of magnesium rich eutectic liquid (with increase in x value) is believed to be consumed by Mg containing 12H' polytype and consequently the densification and grain growth gets significantly inhibited.

In short, high temperature thermodynamic stability of magnesium rich AlN polytype (up to 1850^{o}C) appears to play a pivotal role on the formation of magnesium stabilized alpha-sialon [125]. Similar cationic radius of magnesium cation (Mg^{+2}) as that of aluminum cation (Al^{+3}) causes a replacement by Mg^{+2} ions for Al^{+3} ions, which otherwise would have stabilized alpha sialon [125]. In light of this it is believed that thermodynamic stability of magnesium doped alpha sialons could be increased with help of additives such as calcium oxide or yttrium oxide with a much bigger cationic radii [28,130].

6.2.5 Mechanical properties

Vickers hardness (HV_{10}) and indentation fracture toughness (K_{1c}) of the magnesium stabilized nitrogen rich sialon samples synthesized at 1500^{o}C are listed in **Table 13**. As shown, initially, an increase in the hardness of the samples is observed with increase in x value, which is followed by almost constant hardness and finally a gradual decrease is observed for samples represented by high end x values. An initial increase in hardness from 18.8 GPa (Mg-0.2) to 21.4 GPa (Mg-0.6) is believed to be associated with a shift in phase composition from beta rich two phase alpha+ beta region (where beta sialon is known for a relatively less hardness as compared to alpha phase) to an alpha rich two phase alpha + 12H' phase regime. A gradual decrease in hardness with increase in x value for compositions represented by high end x values is associated with increase in amount of 12H' phase. Z. Yang et al has reported a similar trend for magnesium doped sialon compositions laying along the m=2n line (oxygen rich compositions), sintered at 1800^{o}C [125]. However, relatively higher hardness for nitrogen rich samples (in present study) as compared to oxygen rich samples (in case of Z. Yang et al) may well be attributed to nitrogen rich alpha sialons. The observation is line with study performed by František Lofaj et al. which reveals that a 4% increase in N content would result in nearly the same increase in micro-hardness of RE-Si-Mg-O-N systems [122]. Sample Mg-0.2 with highest amount of beta-sialon phase results in the maximum fracture toughness of 5.4 MPa.m$^{1/2}$.The elongated morphology of beta-sialon is well-known to give rise to toughening mechanisms such as crack deflection, crack bridging and grain pull out [141,144]. In the absence of beta-sialon phase the fracture toughness is seen to decrease with the minimum value of 2.9 MPa.m$^{1/2}$ for the sample Mg-2.2 having the maximum amount of AlN polytype (12H') phase. Thus, the lath/fibrous like morphology of 12H' phase is seen to have deteriorating effect on the fracture toughness of these materials. In light of the present results, the desired mechanical

properties of Mg-doped sialon ceramics could be better tailored by thoughtful selection of initial powder composition.

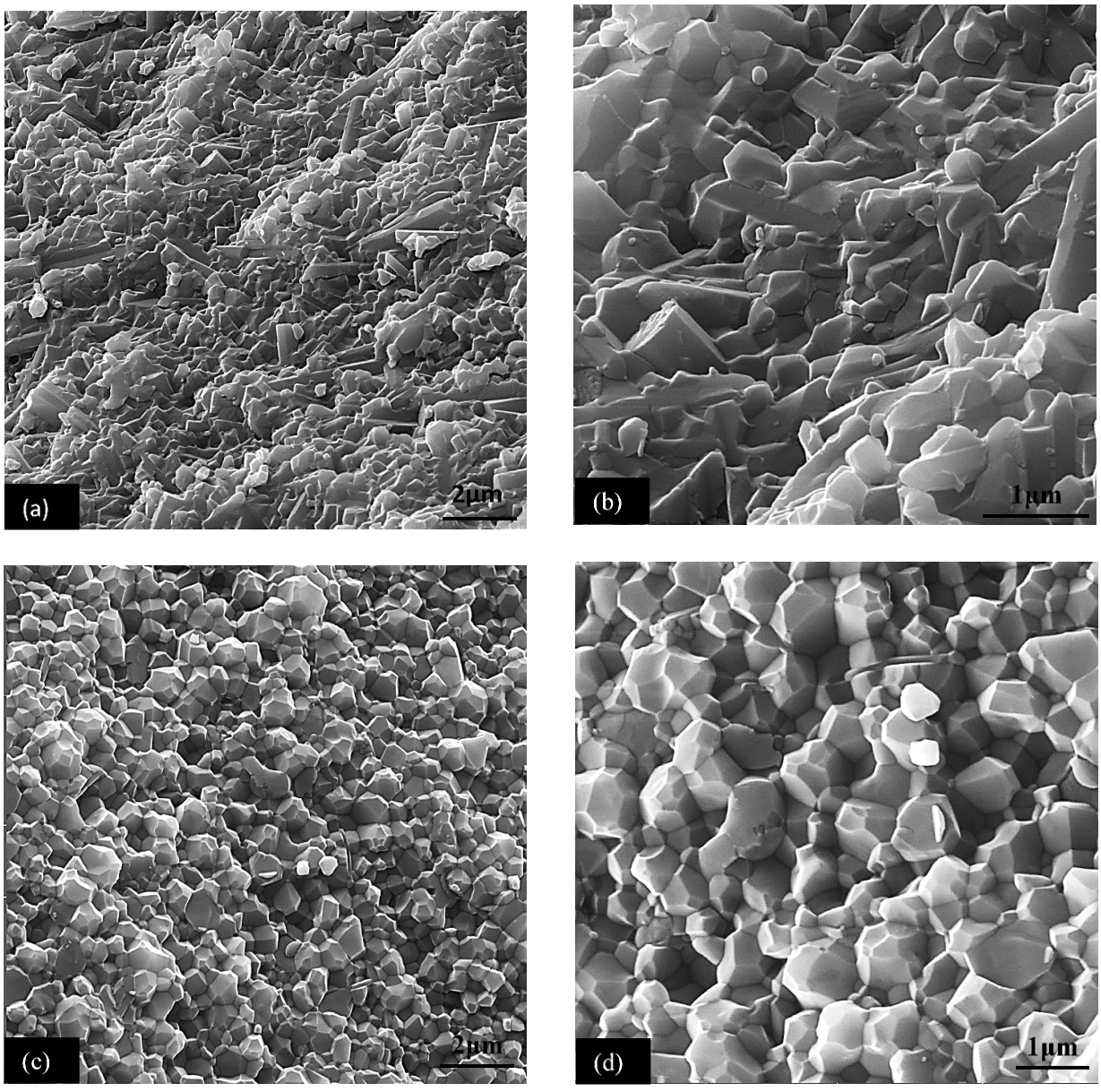

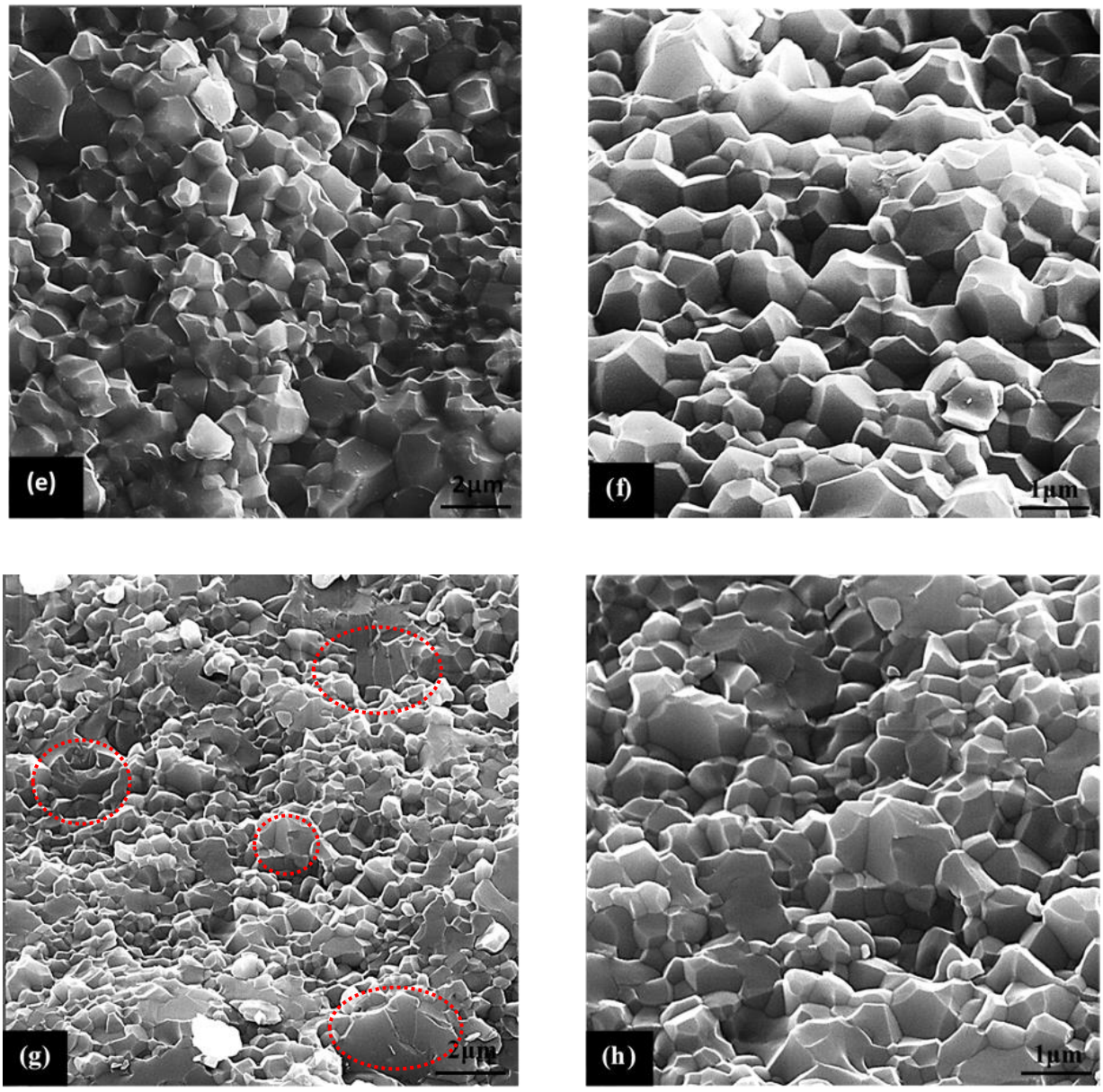
(e)
2µm
(f)
1µm
(g)
2µm
(h)
1µm

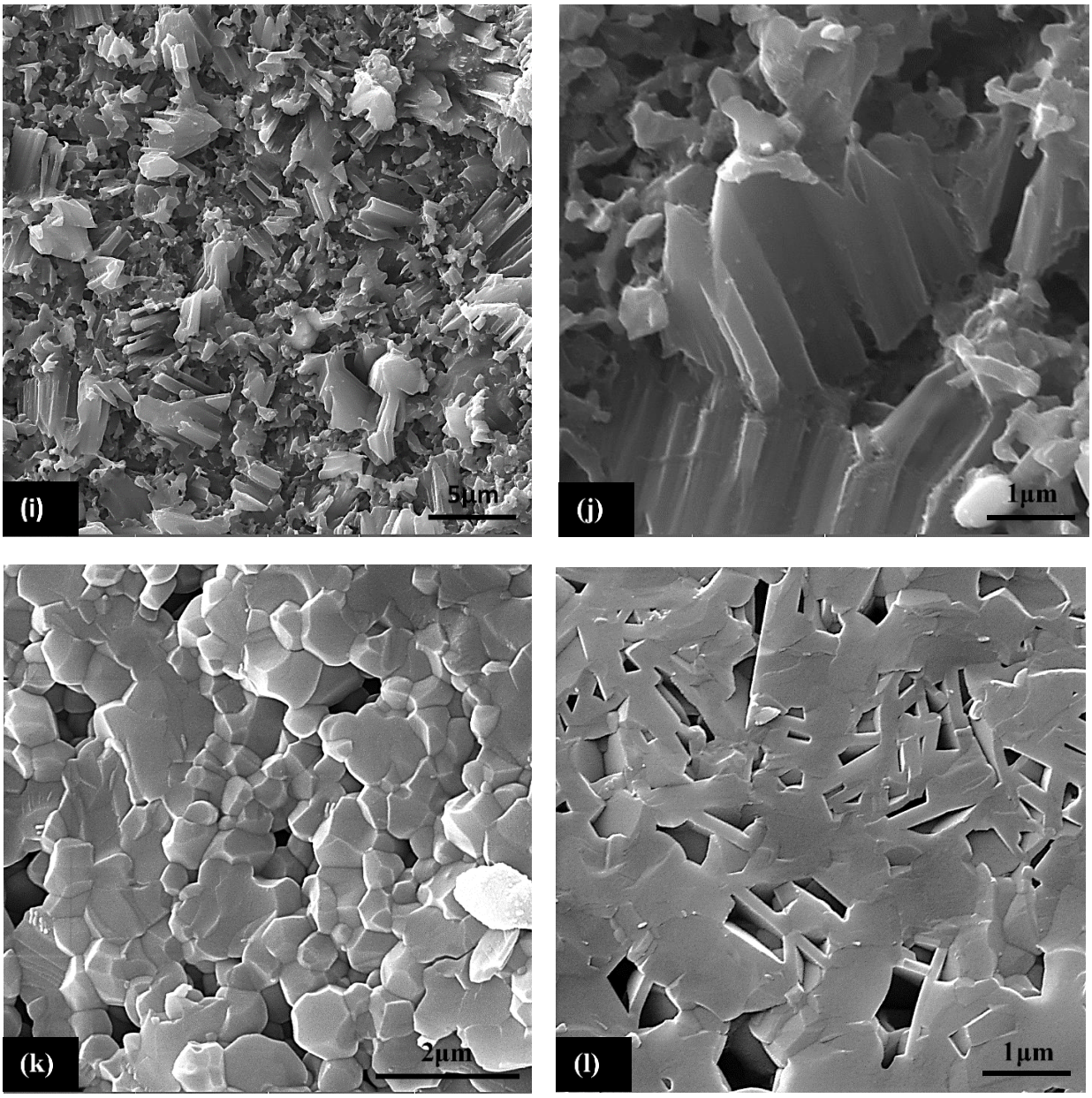

Figure 31 Secondary electron (SE) micrographs showing **(a)** low and **(b)** high magnification fracture surface of sample Mg-0.4, **(c)** low and **(d)** high magnification fracture surface of sample Mg-0.6**, (e)** low and **(f)** high magnification fracture surface of sample Mg-1.0, **(g)** low and **(h)** high magnification fracture surface of sample Mg-1.4, **(i)** low and **(j)** high magnification micrographs of etched surface of sample Mg-1.4 showing AlN polytype, **(k)** fracture surface of sample Mg-2.0 showing equiaxed alpha sialon **(l)** fracture surface of sample Mg-2.0 showing AlN polytype.

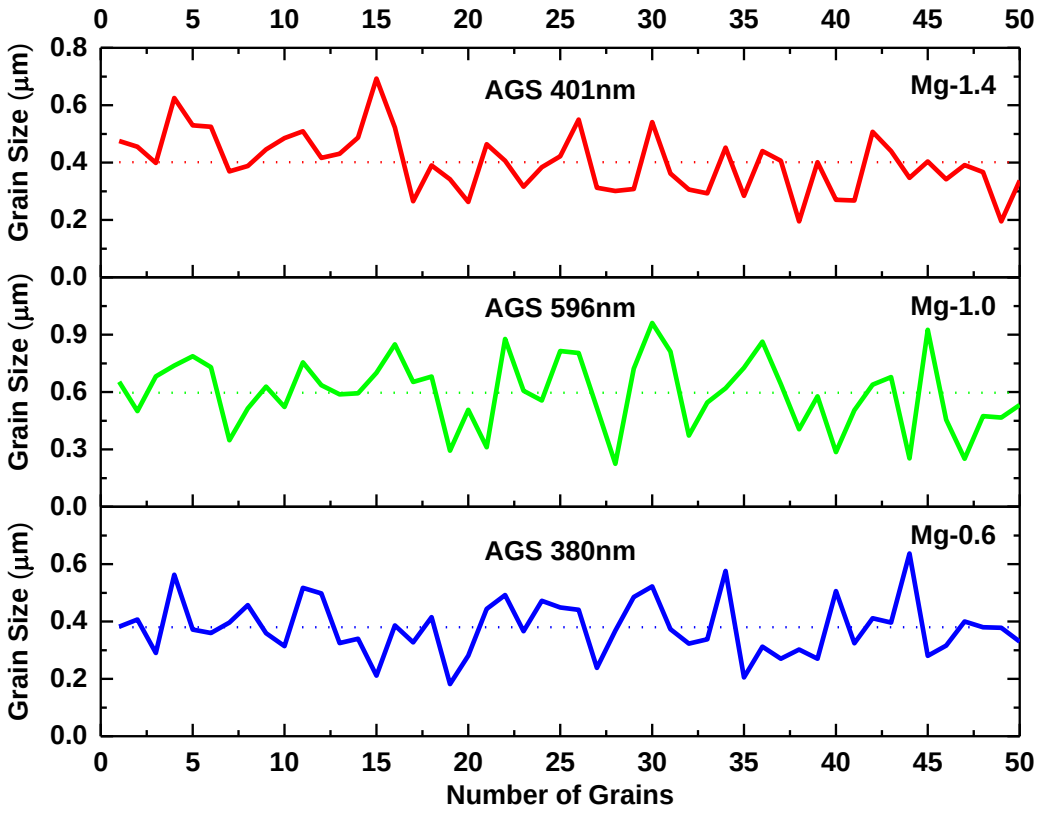

Figure 32 Grain size distribution of nitrogen rich samples synthesized at 1500°C having the sample Id's of Mg-0.6, Mg-1.2 and Mg-2.0 (AGS: Average Grain Size).

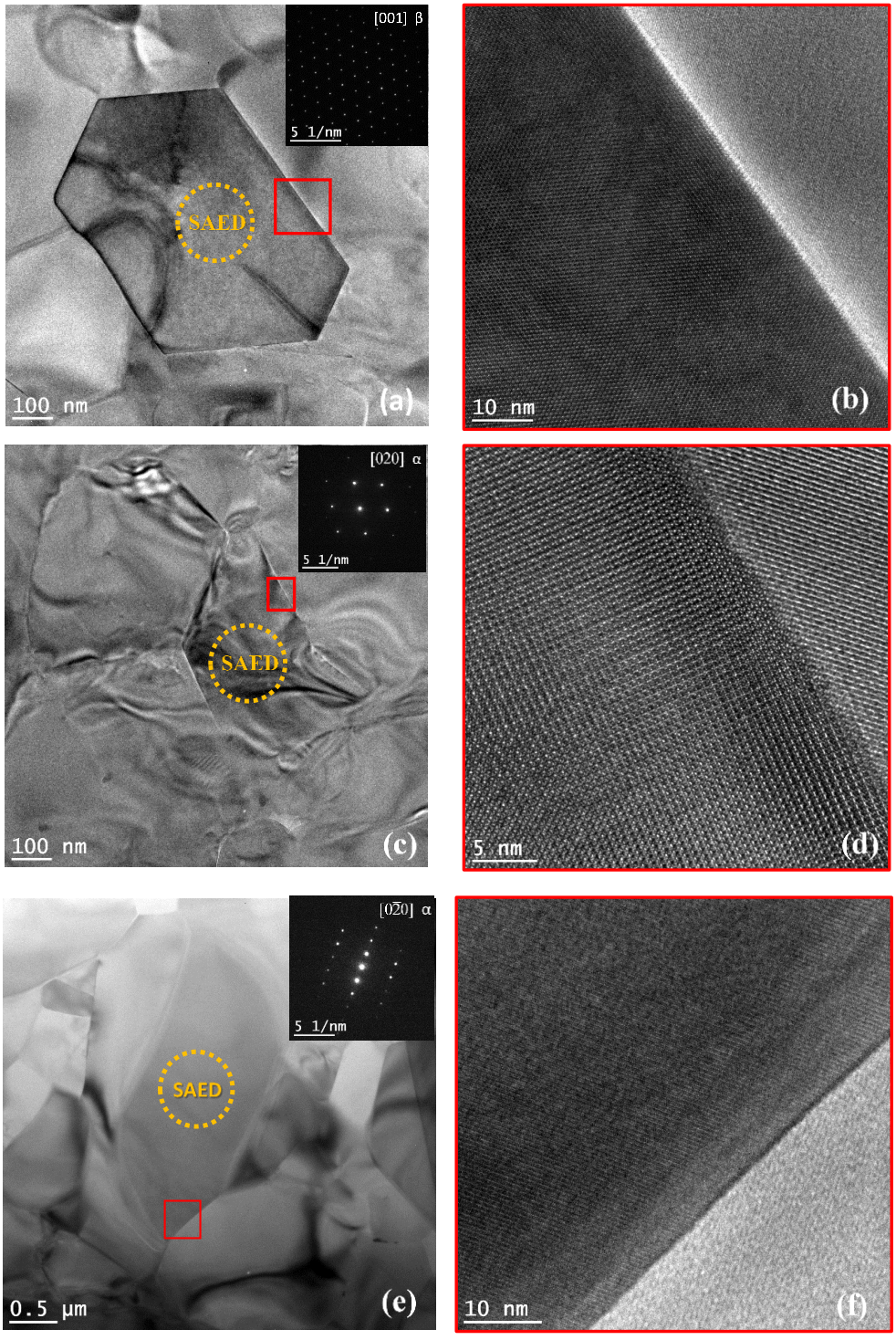
[001] β
5 1/nm
SAED
100 nm
(a)
10 nm
(b)
[020] α
5 1/nm
SAED
100 nm
(c)
5 nm
(d)
[0$\bar{2}$0] α
5 1/nm
SAED
0.5 μm
(e)
10 nm
(f)

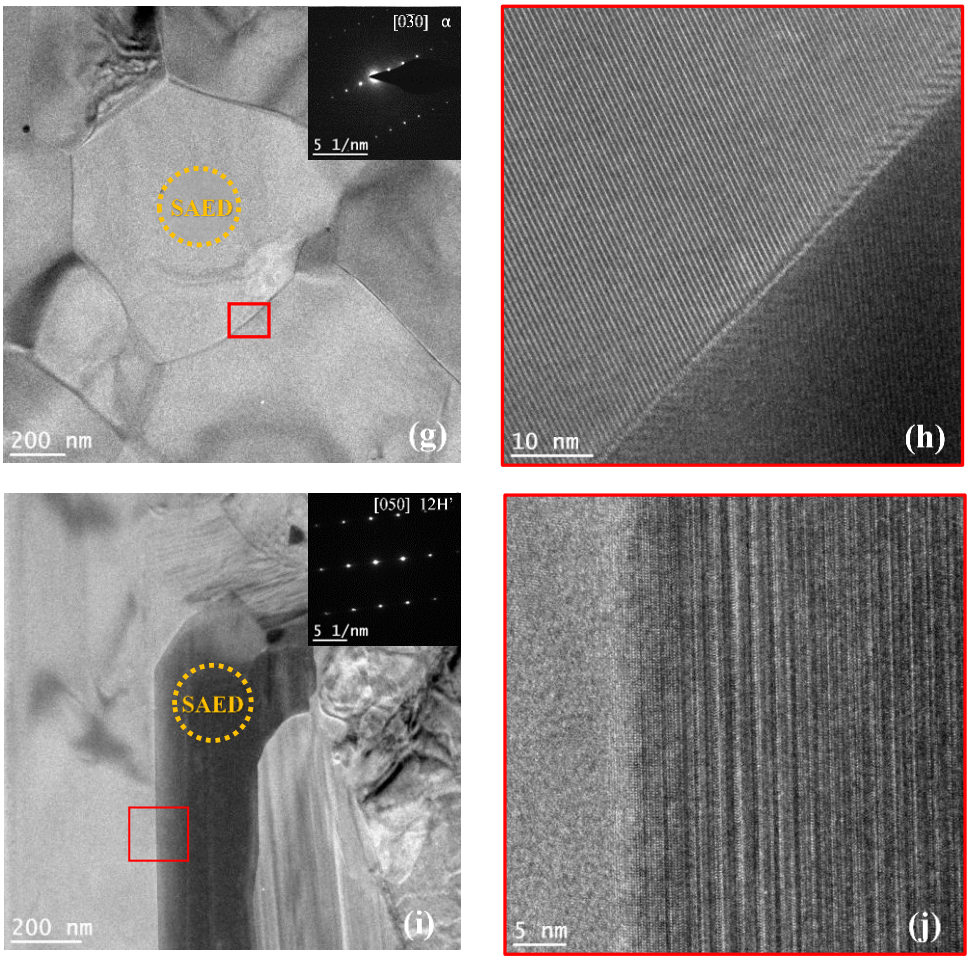

Figure 33 Low and high resolution TEM micrographs along with the SAED patterns acquired from the nitrogen rich samples synthesized at 1500°C using different x values: **(a-d)** Mg-0.4, **(e - f)** Mg-1.2 and **(g-j)** Mg-1.4.

6.3 Conclusion

Several compositions of magnesium doped nitrogen rich sialon ceramic samples having the x value in the range of 0.2-2.2 were selected for the synthesis. Nano sized staring powder precursors along with spark plasma sintering technique enhanced the reaction kinetics and thus helped achieve well densified sialon ceramic samples at comparatively low temperature of 1500°C as compared to

normally reported temperature of 1700°C or greater. Unlike other sialon systems, it is observed that a single phase magnesium stabilized alpha sialon doesn't exist along the nitrogen rich line Si_3N_4-1/2Mg_3N_2:3AlN (on the Mg alpha sialon plane). The densification of the nitrogen rich samples as well as the formation of a stable alpha sialon phase is seen to become difficult at higher x values (more Mg_3N_2 and AlN content). Initially with an increase in x value a corresponding increase in the lattice parameters of alpha sialon unit cell is observed. The maximum achieved content of magnesium cation in the alpha sialon unit cell is observed to be 1.08 (for x=1.6), however with any further increase in x value, increase in lattice parameters became negligible. Similarly, with an increase in x value (0.6 to 1.0) the average grain size is observed to increase followed by a decrease in grain size with further increase in x value (1.0 to 1.4). The unique characteristics of magnesium doped nitrogen rich sialon ceramics can fairly be attributed to the formation and growth of Mg-containing polytype phase (for compositions having higher x value) at the expense of high temperature transient liquid phase which otherwise is essential for densification, formation and grain growth of alpha-sialons. Significantly improved hardness and fracture toughness of 21.4 GPa and 5.4 MPa.$m^{1/2}$ was achieved for magnesium doped nitrogen rich sialon ceramics. Moreover, the absence of intergranular glassy phase in these materials suggests of the high temperature stability and high infrared transmittance of these materials.

CHAPTER 7

EFFECT OF PRECURSOR SIZE ON THE STRUCTURE AND MECHANICAL PROPERTIES OF CALCIUM-STABILIZED SIALON/CUBIC BORON NITRIDE NANOCOMPOSITES

Summary

Calcium-stabilized alpha-sialon ceramics reinforced with cubic boron nitride (cBN) particles were synthesized using spark plasma sintering. The effects of the size of alpha-sialon precursor particle and the influence of the amount of cBN reinforcement on the physical, structural and mechanical characteristics of the composites were studied. Synthesis of the composites at 1500 °C with a holding time of 30 minutes resulted in densified composites. CBN-reinforced alpha-sialon composites synthesized via probe sonication showed particle sizes between 200 nm to 450 nm and showed significantly better mechanical properties than did the unreinforced sialon. A Vickers hardness (H_{V10}) value of as high as 24.0 GPa was measured for this reinforced sialon, as compared to a value of 21.6 GPa for the pure alpha sialon. However, a phase transformation from alpha to beta sialon was observed when using high energy ball milling process condition, where the size of the alpha-forming precursors was decreased to about 100 nm. This phase transformation was accompanied by a simultaneous cubic-to-hexagonal boron nitride phase transformation.

Graphical Abstract

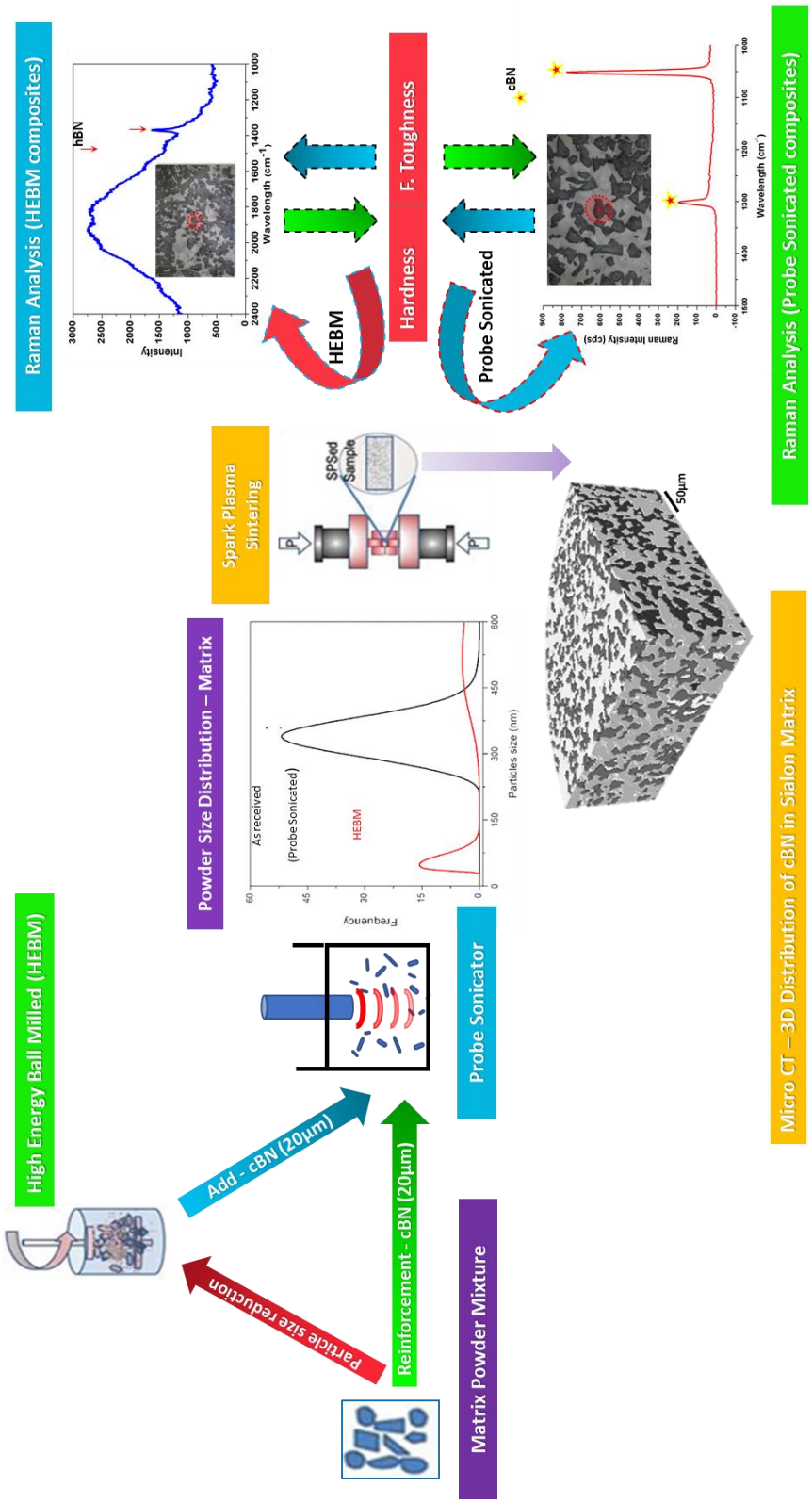

7.1 Introduction

Ceramics are traditionally known as materials that endure severe engineering and operating environments. Silicon nitride ceramics exhibit outstanding thermo-mechanical behavior [1] due to their atomic structure and bonding that is strongly covalent in nature. But these structures formed by silicon and nitrogen have also made it challenging to achieve fully compact and densified materials. The strong chemical bonds characteristic of silicon nitride thus require excessively high temperatures to help achieve compact materials [2,3]. However, the practical complexities of carrying out syntheses at high temperatures, and for a sufficiently long period of time, have led to the development of metal oxide additives to help synthesize fully compact materials at much lower temperatures[1–3,85]. An obvious outcome of this additive modification was the development of sialon (aluminosilicate oxynitride) materials having an additive controlled structure-property relationship [10–12]. Superior hardness of sialon ceramics as compared to silicon nitride have it an ideal candidate for cutting tool materials [87,88]. CeramTec offers cutting tool materials made up of alpha and beta sialon for machining (boring, milling, turning) of cast iron in continuous as well as interrupted cutting mode. The company is already producing and marketing cutting tools made up of Sialon/SiC composites. Since Sialon materials offer better sinterability as compared to silicon nitride, addition of hard reinforcing particles like cBN to the sialon matrix would pave the way for tool materials having improved wear resistance and prolonged lifetime [89].

Sialon materials form a solid solution of silicon nitride, and have been primarily classified into two phases, alpha and beta, having different crystal structures as well as different microstructures and thermomechanical properties. Beta sialon is fashioned by concurrently replacing equal numbers of silicon and nitrogen atoms with aluminum and oxygen atoms, respectively, and has been generally defined by the formula $Si_{6-z}Al_zO_zN_{8-z}$. The alpha-sialon unit cell includes four units

of Si_3N_4, and is where x is less than 2 and is also the product of m and v (valency), and (m+n) (Si-N) bonds are replaced by m (Al-N) bonds and n (Al-O) bonds [10,12,20,41]. While other phases of sialon have been investigated, alpha sialon and beta sialon have been the most intensely considered during the past two decades due to their remarkable mechanical properties, specifically the high hardness of alpha sialon and the modest fracture toughness of beta sialon [16,17]. The inclusion of aluminum oxide, other metal oxides have also been employed as additives to stabilize sialons. Although rare-earth metal oxides have for decades been employed as stabilizing additives in the synthesis of sialons, calcium oxide has lately become a more favored additive due to its higher solubility and stability [24,28–31,90]. Moreover, Ca-based compounds are less expensive and more available [34].

The mechanical properties of ceramics, in particular ceramic cutting tools, have also been improved by adding hard reinforcements that offer good adhesion to the matrix. Cubic boron nitride (cBN), which is known as the second hardest material after diamond, is considered to be an ideal candidate as a reinforcement for ceramic matrixes [145]. Most investigations of sialon/cBN ceramic composites have been done with beta sialon as the matrix. With the addition of 10 vol.% of cBN to the beta-sialon matrix, Vickers hardness and fracture toughness values of up to 15.4 GPa and of 6.8 $MPa.m^{1/2}$, respectively, have been reported [146]. Furthermore, the hardness of this composite was observed to have decreased at a synthesis temperature of 1650 °C. The decrease in the hardness at this temperature was attributed primarily to a transformation of the hard cBN phase to a softer hexagonal phase. The effect becomes more pronounced as the synthesis temperature is increased. However, it has also been reported that higher heating rates could impede this transformation [147]. In this regard, spark plasma sintering is a powder consolidation method that has garnered huge attention for the production of ceramic materials because of its faster

heating rate, as well as its shorter sintering duration and novel pulsed-current-based heating [36,37].

The present study focused on developing fully densified cBN-reinforced alpha-sialon composites at a low synthesis temperature of 1500 °C. Additionally, the effect of the amount of reinforcement and that of the size of the alpha-forming precursors on the structural stability of the alpha phase and hence on mechanical properties of the composites were also explored.

A single-phase calcium-stabilized alpha sialon having the formula $Ca_{0.87}Si_{10}Al_{3.04}O_{1.30}N_{16.09}$ was selected as the matrix material for the syntheses of the composites. Cubic boron nitride particles having an average particle size of 20 µm were employed as the reinforcement. The initial powder mixing techniques as well as the sizes and amounts of reinforcement employed in the syntheses of the sialon composites are summarized in **Table 14** (detailed experimental procedure is mentioned in chapter 3). Mixture of composites prepared (details mentioned in chapter 3) were sintered using spark plasma sintering (SPS) at 1500°C for 30 min.

Table 14 Classification of the synthesized composites according to reinforcement particle size, reinforcement weight percent, and mixing technique.

Sample ID*	cBN Particle Size (um)	cBN Wt.%	Mixing Technique
1P	-	-	P
2P	20	10	P
3P	20	20	P
4P	20	30	P
5H	20	10	H
6H	20	20	H
7H	20	30	H

*P and H denote probe sonication and high-energy ball milling, respectively.

7.2 Results and Discussion

7.2.1 Powder analysis

Figure 34 (a) shows the FESEM micrograph of the as-received cBN (20 μm) particles, which confirmed the particle size specification provided by the manufacturer. **Figure 34 (b and c)** shows an XRD plot and Raman spectrum of the as-received cBN particles and confirmed them to have the cubic phase structure. In order to assess the stability of cBN particles at high temperatures, XRD was performed at 100, 1200, 1300, 1400 and 1500 °C (**Figure 35**). An FESEM micrograph of cBN particles exposed to 1500 °C for 30 minutes is shown in **Figure 35 a**. According to the FESEM micrograph, the cBN particles retained their sharpness at the high temperature, and neither any distortion nor cracking nor deterioration was observed. Similarly, the XRD spectra confirmed the presence of single-phase cBN particles at various temperatures up to 1500 °C. Particle sizes were determined using a dynamic light scattering analyzer. The powder mixture of the alpha-sialon matrix (without cBN) prepared via probe sonication (1P to 4P) showed particle dimensions between 200 nm and 450 nm whereas the mixtures prepared through high-energy ball milling (5H to 7H, without cBN) displayed dimensions of primarily 50-125 nm (**Figure 36)**. It was observed (**Figure 36)** from the HEBM sample that the sizes of the particles decreased due to the effective ball processing. EDX elemental maps **(Figure 37)** acquired from both the samples (probe sonication and HEBM) showed similar results, with comparably high levels of homogeneity. According to the EDX analysis N/O weight ratio of 2.16 for probe sonicated powder mixture was observed to decrease to 0.79 for HEBM powder mixture. This in turn confirmed the presence of higher oxygen content in the HEBM powder mixture.

Figure 38 shows a post-synthesis micro-CT (μCT) analysis of probe-sonicated sialon/cBN composite sample 4P. A 3-mm-diameter core was sectioned and scanned using a voltage of 60 kV and current of 165 μA, and N-Reckon software was used for the reconstruction of projected images with the help of two other computer programs, namely CT-AN and CT-Vol, which further processed the projections to generate the 3D model. The 3D distribution cBN-reinforced particles (dark grey in the **figure 38**) within the alpha-sialon matrix (light grey) confirmed a good level of homogeneity at the micron level and higher. A similar distribution was observed for cBN particles embedded in the high-energy ball milled sialon matrix.

7.2.2 Synthesis and densification

The plots in **figure 39** show the densities of the synthesized composites as a function of the weight percentage of reinforcements (cBN). The pure alpha-sialon sample 1P displayed the highest density, with a value of 3.19 g/cm^3. As the weight percent of the reinforcement was increased, the density slightly decreased, with sample 4P displaying a density of 3.10 g/cm^3. Nevertheless, a densification of about 96 % was attained for the samples reinforced with 30 weight percent cBN (density of cBN = 3.45 g/cm^3) having a particle size of 20 um as compared to the pure alpha sialon. J. C. Garrett and Feng Ye have reported similar trends in their studies where the density of Sialon/cBN composites is reported to have decreased with increase in amount of cBN reinforcements [146,148]. Although, in literature, there is no clear explanation for the said decrease in density but a possible explanation might be that it is due to the difference in coefficient of thermal expansion of Sialon ($3*10^{-6}/^oC$) and cBN ($1.2*10^{-6}/^oC$) which result in the formation of void spaces at the Sialon/cBN interface. Similar effect of cBN addition on the density of cBN–Al_2O_3 and cBN–WC–Co composites has also been reported in the literature [149,150]. The heating nature of SPS, i.e. pulsed-current, together with larger surface areas of the nano precursors, helped

the densification at lower synthesis temperature; also, CaO, as a densifying agent, resulted in an extra amount of liquid phase during the initial stage of synthesis (~ 800 to 1200 °C), which also facilitated densification. Higher surface area of the nano/submicron powder particles has been shown to act as the driving force promoting the synthesis to gain thermal equilibrium. Based on the equation reported by Hansen and coworkers, the rate of synthesis gets enhanced four-times provided that the size of the starting powder material is decreased by an order of magnitude [151]. But, a similar decline in densities of ball milled alpha-sialon composites reinforced with 20 um cBN was observed due to the phase transformation of cBN into hBN (density of hBN = 2.1 g/cm^3).

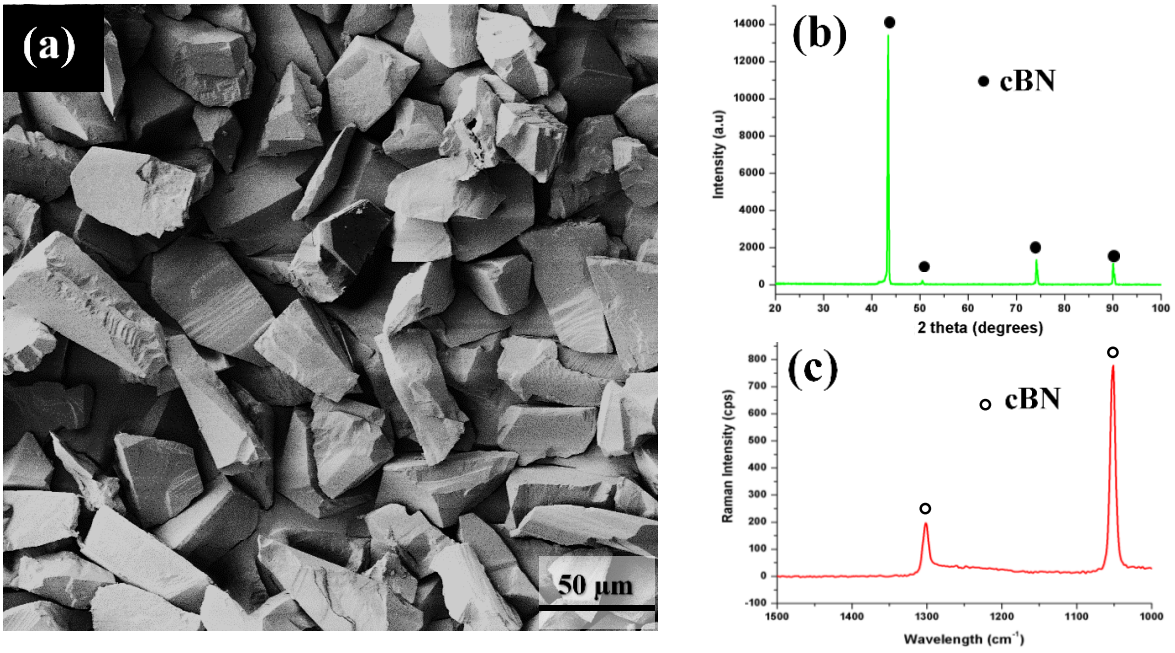

Figure 34 (a) FESEM micrograph, (b) XRD spectrum, and (c) Raman spectrum of the as-received cBN particles.

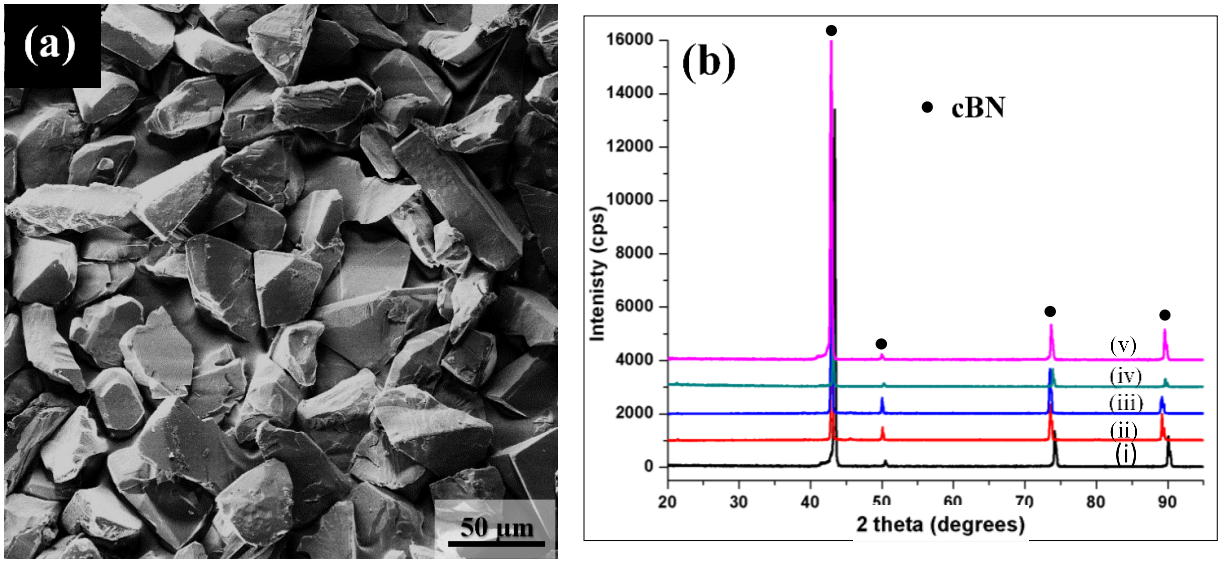

Figure 35 (a) FESEM micrograph of the cBN particles heated up to 1500 °C and held there for 30 minutes. (b) XRD plots of the cBN particles at (i) 100 °C, (ii) 1200 °C, (iii) 1300 °C, (iv) 1400 °C and (v) 1500 °C, which showed characteristic peaks of single-phase cBN.

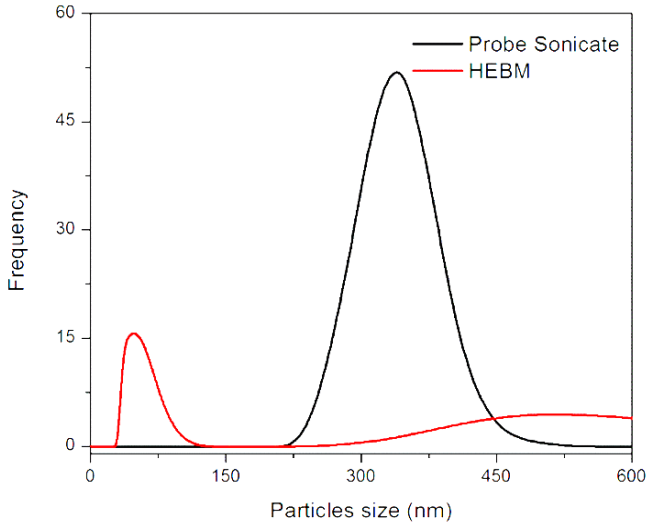

Figure 36 Particle size distributions of the powder mixtures obtained via probe sonication and high-energy ball milling.

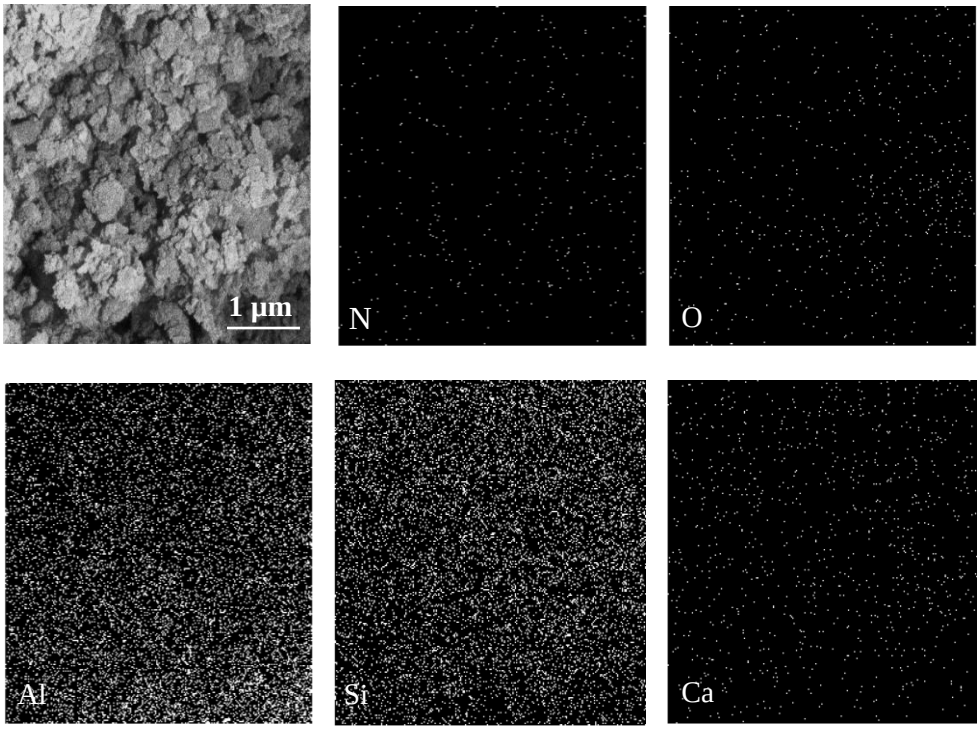

Figure 37 Post mixing EDX mapping of sample 1P revealed a homogenized elemental dispersion in the starting mixture.

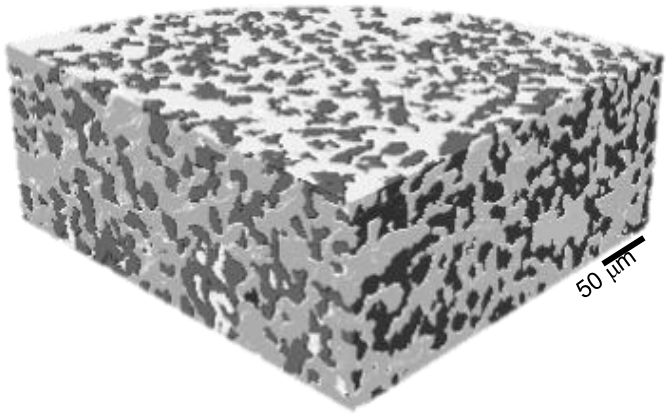

Figure 38 A 3D micro-CT cutaway section of the probe-sonicated synthesized sialon/30 wt. % cBN composite (sample 4P) depicting a quite homogenous distribution of cBN particles (dark grey color) within the sialon matrix (light grey color).

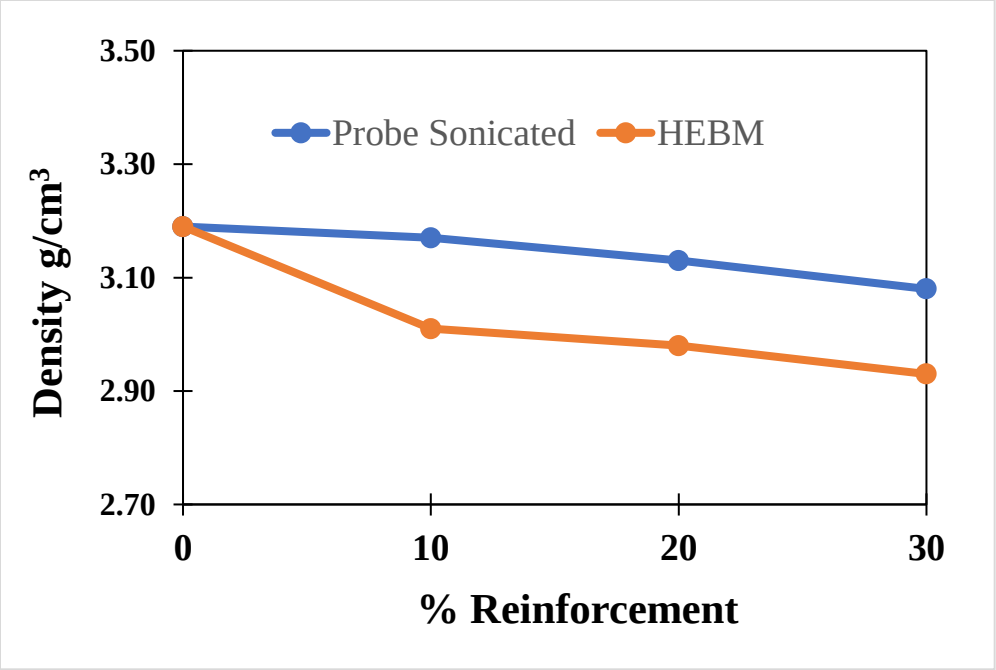

Figure 39 Densities of the composites as a function of weight percent of reinforcement.

7.2.3 Phase formation

X-ray diffraction patterns of the synthesized samples 2P, 3P and 4P having 10, 20 and 30 weight percent of 20 um cBN are shown in **figure 40**. For the samples 5H to 7H, the diffraction patterns are shown in **figure 41.**

Composites prepared via probe sonication showed the presence of a pure Ca-alpha-sialon ($Ca_{0.68}Si_{10}Al_{2.04}O_{0.68}N_{15.38}$) phase according to the calculated values of m and n. Aside from the alpha-sialon phase stabilized by pure calcium, no evidence of a transformation from cBN to HBN was indicated by their x ray-diffraction patterns. However, the patterns from high-energy ball milled samples 5H to 7H suggested a partial alpha-to-beta transformation for the sialon matrix and a considerable cBN-to-hBN transformation.

Raman spectroscopy of the reinforcing boron nitride particles was performed in order to confirm the cBN-to-hBN phase transformation. **Figure 42** shows Raman spectra of reinforcing boron nitride particles from composite sample 4P. The presence of peaks at 1056 cm^{-1} and 1307 cm^{-1}, for all of the six randomly chosen boron nitride particles, confirmed the presence of the cBN phase and clearly indicated that there was no transformation of cBN particles to the soft hBN phase. **Figure 43** shows Raman spectra of reinforcing boron nitride particles for HEBM composite sample 7H. Consistent with the XRD results, the Raman spectra of the boron nitride particles also confirmed the presence of the hBN phase, showing a peak at 1367 cm^{-1}, along with a broad asymmetric peak. The asymmetric and broad nature of the latter Raman peak was due to stress-induced lattice distortion experienced by the boron nitride particles [152].

The oxide content associated with HEBM samples facilitated a partial transformation of stable alpha sialon into beta sialon ($Si_{10}Al_2O_2N_{14}$) at the synthesis temperature of 1500 °C. This transformation was due to wetting of the nitride (Si_3N_4/AlN) powder particles [94], where wetting occurred in the presence of a liquid phase while formation of eutectic oxide melt occurred in the range of 820 to 990 °C depending upon the starting mixture. Additionally, Z. Kesic et. al. reported in a study that during milling, small amount of CaO reacts with CO_2 in the air to form $CaCO_3$ [153]. The decomposition of $CaCO_3$ at higher temperatures becomes a source of extra oxygen, which in turn facilitates formation of beta-sialon [154]. The stress-induced by elongated morphology of beta sialon and the occurrence of liquid phase, both, most likely resulted in the cBN-to-hBN transformation for the HEBM-prepared samples. The reaction sequence can be expressed as shown in equation 2 below. Conceivably a change in the enthalpy (ΔH) of the system during the alpha-to-beta transformation, the formation of the extra liquid phase in the presence of

oxygen in the system, and the morphological change from equiaxed alpha sialon to elongated beta-sialon caused this transformation of the high-temperature-stable cBN phase to hBN.

$CaO \rightarrow (CaCO_3) + Si_3N_4 + AlN + SiO_2 \approx$ alpha sialon + beta sialon + calcium-enriched liquid phase (eq. 2)

7.2.4 Microstructural development

An FESEM micrograph of a pure alpha-sialon sample (1P) etched using a hydrofluoric acid solution is shown in **figure 44 (a).** Fully dense single-phase equiaxed alpha-sialon grains were observed in the micrograph, validating the single-phase alpha region defined by the values of m=1.6 and n=1.2. A backscattered FESEM micrograph of the composite sample 4P, containing the cBN reinforcement with a particle size of 20 um, is shown in **figure 44 (b)**. Cubic BN and alpha sialon can be distinguished easily in the micrograph due to the difference in their weighted mean BSE coefficient. The cBN grains (black) were observed to be homogeneously dispersed in a continuous alpha-sialon matrix. No pore was found in any of the samples (see the 3D reconstruction of sample 4P in **Figure 38)**.

A micrograph of a polished sample of the HEBM sialon/cBN composite is shown in **figure 45 (a).** Here, a uniform distribution of reinforcement particles within the matrix was clearly observed. Hexagonal boron nitride reinforcements appeared damaged, cracked and disjointed from the matrix, most probably due to the stress-induced cBN-to-hBN phase transformation and the formation of the ultra-fine freshly transformed grains of hBN, which in general showed a fine lathlike morphology. **Figure 45 (b)** shows an etched image of the same sample. Here, a needle-shaped, elongated morphology of the β-$Si_{10}Al_2O_2N_{14}$ grains was observed. This observation provided more evidence for the presence of the beta-sialon phase. The transformation from the

alpha phase to the beta phase at similar processing conditions was likely due to the higher content of oxide and liquid associated with the smaller particle size of the initial HEBM powder mixture as described above in the phase formation section. Roman Shuba and I-Wei Chen have also reported that "as the powders experienced increasing oxidation because of mixing, the densification temperature decreased, the amount of residual glass increased, and alpha-Sialon was destabilized and replaced by beta-Sialon and AlN polytypes during hot pressing."[154].

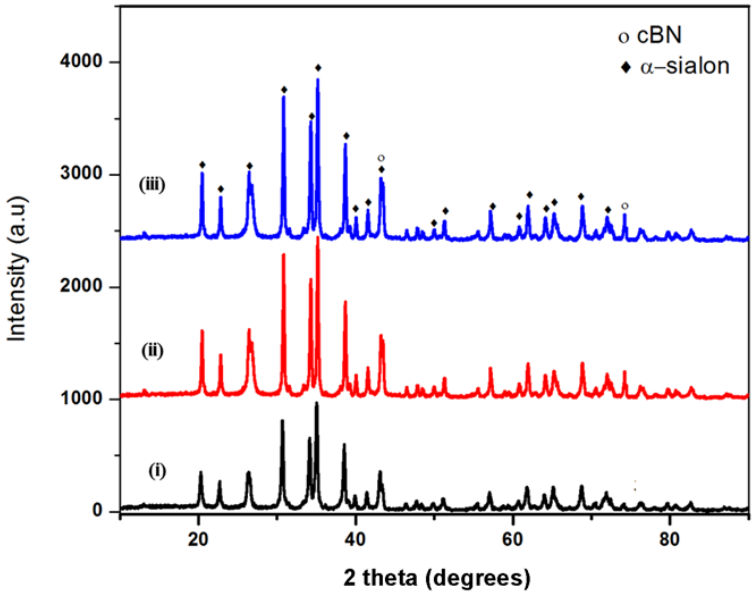

Figure 40 XRD pattern of composite samples (probe sonicated) synthesized at 1500°C, with a holding time of 30 min. **(i)** 2P, **(ii)** 3P and **(iii)** 4P. Alpha-sialon and cBN peaks matched those in ICDD # 00-042-0252 and 01-089-1498, respectively.

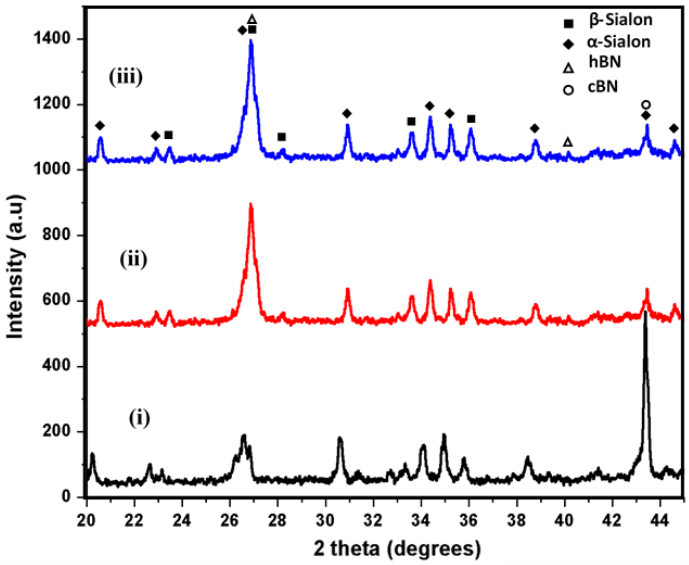

Figure 41 XRD pattern of composite samples (HEBM) synthesized at 1500°C, with a holding time of 30 min. **(i)** 5H, **(ii)** 6H and **(iii)** 7H. Beta-sialon/BN composite peaks matched those in ICDD # 00-048-1615 (β-$Si_{10}Al_2O_2N_{14}$), 01-089-1498 (cBN) and 01-07708869 (hBN).

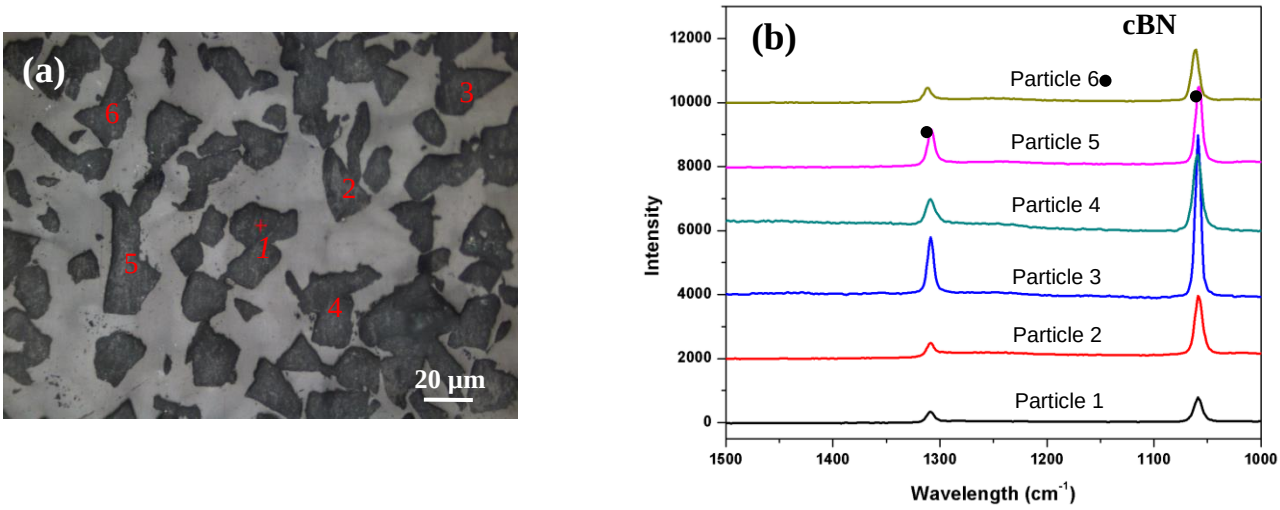

Figure 42 (a) Optical image of the synthesized sample 4P showing cBN particles embedded in a probe-sonicated sialon matrix. (b) Raman spectra of the particles highlighted in panel (a), showing characteristic cBN peaks.

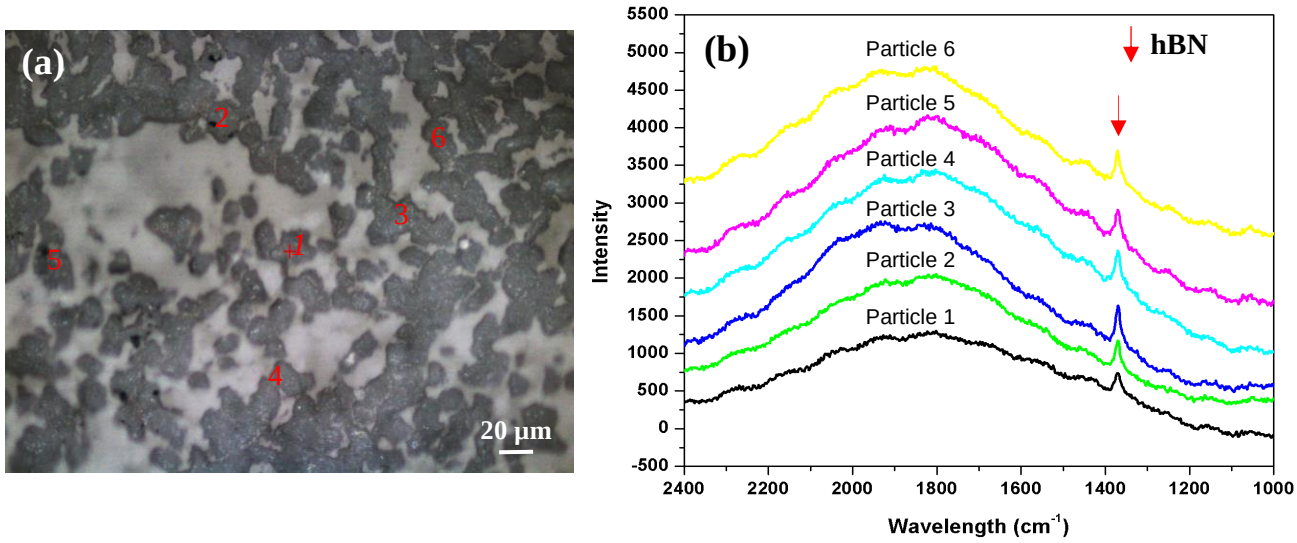

Figure 43 (a) Optical image of the synthesized sample 7H showing hexagonal boron nitride particles embedded in an HEBM sialon matrix. (b) Raman spectra of the particles highlighted in panel (a), each showing a characteristic hBN peak along with a broad asymmetric peak [152].

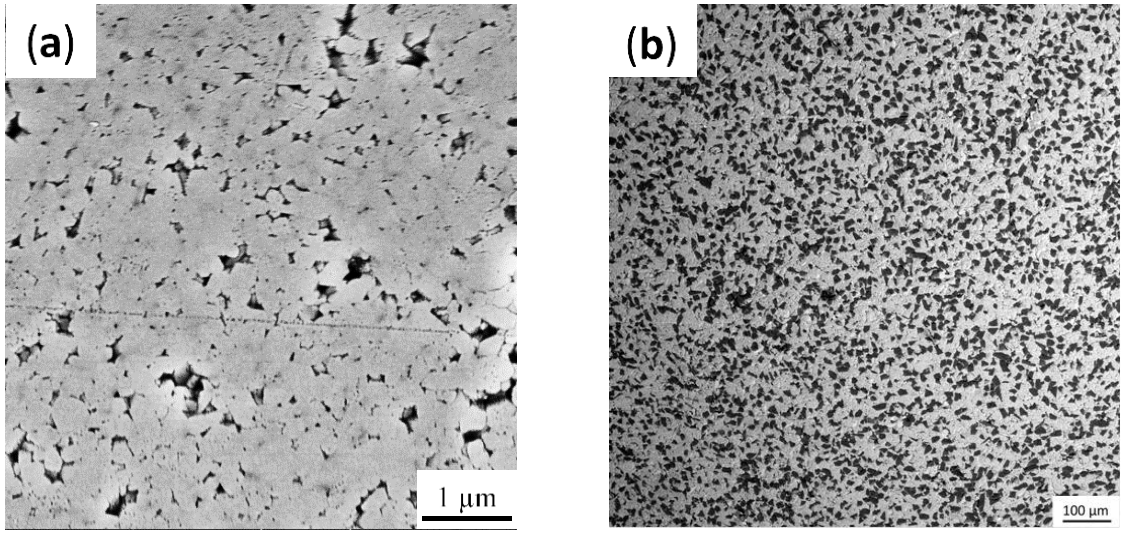

Figure 44 Back-scattered electron (BSE) FESEM micrographs of alpha-sialon ceramics (a) without cBN reinforcement (sample 1P), and (b) with 30 wt. % cBN (sample 4P)

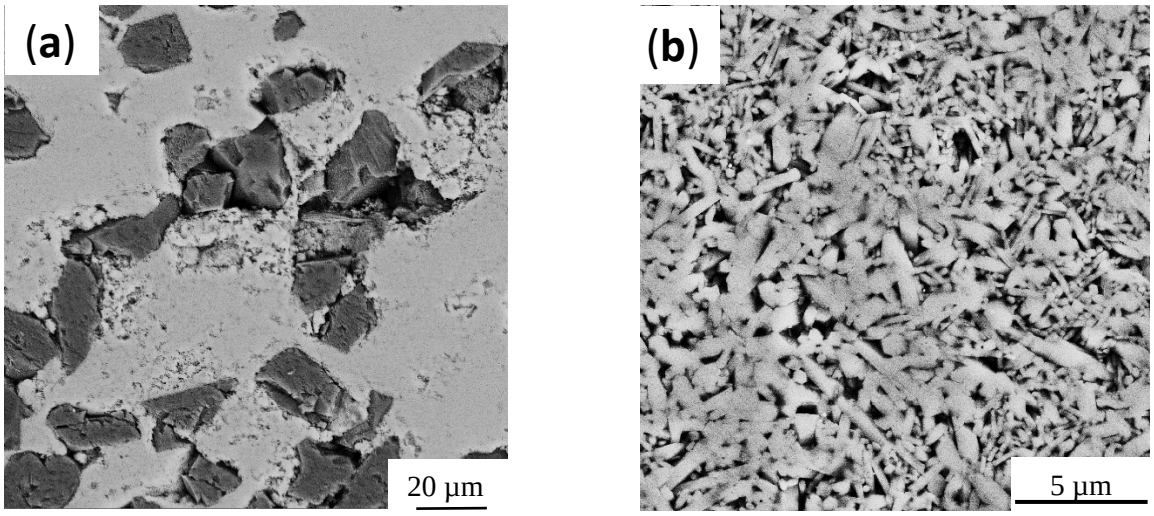

Figure 45 Back-scattered electron (BSE) FESEM micrographs of HEBM beta-sialon /hBN composite sample 7H. (a) The as-polished surface, revealing cracked hBN grains. (b) Etched surface, revealing the presence elongated beta phase structures.

7.2.5 Mechanical properties

Table 15 summarizes the results of mechanical tests of the pure sialon, as well as the cBN-reinforced sialon composites. For the samples prepared via sonication (samples 1P to 4P), addition of cBN was associated with an increase in Vickers hardness values, indicating a strengthened matrix. As the weight percent of cBN was increased from 0 to 30%, the hardness (H_{V10}) value increased from 21.6 GPa to 24.0 GPa. However, a decrease in fracture toughness with the increase in filler content was observed. A summarized list of mechanical properties representative of silicon nitride based materials is summarized in **Table 16**.

The composites prepared via high-energy ball milling (samples 5H to 7H) showed a decrease in hardness upon addition of cBN. The decrease in hardness was associated with the phase transformation from both hard alpha sialon to soft beta sialon and the transformation of the hard cBN phase to the soft hBN phase. However, the fracture toughness increased as cBN was added,

and this increase in fracture toughness is a typical characteristic of the elongated morphology of beta-sialon grains and the hBN phase.

Table 15 Mechanical properties of the samples.

Sample ID	Hardness - HV_{10} (GPa)	Fracture Toughness ($MPa \cdot m^{1/2}$)
1P	21.6 ± 0.6	7.30 ± 1.3
2P	21.8 ± 0.5	9.03 ± 0.8
3P	23.1 ± 0.6	6.70 ± 0.8
4P	24.0 ± 0.5	5.67 ± 0.9
5H	15.5 ± 0.4	7.95 ± 0.6
6H	11.6 ± 0.3	11.51 ± 0.9
7H	9.4 ± 0.6	12.46 ± 1.2

Table 16 Properties of silicon nitride based materials.

Material	HV_{10} (GPa)	K_{1c} ($MPa.m^{1/2}$)	Ref
α-Si_3N_4	<20	~3	[17]
β-Si_3N_4	<16	4-7	[17]
Y-α-Sialon	17.6-19.4	3.4-6.2	[71,72]
Ca-α-Sialon	17.7-19.8	4.4-5.6	[28]
Ca/Mg-α-Sialon	18.3-20.5	4.9-5.6	[28]
β sialon/cBN (10.wt %)	15.4	6.3	[146]
Y-α-Sialon/cBN (10.wt %)	21.0 (HV_5)	5.2	[148]
Y-α-Sialon /cBN (10.wt %)	15.9 (HV_5)	8	[148]
Commercial β-Sialon (Int.Syalon101)	14.7	7.7	[77]
Commercial α/β Sialon (Int. Syalon 050)	19.81	6.5	[78]

7.3 Conclusions

Sialon composites reinforced with cBN and prepared via two different mixing routes, probe sonication and High Energy Ball Mill (HEBM), were synthesized by using SPS at 1500 °C for 30 minutes under a constant pressure of 50 MPa. A uniform dispersion of the cBN particles in the sialon matrix was achieved by both mixing routes. The Ca-alpha-sialon/30%cBN composite showed a Vickers hardness (HV_{10}) of 24 GPa, greater than the 21.6 GPa Vickers hardness of the pure alpha-sialon matrix. In our work probe-sonicated calcium-stabilized alpha-sialon/cBN composites showed remarkable mechanical properties. The smaller particle size of the alpha-forming precursors from HEBM resulted in a partial phase transformation from alpha to beta sialon along with a simultaneous transformation of reinforcing cBN particles to the hexagonal BN phase due to a change in alpha to beta phase, formation of a liquid phase, and morphological changes of sialon. The observed effect of the size of precursor powders on the stability of alpha sialon at a temperature of 1500 °C is due to the higher oxide content associated with the higher specific surface area of the starting HEBM precursors.

CHAPTER 8

SYNTHESIS OF HARD AND TOUGH CALCIUM STABILIZED A-SIALON/SIC CERAMIC COMPOSITES USING NANO-SIZED PRECURSORS AND SPARK PLASMA SINTERING

Summary

SiC-reinforced Ca-α-Sialon ceramic composites were synthesized using nano-sized precursors and spark plasma sintering at 1500 °C for 30 min by adding 10, 20 and 30 wt. % of SiC into the Sialon matrix. Almost complete densification was achieved for all the samples. The second-phase SiC particles were found to be homogeneously dispersed in the α-Sialon matrix. The effects of the amount of loaded SiC on the mechanical properties of the ceramic composites were studied. A remarkable combination of hardness and toughness values, specifically 24.53 GPa (HV_{10}) and 11.0 $MPa.m^{1/2}$, respectively, was obtained for the composite ceramic containing 30 wt.% SiC, whereas hardness and fracture toughness values of only 21.1 GPa (HV_{10}) and 7.3 $MPa.m^{1/2}$, respectively, were obtained for the monolithic α-Sialon ceramic. The increase in fracture toughness was fairly attributed to the crack deflection, crack bridging and grain pullout mechanisms caused by the finely dispersed SiC particles.

Graphical Abstract

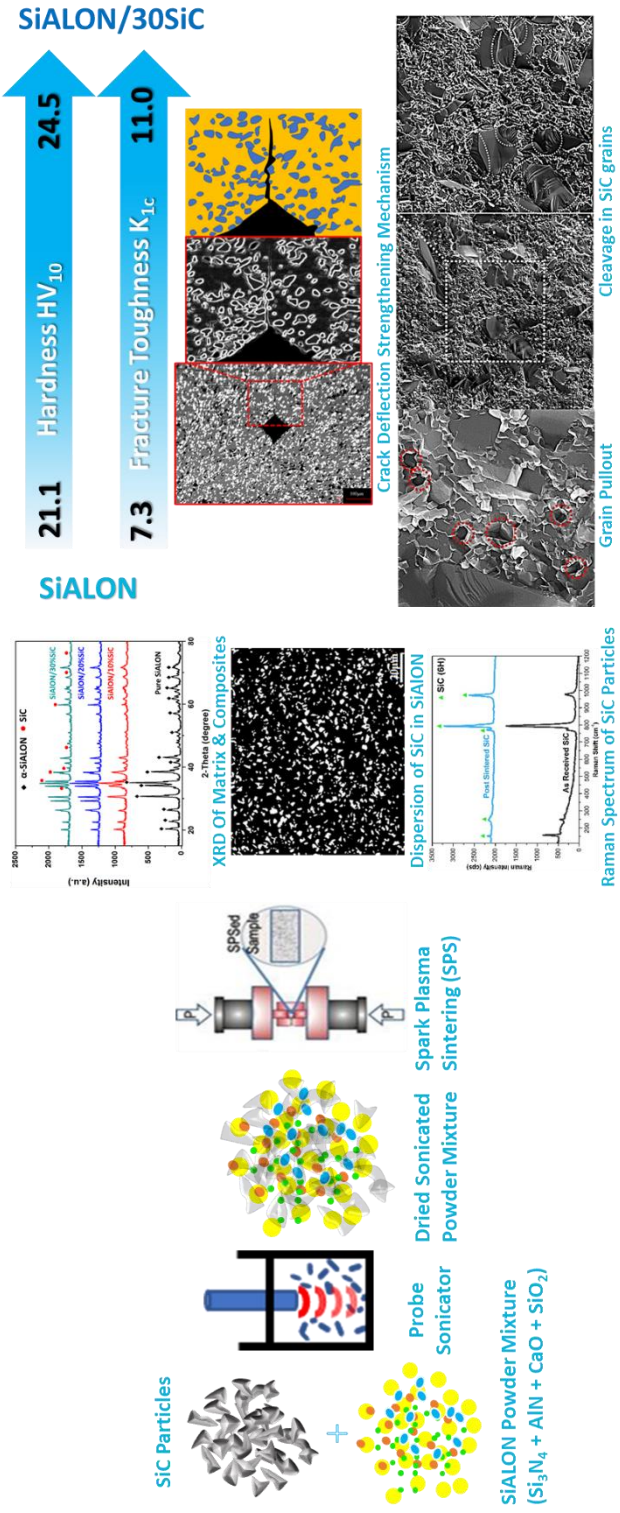

8.1 Introduction

Silicon nitride (Si_3N_4)-based ceramics, such as Sialons, exhibit a remarkable combination of mechanical and thermal properties, particularly high fracture toughness, hot hardness and thermal shock resistance, which make them a suitable candidate to be used in harsh environments and high-temperature applications [155,38,156]. Sialon ceramics are regarded as solid solutions of Si_3N_4, in which some of the Si and N atoms are replaced by Al and O atoms, respectively [12,20,41,10]. Owing to their prominent mechanical properties, α-Sialon (having elevated hardness) and β-Sialon (having modest fracture toughness) have been the most investigated phases of Sialon ceramics during the past two decades [17,16].

We previously developed a single-phase α-Sialon ceramic from nano sized precursors using calcium oxide as a sintering additive and utilizing spark plasma sintering for consolidation [93]. Due to the high solubility of calcium (Ca) in α-sialon, calcium oxide (CaO) as a sintering additive has shown to not only help stabilize the α-sialon phase [29,28], but also to help achieve well densified sialon ceramics at lower sintering temperatures of 1500 and 1600^{o}C [94]. Moreover, calcium compounds are relatively cheap as they could readily be obtained from many mineral resources such as fly ash [34]. The use of spark plasma sintering (SPS) has garnered active attention in the synthesis of ceramic materials due to its higher heating rate and its novel pulsed-current-based heating, assisting in the compaction of ceramics at temperatures lower than those of conventional consolidation techniques [37,157].

One of the methods developed to enhance the mechanical properties of monolithic ceramics involves the addition of second-phase particulates to the matrix, forming ceramic composites. W.-L. Wang et.al has reported work on the improvement of mechanical properties of alumina ceramic by incorporating boron nitride nanotubes [158]. J. Zhang et. al in a study on alumina-cBN

composites revealed that addition of metals like Al or Ni results in strengthening the matrix-reinforcement interfacial bonding and consequently the hardness of the composites [159]. Bilal et. al in their work on calcium-stabilized sialon/cBN nanocomposites, reported that the Vickers hardness (HV_{10}) of 24.0 GPa was achieved for alpha silaon reinforced with 30wt.% cBN, as compared to that of 21.6 GPa for the pure alpha sialon matrix [91]. In an effort to improve the mechanical properties of monolithic alumina ceramics, Muzammil et.al reported that reducing matrix particle size to 150nm resulted in the improved hardness of 29GPa for Alumina(150nm)/30wt.% cBN composites [152]. Many efforts have been expended during the last two decades to improve the toughness and strength of ceramic materials. For example, adding TiB_2 particles to the alumina matrix has shown to improve the fracture toughness, hardness and wear resistance of the composite [160]. Similarly, mechanical properties such as wear resistance, cutting ability, hardness, transverse rupture strength and indentation resistance are reported to improve with the additionon of zirconia (20% by mass) into alumina ceramics [161]. The bending strength of alumina ceramic having one weight percent of multi-walled carbon nanotubes as a reinforcement, is reported to be about 10% greater than that of monolithic alumina [98,162].

An effective method to improve the flexure strength and toughness of the alumina matrix involves adding SiC particles with a range of particle sizes to the matrix [163]. Likewise, adding second-phase particles such as silicon carbide (SiC) to hard monolithic α-sialon ceramics may be a way to further enhance the fracture toughness and wear resistance of composite ceramics without deteriorating any of their mechanical properties [164].

However, various researchers failed to successfully develop such composites with higher fracture toughness values due to the malfunctioning of self-toughening mechanisms particularly in composites with higher weight fractions of SiC [165,92,166]. This reduction in fracture toughness

was attributed to inhibition of anisotropic grain growth. The sintering techniques such as gas-pressure sintering, hot-pressing and liquid phase sintering owing to their lower heating rates have also resulted in the deprivation of elongated grains [165,166].

In recent years, Limeng Liu et al. employed spark plasma sintering at 1800 °C with Y_2O_3 as a sintering additive. They successfully obtained self-toughened microstructure in the α-sialon/α-SiC composites claiming elongation of both the sialon and SiC grains [38]. The elongation of the grains was attributed to the higher heating rates (100 °C/min in this case). However, they did not utilize nano-sized starting powders nor CaO as sintering additive and their sintering temperatures were very high (1800ºC).

In this study, previously reported calcium stabilized monolithic α-sialon prepared from nano precursors [93] is reinforced with micron-sized silicon carbide (SiC) particles and subjected to spark plasma sintering at a relatively low temperature of 1500ºC to develop α-sialon/SiC ceramic composites. Densification, phase formation and the resultant mechanical properties are evaluated and discussed.

The chemical composition selected for the matrix was $Ca_{0.8}Si_{9.2}Al_{2.8}O_{1.2}N_{14.8}$. **Table 17** shows the ID's of investigated samples along with the corresponding amounts (in wt. %) of reinforcement and nano-sized staring powder precursors (powder specifications are mentioned in chapter 3). As-received SiC powder with an average particle size of 11 μm was high energy ball milled and the particle size after milling was estimated to be 2 μm which was based on five measurements acquired using a Microtrac particle size analyzer (Model S3500/Turbotrac). **Figure 46 (a&b)** depicts the SEM micrographs of the as received and ball milled SiC particles. A plot of the dynamic light scattering (DLS) showing the detailed size distribution of the SiC particles after ball milling

is shown in **figure 47**. Mixture of composites prepared using ultrasonic probe sonicator (procedure mentioned in chapter 3) were sintered using spark plasma sintering (SPS) at 1500°C for 30 min.

Table 17 Amounts in wt. % of chemical powder reactants mixed with SiC reinforcement to synthesize $Ca_{0.8}Si_{9.2}Al_{2.8}O_{1.2}N_{14.8}$/SiC ceramic composites.

Compositions	**$Ca_{0.8}Si_{9.2}Al_{2.8}O_{1.2}N_{14.8}$**				**SiC**
	α-Si_3N_4	**AlN**	**CaO**	**SiO_2**	
0SiC	71.07	19.37	7.57	2.03	0
10SiC	63.96	17.43	6.81	1.83	10
20SiC	56.86	15.50	6.06	1.62	20
30SiC	49.75	13.56	5.30	1.42	30

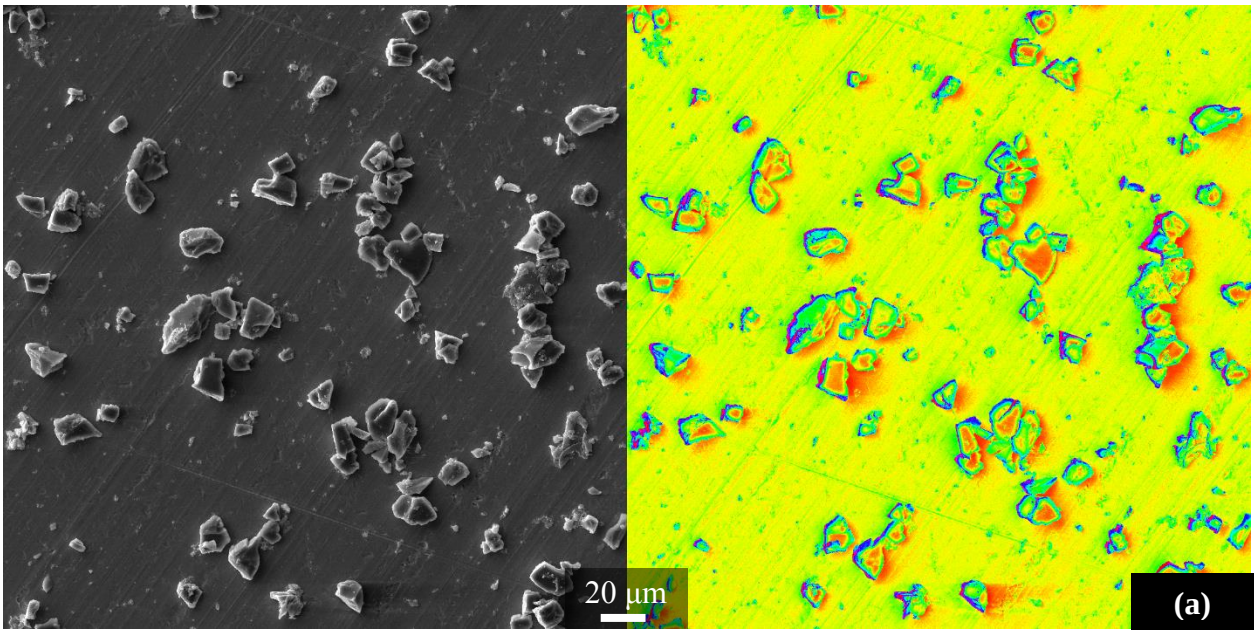

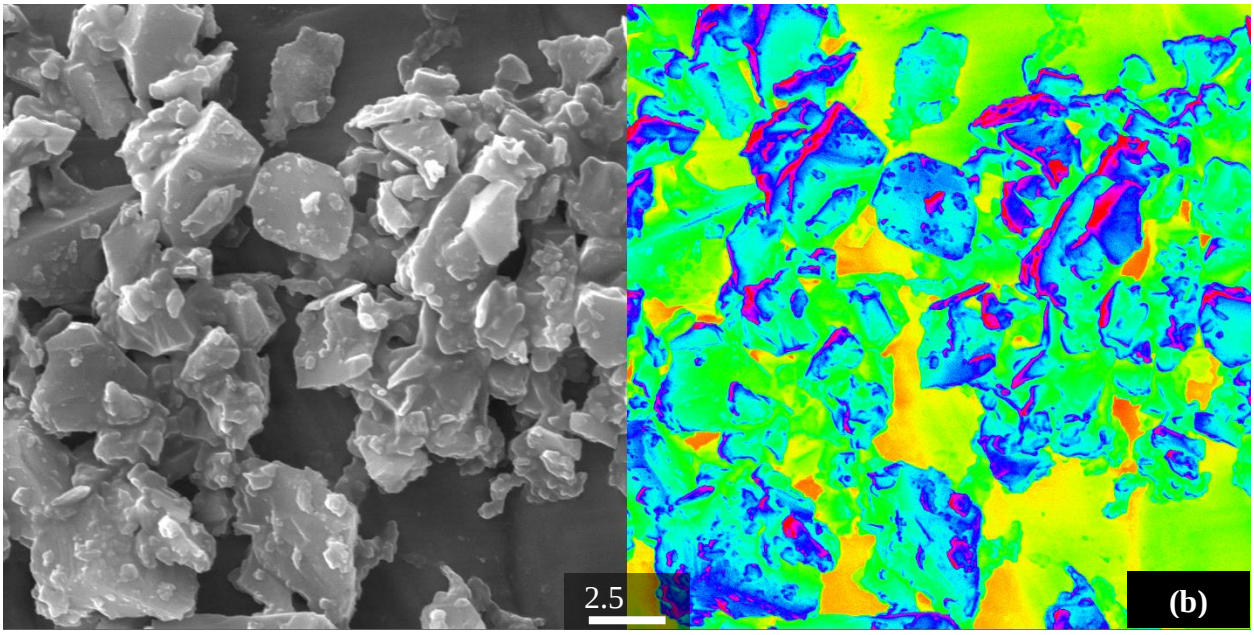

Figure 46 Secondary electron (SE) and coloured micrographs of SiC partiless **(a)** in as received condition **(b)** post ball milling condition.

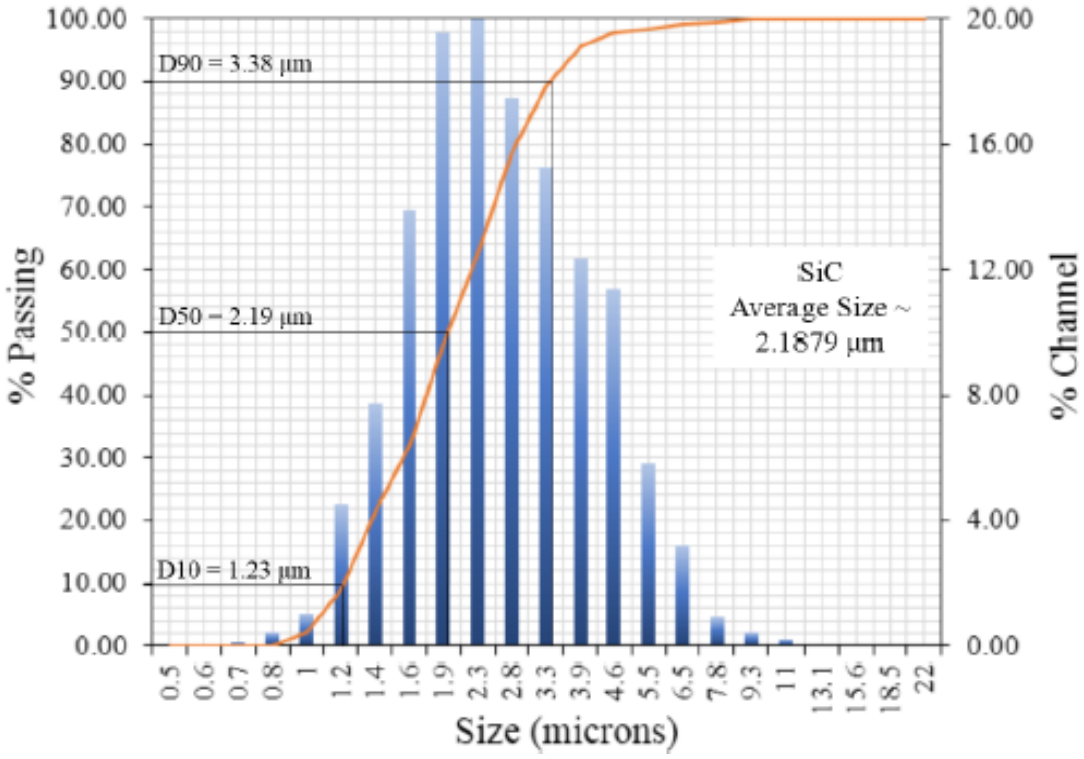

Figure 47 DLS-determined particle size distribution of SiC particles after high-energy ball milling.

8.2 Results and Discussion

8.2.1 Sintering and Densification

The experimental and calculated densities along with the densification level for all the samples are shown in **Table 18**. Considering the reported density values of 3.07g/cm^3 and 3.17g/cm^3 at 1700^{o}C and 1750^{o}C, respectively, for dense hot-pressed oxygen rich calcium alpha-sialon (having a composition of $Ca_{0.5}Si_{10.5}Al_{1.5}O_{0.5}N_{15.5}$) [25], pure α-sialon sample (0SiC) having a measured density of 3.19g/cm^3 is presumed to be as fully densified. The calculated densities in **Table 18** were estimated using the rule of mixture, taking the constituent phase densities of pure α-sialon and reinforced SiC as 3.19 g/cm^3 and 3.21 g/cm^3 respectively [167]. Comparing the experimental and theoretical densities suggested that the sintered samples had reached a percent densification greater than 99.9 %. The inherently high heating rates employed during the synthesis appeared to account for the effectiveness of SPS in achieving rapid and complete densification even at a relatively low temperature. However, a slight decrease in density was noticed in samples with higher loading of SiC particles. Similar trends have been reported in Sialon/cBN composites where the density of Sialon/cBN composites is seen to have decreased with increase in amount of cBN reinforcements [91,146,148].

Table 18 Density values of α-sialon/SiC ceramic composite samples sintered at 1500°C with a 30 min holding time.

Sample ID	**0SiC**	**10SiC**	**20SiC**	**30SiC**
Experimental density (g/cm^3)	3.19	3.191	3.192	3.193
Calculated density (g/cm^3)	--	3.191	3.193	3.195
Percentage densification	--	99.99	99.97	99.95

8.2.2 Phase Structure

Figure 48 shows the X-ray diffraction (XRD) pattern of monolithic α-sialon, denoted as **0SiC**, along with the patterns of the 10 wt. %, 20 wt. % and 30 wt. % α-sialon/SiC ceramic composites. The pattern for the 0 wt. % SiC sample indicates that the sample comprise of single-phase α-sialon ($Ca_{0.68}Si_{9.96}Al_{2.04}O_{0.68}N_{15.32}$). For the composite samples, peaks corresponding to SiC phase (polytype 6H) are detected, where the intensities of these peaks are observed to increase with higher amount of reinforcement. Moreover, no peaks other than those belonging to the incorporated SiC particles and α-sialon matrix are to be found. These XRD results indicate that there wasn't any post sintering polymorphic change in the starting SiC (6H polytype) particles. Furthermore, had there been any reaction between the matrix and SiC particles during the synthesis process, the reaction product/s (beyond the detection limit of XRD or amorphous in nature) were not detected by XRD.

Raman analysis of the SiC particles before (as received) and after sintering process (embedded in 30SiC sample) is shown in **figure 49**. Normally, SiC polytypes (6H, 4H and 15R) are distinguished with the aid of Raman peak values at ~151cm^{-1} for 6H, 203cm^{-1} for 4H and 171cm^{-1} for 15R [168]. The presence of peak at ~153.08cm^{-1} for both as received and post-sintered SiC particles confirm that the sintering conditions has not caused any polymorphic transformation for the 6H SiC particles (**see figure 49 a and b**).

It should also be noted that the lack of a phase transformation of SiC is due to the relatively low processing temperatures of 1500°C. In our final assembly, α-SiC (6H) remained same as the initial SiC (6H), which perhaps is due to the thermodynamic stability of α-SiC up to a temperature of as high as 2100°C [155].

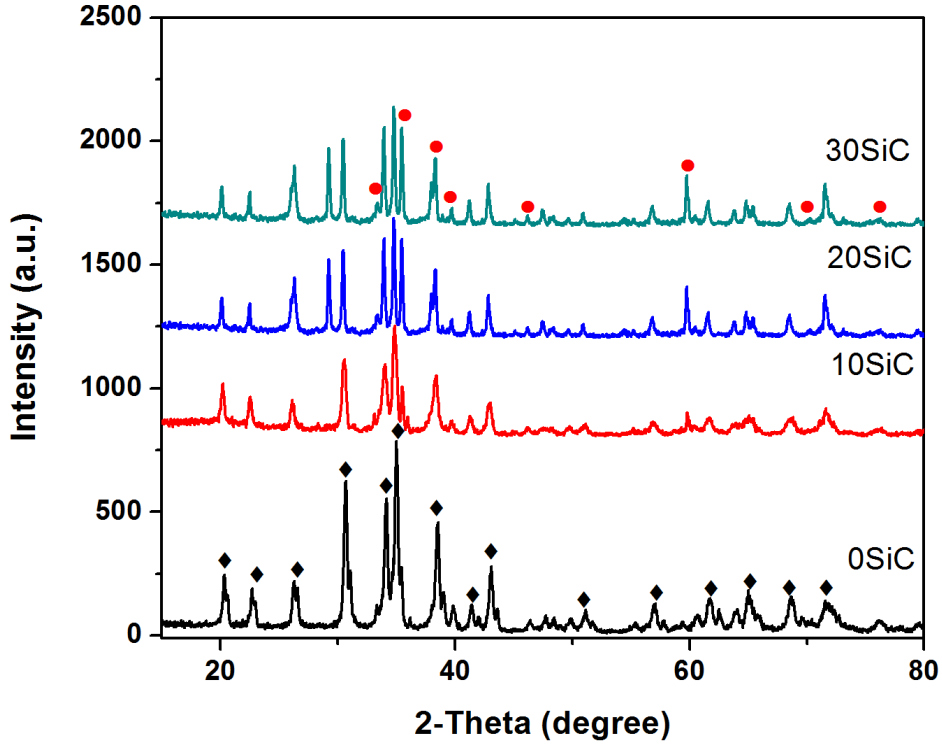

Figure 48 XRD patterns of monolithic α-sialon, and 10 wt. %, 20 wt. % and 30 wt. % α-sialon/SiC ceramic composites. (♦) α-sialon ($Ca_{0.68}Si_{9.96}Al_{2.04}O_{0.68}N_{15.32}$) and (●) SiC.

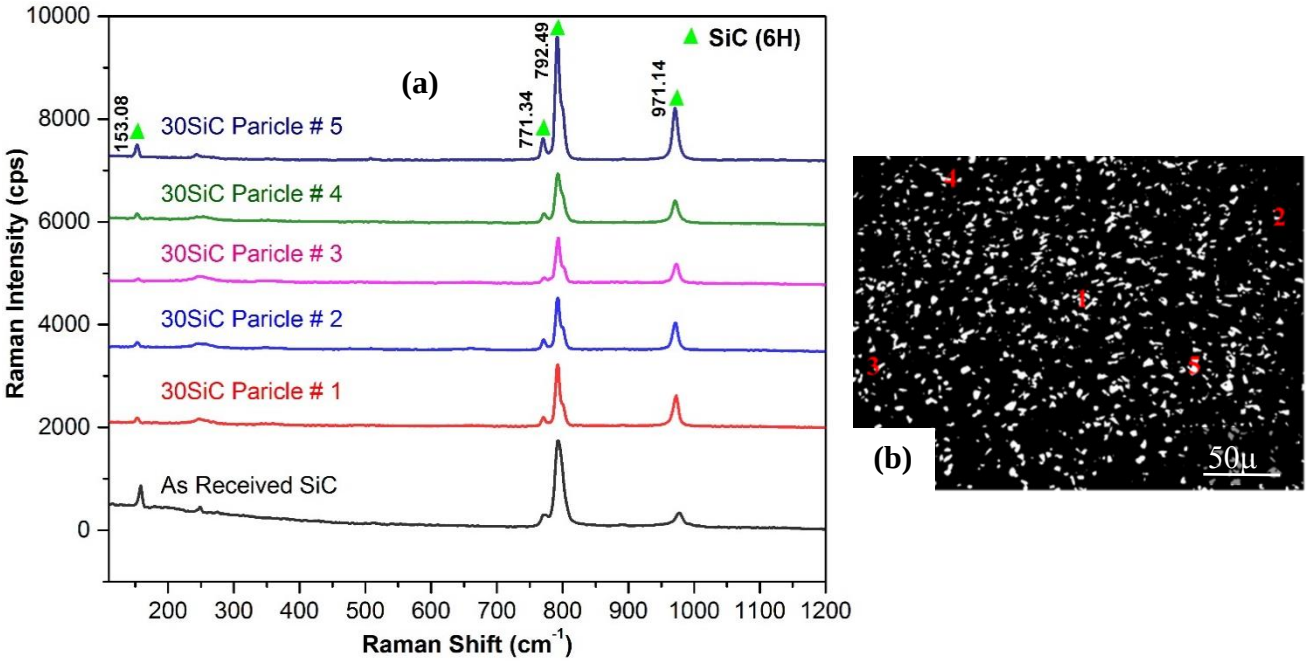

Figure 49 (a) Raman spectrum of as received and post sintered (Sample 30SiC) SiC particles, **(b)** Optical image of 30SiC sample representing the particles from which Raman spectrum is acquired.

8.2.3 Microstructure Evaluation

Figure 50 (a), **(b)** and **(c)** show the optical micrographs acquired from the polished surfaces of the samples 10SiC, 20SiC and 30SiC respectively. The uniform distribution of white SiC particles in the black alpha Sialon matrix confirms that ultrasonic probe sonication was sufficient to achieve adequate level of homogeneity of second phase particles.

Figure 51 shows the secondary electron micrograph of 30SiC sample (polished condition) acquired at low accelerating voltage of 5kV. At high accelerating voltages the signal from the matrix suppressed signals from the SiC particles. Although, not very clear but the dispersion of SiC was relatively evident at 5kV. EDX point analysis of thirteen particles acquired (at 5kV) from the same region confirmed all of them to be SiC (EDX spectrum for one particle is shown in **figure 51b**).

Figure 52 (a-c) shows micrographs of fractured surfaces of 0SiC and 30SiC samples. In the image **(figure 52a)** of sample 0SiC (with no reinforcements and a relatively low fracture toughness), classical intergranular type of fracture without any tearing of grains is not observed. The red circles shown in **figure 52b**, for sample Id: 30SiC, represent grain pullout. The pullout could either be of SiC or matrix grains. As shown in **figure 52c** presence of sharp step like features inside the SiC grains representative of cleavage or delamination is very obvious (see white circles in the magnified view). Such grain pull out and cleavage steps have been reported as an important factors in enhancing the fracture toughness of the ceramic composites having higher amounts of SiC [170–172].

We performed the Vickers indentation test on the monolithic α-sialon sample (0SiC) and sample with 30 wt.% of SiC (30SiC), and the indents recorded for the said samples are shown in the

micrographs of **figure 53 (a, b) and (c, d)**, respectively**.** Micrograph for sample 0SiC reveals cracks that are apparently growing rapidly with no notable deflections along the path of the crack propagation **(figure 53b)**. In contrast, the indentation on sample 30SiC yielded cracks showing multiple deflections, and in the higher-magnification images **(figure 53d)**, crack bridging is observed. Crack bridging can occur where the stress intensity at the crack is reduced by bowing of the crack and the grains remain intact behind the crack [173]. Apparently the crack bridging phenomenon also helped in enhancing the fracture toughness of the composite samples [174].

Moreover, indent on the un-etched polished sample with 30 wt. % of SiC (30SiC) as observed under light microscope is shown **Figure 54a**. The magnified image along with the schematic representation of the same **(figure 54 b and c)** provides a clear evidence of SiC particles deflecting the crack. We can fairly say that irrespective of the variation in size, uniformly distributed hard SiC particles force the crack to change its directions, and hence slowed down the propagation of the crack. Such crack deflection along with crack bridging, grain pullout and delamination have contributed considerably to the increase the fracture toughness of the composite samples[175].

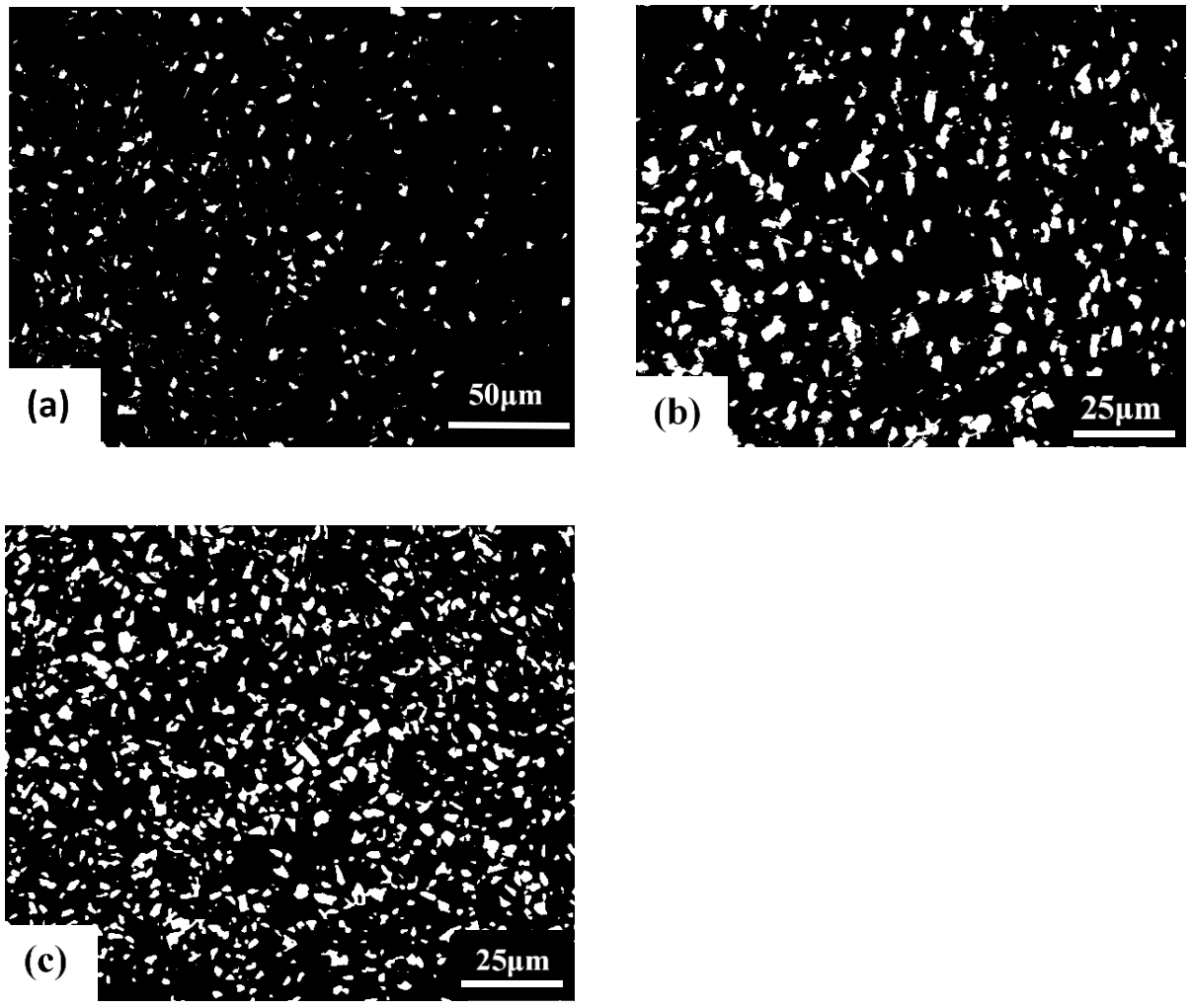

Figure 50 Optical micrographs of **(a)** 10SiC, **(b)** 20SiC and **(c)** 30SiC samples.

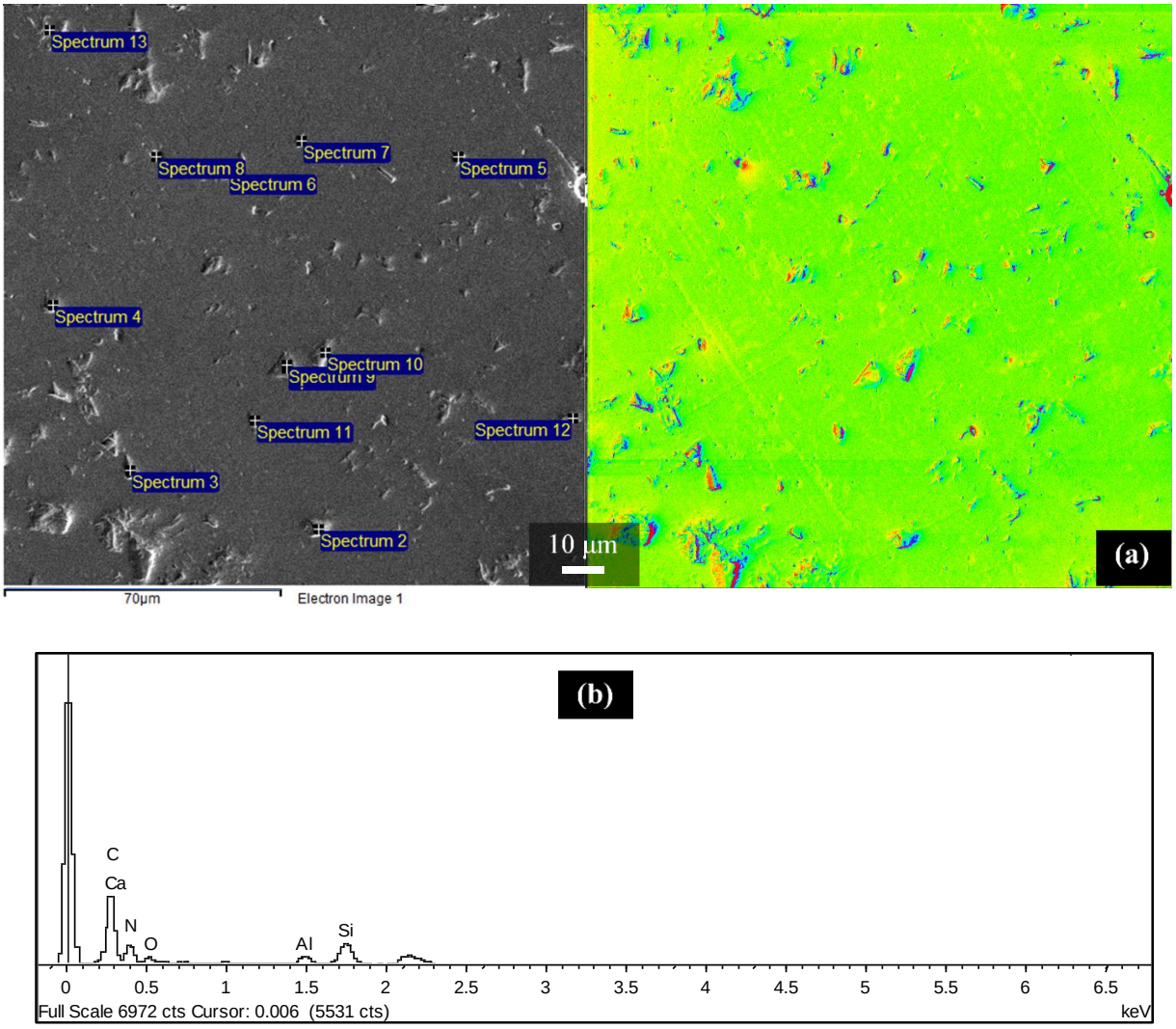

Figure 51 (a) secondary electron micrograph of 30SiC sample and **(b)** EDX spectrum for a SiC particle acquired at low accelerating voltage of 5kV.

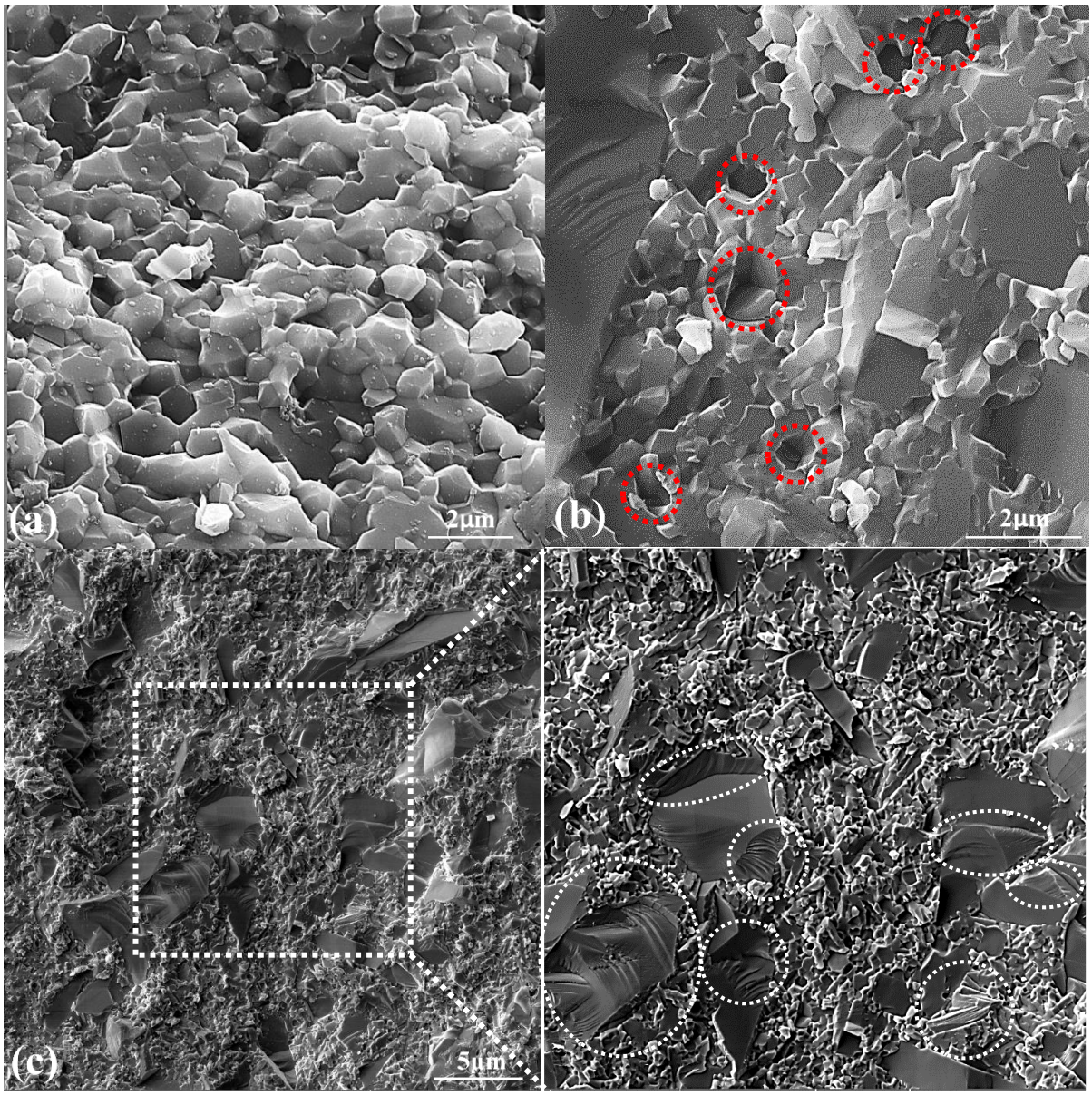

Figure 52 Fracture surface micrographs of (a) monolithic α-sialon acquired in SE mode, (b) 30 wt.% α-sialon/SiC ceramic composite acquired in SE mode at an accelerating voltage of 20kV and (c) 30 wt.% α-sialon/SiC ceramic composite acquired in SE mode at an accelerating voltage of 5kV.

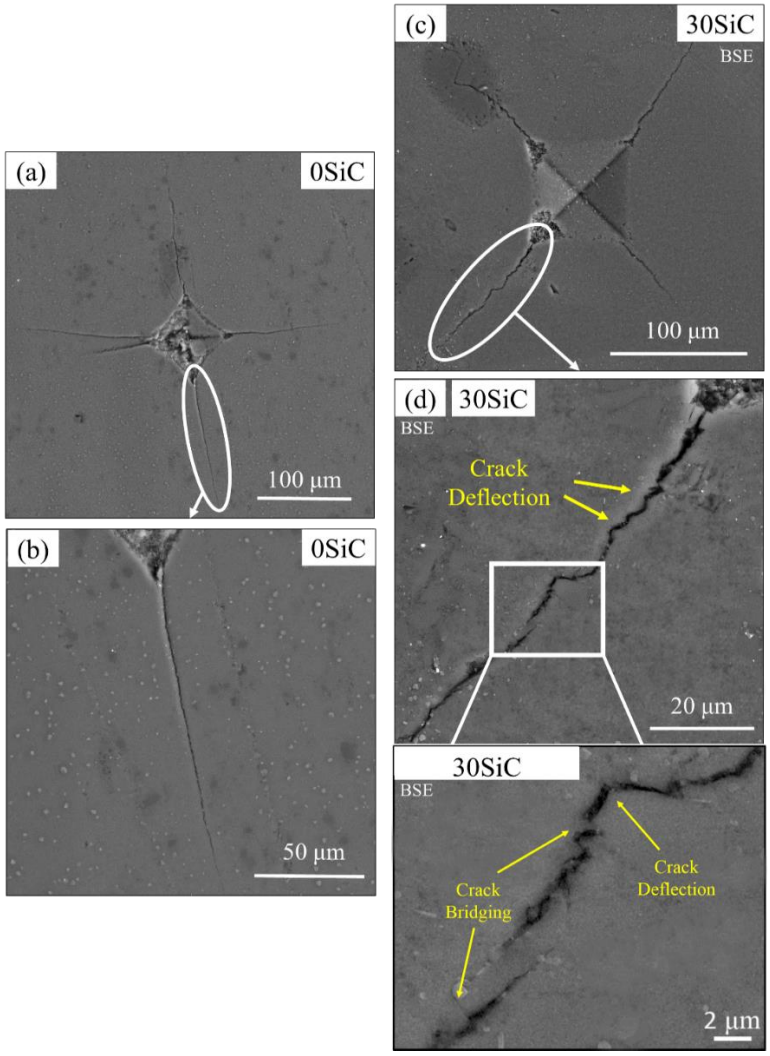

Figure 53 BSE images comparing indentations and crack propagations in **(a, b)** monolithic α-sialon indicate nearly a straight line and in **(c, d)** the 30 wt. % α-sialon/SiC composite indicate multiple deflections due to the presence of SiC particles.

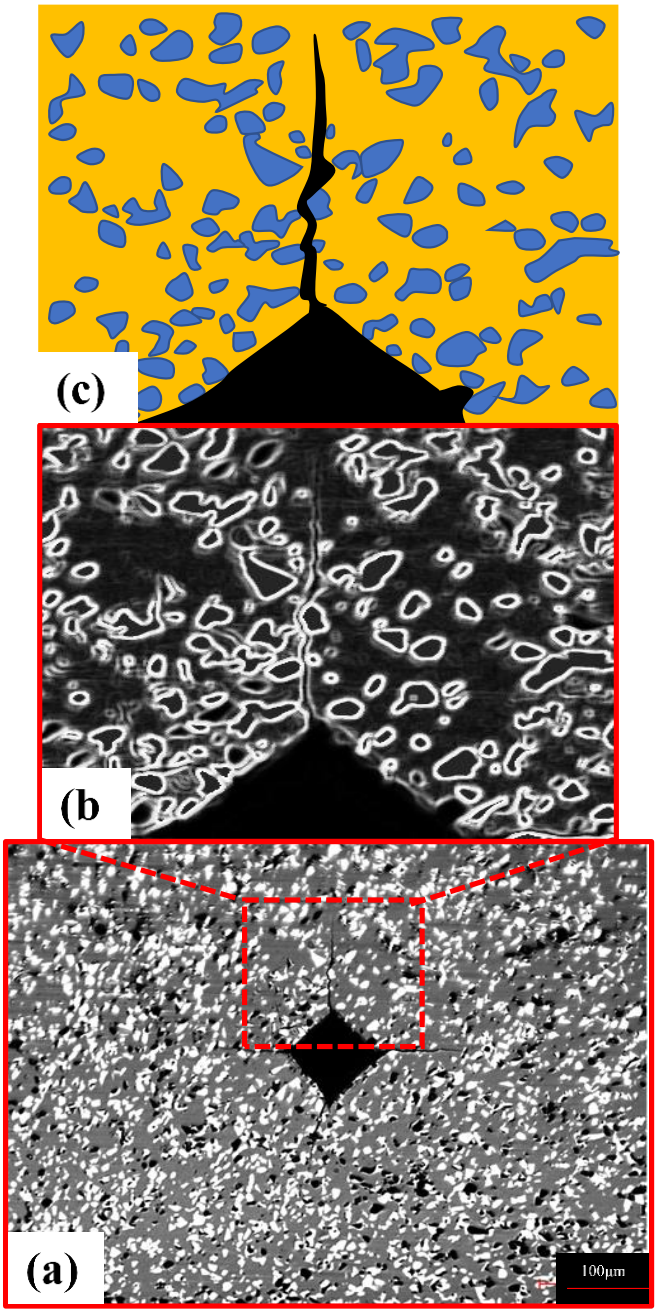

Figure 54 (a) Optical micrograph of the Vickers hardness indent recorder for sample 30SiC and **(b)** represents the magnified image being processed to show crack initiation and propagation zone and **(c)** schematic representation of the magnified image in (b),The crack deflection by SiC particles can be clearly observed

8.2.4 Mechanical Properties

Vickers hardness (HV_{10}) and fracture toughness (K_{1C}), of the reinforced composite ceramics are shown in **Table 19.** Low temperature synthesis of Ca-α-SIALON matrix using nano precursors, reinforced with SiC particles, yielded remarkable mechanical properties as compared to the already reported data for the similar systems (a summarized literature is presented in **Table 20**). Sialons have usually been reported to be sintered at quite high temperatures (1700 or 1800^{o}C), however in present case, very hard and tough ceramics are being developed at a relatively low temperature of 1500^{o}C, primarily due to the nano sizes of the starting powder precursors. The hardness is seen to increase with increasing amounts of SiC reinforcement, and apparently, this trend is due to the relatively high hardness of SiC as well as its uniform distribution throughout the sialon matrix [169]. Including 30 wt. % of SiC in monolithic α-sialon resulted in 16 % and 63 % increases in the hardness and fracture toughness values, respectively. Such increase represents a promising achievement of the present work.

Table 19 Mechanical properties of α-sialon/SiC ceramic composites.

Sample ID	**0SiC**	**10SiC**	**20SiC**	**30SiC**
HV_{10} (GPa)	21.1 ± 0.4	21.5 ± 0.3	23.1 ± 0.4	24.5 ± 0.2
K_{IC} (MPa.m$^{1/2}$)	7.3 ± 0.8	9.1 ± 0.7	10.5 ± 0.3	11.0 ± 0.5

Table 20 Mechanical Properties of Si_3N_4 based materials.

Material	**HV_{10} (GPa)**	**K_{1c} (MPa.m$^{1/2}$)**	**Ref**
α-Si_3N_4	<20	~3	[17]
β-Si_3N_4	<16	4-7	[17]
Y-α-Sialon	17.6-19.4	3.4-6.2	[170,71]
Ca-α-Sialon	17.7-19.8	4.4-5.6	[28]
Ca/Mg-α-Sialon	18.3-20.5	4.9-5.6	[28]
Commercial β-Sialon (Int.Syalon101)	14.7	7.7	[77]
Commercial α/β Sialon (Int. Syalon 050)	19.81	6.5	[78]

β sialon/cBN (10.wt %)	15.4	6.3	[146]
Y-α-Sialon /SiC (5-40.wt %)	19.9-22.8	5.6-8.2	[38]
Y-α-Sialon /SiC (80.wt %)	19.1-21.7	3.9-4.5	[176]
Y-α-Sialon /SiC (40.wt %)	22.2	8.5	[177]
Y-α-Sialon/cBN (10.wt %)	21.0 (HV_5)	5.2	[148]
Ca-α-Sialon /cBN (30.wt %)	24.0	5.7	[91]

8.3 Conclusions

The synthesis, densification, and mechanical properties of α-sialon/SiC composite ceramics were investigated. These composites consisted of a Ca-α-sialon matrix reinforced with 10, 20 or 30 wt. % of a SiC particles. These samples were prepared from nano--sized precursors (matrix) and were made by applying spark plasma sintering (SPS) at 1500 °C for 30 min. Their densities were close to the respective theoretical densities, revealing that rapid densification could be achieved at a relatively low temperature due to the inherent capabilities provided by SPS.

The dispersions of second-phase particles with in the Sialon matrix was found to be quite uniform. The nature of the SiC in the final assembly remained the same as that of the as received SiC, i.e. no evidence of a polymorphic phase transformation of SiC was witnessed.

The Vickers hardness and fracture toughness values of the sintered ceramics were measured, and found to increase as the amount of SiC in the ceramic increased (from 10 to 30 wt.%). The increased fracture toughness was attributed to the introduction and availability of toughening mechanisms such as crack deflection, crack bridging, grain pull-out and cleavage fracture of SiC particles, while the increased Vickers hardness was attributed to the quite uniform dispersion and high hardness of the reinforcing particles as well as to the good consolidation resulting from the use of SPS and in particular from the incorporation of the nano sized precursors.

For α-sialon composites reinforced with SiC (2 μm) particles, the highest hardness value of 24.53 GPa (HV_{10}) and highest fracture toughness value of 11.0 $MPa.m^{1/2}$ were achieved for the composite containing 30 wt. % of SiC. In contrast, the monolithic α-sialon ceramic showed a hardness value of only 21.1 GPa (HV_{10}) and a fracture toughness value of only 7.3 ($MPa.m^{1/2}$).

Chapter 9

Conclusions and Recommendations

9.1 Conclusions

In the first part of this thesis, Ca-stabilized alpha sialon samples were synthesized from aluminum nitride (AlN) precursors of particle sizes of 50 nm and 1 μm using spark plasma sintering (SPS) at 1500°C. Alpha sialon phase was observed in all samples. The formation of alpha sialon in the sample produced from nano-sized AlN particles most likely resulted from the formation of large amount of liquid phase due to the high reactivity of AlN. However, incomplete dissolution of micron sized AlN precursor at 1500°C restricted the completion of intended reaction and hence the complete development of alpha sialon.

Calcium stabilized nitrogen rich sialons having compositions along the Si_3N_4-1/2Ca_3N_2:3AlN line were synthesized at sintering temperature of 1500°C. Enhanced reaction kinetics due to nano size precursors and high heating rates achieved with aid of non-conventional SPS process helped in development of well densified nitrogen rich sialon ceramics. Alpha sialon phase for the samples having Ca content (x) in the range of $0.15<x<1.83$ was obtained. Formation of single phase nitrogen rich alpha sialons was achieved for samples having nominal x value in the range of $0.4 < x < 1.6$. Increase in the lattice parameters of alpha sialon unit cell was observed to have a linear relationship with the amount of Ca^{+2} ions incorporated in the alpha structure. Increasing x value resulted in an increase in the average grain size from 286nm to 468nm. Moreover, higher amount of Ca_3N_2 starting powder was observed to facilitate the growth of elongated alpha sialon grains. Calcium stabilized nitrogen rich sialon ceramic having a very promising hardness and fracture toughness, of 22.4GPa and 5.7 $MPa.m^{1/2}$, respectively was developed. Furthermore, the absence

of a glassy grain boundary phase in nitrogen rich sialons makes them potentially viable candidates for high temperature application.

Several compositions of magnesium (Mg) doped nitrogen rich sialon ceramic samples having the x value in the range of 0.2-2.2 were synthesized. Nano sized starting powder precursors along with SPS technique enhanced the reaction kinetics and thus helped achieve well densified sialon ceramic samples at comparatively low temperature of 1500°. Unlike other sialon systems, it was observed that a single phase magnesium stabilized alpha sialon didn't form along the nitrogen rich line Si_3N_4-1/2Mg_3N_2:3AlN (on the Mg alpha sialon plane). The densification of the nitrogen rich samples as well as the formation of a stable alpha sialon phase became difficult at high x values (more Mg_3N_2 and AlN content). Initially with an increase in x value a corresponding increase in the lattice parameters of alpha sialon unit cell was observed. The maximum achieved content of magnesium cation in the alpha sialon unit cell was determined to be 1.08 (for x=1.6), however with any further increase in x value, increase in lattice parameters became negligible. Similarly, an increase in x value (0.6 to 1.0) induces an increase in the average grain size of alpha sialon, which in turn decreases for higher x values (1.0 to 1.4). The unique characteristics of magnesium doped nitrogen rich sialon ceramics can fairly be attributed to the formation and growth of Mg-containing polytype phase (for compositions having higher x value) at the expense of high temperature transient liquid phase which otherwise is essential for densification, formation and grain growth of alpha-sialons. Hardness and fracture toughness of 21.4 GPa and 3.5 MPa.$m^{1/2}$, respectively, was achieved for magnesium doped nitrogen rich sialon ceramics. Moreover, the absence of intergranular glassy phase in these materials, indicates a high temperature stability in addition to a reported high infrared transmittance.

Sialon/cBN and Sialon/SiC composites were prepared using SPS at 1500°C. The influence of the amount of reinforcement on the physical, structural and mechanical characteristics of the composites was studied.

For the composites, calcium-stabilized alpha-sialon/cBN composites showed remarkable mechanical properties. The Ca-alpha-sialon/30%cBN composite showed a Vickers hardness (HV_{10}) of 24.0 GPa, For alpha-sialon composites reinforced with SiC (2 μm) particles, the highest hardness value of 24.5 GPa (HV_{10}) and highest fracture toughness value of 11.0 MPa.$m^{1/2}$ were achieved for the composite containing 30 wt. % of SiC. In contrast, the monolithic alpha-sialon ceramic showed a hardness value of only 21.1 GPa (HV_{10}) and a fracture toughness value of 7.3 (MPa.$m^{1/2}$).

9.2 Contribution

The important contribution of this work to the existing literature is summarized below:

1. The novel approach of changing particle size from micro to nano level combined with the SPS process resulted in the formation of alpha-sialon ceramic at much lower than previously reported sintering temperature i.e. 1500^{o}C as compared to 1700/1800^{o}C.

2. Phase stability regime for the calcium stabilized nitrogen rich sialons was developed at temperature of 1500^{o}C. Well densified, glass free, nitrogen rich sialon ceramic materials, having Ca content (x) in the range of $0.15<x<1.83$ were synthesized. Single phase alpha sialon having a high hardness of 22.4GPa and a fracture toughness of 5.7 MPa.$m^{1/2}$ was developed.
3. An empirical relationship was developed between the lattice parameters (a &c) and the content (x) of alkaline metal cation (Ca^{+2}) in the alpha sialon unit cell.
4. Magnesium-doped nitrogen rich sialon ceramics were developed for the very first time.

5. Phase stability regime for the magnesium stabilized nitrogen rich sialon ceramic along the Si_3N_4-1/2Mg_3N_2:3AlN line was developed. Unlike other sialon systems, it was observed that a single phase magnesium stabilized alpha sialon doesn't exist along the nitrogen rich line. Magnesium doped nitrogen rich sialon sample having the maximum amount of alpha phase depicted remarkable hardness (HV_{10}) of 21.4GPa and a fracture toughness of 3.5 MPa.$m^{1/2}$.

9.3 Future Work

In light of the work performed under this thesis, it is recommended that development of phase boundary between alpha and alpha/beta phases and the boundary between alpha and AlN polytypes would be a good value addition to the already available literature. The development of the complete phase boundary of single phase calcium alpha sialon at 1500^oC would thus be a significant scientific addition to the existing literature and would offer a guide map to synthesize low temperature, economically more favorable, sialon phase/phases along with corresponding mechanical properties to meet the desired requirements for a variety of applications.

References

[1] F.L. Riley, Silicon Nitride and Related Materials, J. Am. Ceram. Soc. 83 (2004) 245–265.

[2] S. Hampshire, Silicon Nitride Ceramics, Mater. Sci. Forum. 606 (2009) 27–41.

[3] Stuart Hampshire, Role Of Additives In The Pressureless Sintering Of Nitrogen Ceramics For Engine Applications, Met. Forum. 7 (1984).

[4] G.E. Gazza, Hot-Pressed Si_3N_4, J. Am. Ceram. Soc. 56 (1973) 662–662.

[5] R.E. Loehman, D.J. Rowcliffe, Sintering of Si_3N_4-Y_2O_3-Al_2O_3, J. Am. Ceram. Soc. 63 (1980) 144–148.

[6] K.S. Mazdiyasni, C.M. Cooke, Consolidation, Microstructure, and Mechanical Properties of Si_3N_4 Doped with Rare-Earth Oxides, J. Am. Ceram. Soc. 57 (1974) 536–537.

[7] K. Negita, Effective sintering aids for Si3N4 ceramics, J. Mater. Sci. Lett. 4 (1985) 755–758.

[8] Y.R. Xu, X.R. Fu, D.S. Yan, Creep behavior of hot-pressed silicon nitride ceramics with rare-earth oxides and alumina additives, Phys. B+C. 150 (1988) 276–282.

[9] N. Hirosaki, A. Okada, K. Matoba, Sintering of Si3N4 with the Addition of Rare-Earth Oxides, J. Am. Ceram. Soc. 71 (1988) C–144–C–147.

[10] S. Hampshire, H.K. Park, D.P. Thompson, K.H. Jack, α′-Sialon ceramics, Nature. 274 (1978) 880–882.

[11] Y. Oyama, O. Kamigaito, Solid Solubility of Some Oxides in Si_3N_4, Jpn. J. Appl. Phys. 10 (1971) 1637–1637.

[12] K.H. Jack, W.I. Wilson, Ceramics based on the Si-Al-O-N and Related Systems, 238 (1972) 28.

[13] C. Greskovich, C.R. O'Clair, Sialon Ceramics, US. Patent No. 93687, 1977.

[14] S. Prochazka, C. D. Greskovich, Development of a Sintering Process for High-Performance Silicon Nitride, AMMRC. (1987).

[15] F.F. Lange, Effect of Microstructure on Strength of Si3N4-SiC Composite System, J. Am. Ceram. Soc. 56 (1973) 445–450.

[16] V.A.A. Izhevskiy, L.A.A. Genova, J.C.C. Bressiani, F. Aldinger, Progress in SiAlON ceramics, J. Eur. Ceram. Soc. 20 (2000) 2275–2295.

[17] T. Ekstrom, M. Nygren, SiAION Ceramics, J. Am. Ceram. Soc. 75 (1992) 259–276.

[18] I.H. Shin, D.J. Kim, Growth of elongated grains in α-SiAlON ceramics, 2001.

[19] I.-W. Chen, A. Rosenflanz, A tough SiAlON ceramic based on |[alpha]|-Si_3N_4 with a

whisker-like microstructure, Nature. 389 (1997) 701–704.

[20] K.H. Jack, Sialons and related nitrogen ceramics, J. Mater. Sci. 11 (1976) 1135–1158.

[21] H. Mandal, New developments in α-SiAlON ceramics, J. Eur. Ceram. Soc. 19 (1999) 2349–2357.

[22] G. Pezzotti, T. Wakasugi, T. Nishida, R. Ota, H.-J. Kleebe, K. Ota, Chemistry and inherent viscosity of glasses segregated at grain boundaries of silicon nitride and silicon carbide ceramics, J. Non. Cryst. Solids. 271 (2000) 79–87.

[23] Z.-K. Huang, T.-Y. Tien, Solid-Liquid Reaction in the System Si_3N_4-$Y_3Al_5O_{12}$-$Y_2Si_2O_7$ under 1 MPa of Nitrogen, J. Am. Ceram. Soc. 77 (1994) 2763–2766.

[24] S. Bandyopadhyay, M.. Hoffmann, G. Petzow, Effect of different rare earth cations on the densification behaviour of oxygen rich α-SiAlON composition, Ceram. Int. 25 (1999) 207–213.

[25] Z.-K. Huang, P. Greil, G. Petzow, Formation of alpha-Si3N4 Solid Solutions in the System Si_3N_4-A1N-Y_2O_3, J. Am. Ceram. Soc. 66 (1983) C–96–C–97.

[26] Z.-K. Huang, W.-Y. Sun, D.-S. Yan, Phase relations of the Si_3N_4-AIN-CaO system, J. Mater. Sci. Lett. 4 (1985) 255–259.

[27] P.L. Wang, C. Zhang, W.Y. Sun, D.S. Yan, Characteristics of Ca-α-sialon—Phase formation, microstructure and mechanical properties, J. Eur. Ceram. Soc. 19 (1999) 553–560.

[28] P.L. Wang, C. Zhang, W.Y. Sun, D.S. Yan, Formation behavior of multi-cation α-sialons containing calcium and magnesium, Mater. Lett. 38 (1999) 178–185.

[29] P.. Wang, Y.. Li, D.. Yan, Effect of dual elements (Ca, Mg) and (Ca, La) on cell dimensions of multi-cation α-sialons, J. Eur. Ceram. Soc. 20 (2000) 1333–1337.

[30] Y. Menke, V. Peltier-Baron, S. Hampshire, Effect of rare-earth cations on properties of sialon glasses, J. Non. Cryst. Solids. 276 (2000) 145–150.

[31] M. Herrmann, S. Höhn, A. Bales, Kinetics of rare earth incorporation and its role in densification and microstructure formation of α-Sialon, J. Eur. Ceram. Soc. 32 (2012) 1313–1319.

[32] G.Z. Cao, R. Metselaar, G. Ziegler, Relations between composition and microstructure of sialons, J. Eur. Ceram. Soc. 11 (1993) 115–122.

[33] H. Mandal, D.P. Thompson, α→β Sialon Transformation in Calcium-containing α-SiAlON Ceramics, J. Eur. Ceram. Soc. 19 (1999) 543–552.

[34] J.W.T. Van Rutten, H.T.T. Hintzen, R. Metselaar, Densification behaviour of Ca-α-sialons, Ceram. Int. 27 (2001) 461–466.

[35] M. Belmonte, J. González-Julián, P. Miranzo, M.I.I. Osendi, Spark plasma sintering: A

powerful tool to develop new silicon nitride-based materials, J. Eur. Ceram. Soc. 30 (2010) 2937–2946.

[36] L. Liu, F. Ye, Y. Zhou, Z. Zhang, Q. Hou, Fast bonding α-SiAlON ceramics by spark plasma sintering, J. Eur. Ceram. Soc. 30 (2010) 2683–2689.

[37] D. Salamon, Z. Shen, P. Šajgalík, Rapid formation of α-sialon during spark plasma sintering: Its origin and implications, J. Eur. Ceram. Soc. 27 (2007) 2541–2547.

[38] L. Liu, F. Ye, Z. Zhang, Y. Zhou, Elongation of α-SiC Particles in Spark Plasma Sintered α-SiAlON/α-SiC Composites, J. Am. Ceram. Soc. 94 (2011) 336–339.

[39] R.R. Wills, I. Sekercioglu, D.E. Niesz, The Interaction of Molten Silicon with Silicon Aluminum Oxynitrides, J. Am. Ceram. Soc. 63 (1980) 401–403.

[40] Ekstrom Thommy; Kall P O; Nygren Mats; Olsson P O, Dense single-phase beta-sialon ceramics by glass-encapsulated hot isostatic pressinge, J.Mater.Sci. 24 (1989) 1853–61.

[41] G.Z. Cao, R. Metselaar, .alpha.'-Sialon ceramics: a review, Chem. Mater. 3 (1991) 242–252.

[42] D. Stutz, P. Greil, G. Petzow, Two-dimensional solid-solution formation of Y-containingα-Si3N4, J. Mater. Sci. Lett. 5 (1986) 335–336.

[43] S. Slasor, D.P. Thompson, Preparation and Characterization of Yttrium α'-Sialons, in: Non-Oxide Tech. Eng. Ceram., Springer Netherlands, Dordrecht, 1986: pp. 223–230.

[44] S. Slasor, D.P. Thompson, Two-dimensional solid solution formation of Y-containing α-Si_3N_4, J. Mater. Sci. Lett. 6 (1987) 315–316.

[45] Z.-K. Huang, T.-Y. Tien, T.-S. Yen, Subsolidus Phase Relationships in Si_3N_4-AlN-Rare-Earth Oxide Systems, J. Am. Ceram. Soc. 69 (1986) C–241–C–242.

[46] D. Thompson, W. Sun, P. Walls, O'-- beta' and alpha'-- beta' Sialon Ceramics, in: Ceram. Mater. Components Engines, 1986: pp. 643–650.

[47] S.I. Raider, R. Flitsch, J.A. Aboaf, W.A. Pliskin, Surface Oxidation of Silicon Nitride Films, J. Electrochem. Soc. 123 (1976) 560.

[48] S.C. Singhal, Thermodynamic analysis of the high-temperature stability of silicon nitride and silicon carbide, Ceramurg. Int. 2 (1976) 123–130.

[49] T. Sakai, M. Iwata, Effect of oxygen on sintering of AlN, J. Mater. Sci. 12 (1977) 1659–1665.

[50] O'Meara, C.. Dunlop, G.L.. Pompe, High-Technology Ceramics, in: Proceeding World Congr. High Tech Ceram., 1987: p. 265.

[51] E.M. Levin, H.F. McMurdie, Phase diagrams for ceramists, 1975 supplement, (1975).

[52] S. Hampshire, K. Jack, Special ceramics, in: Brit. Ceram. Soc, 1981: p. 37.

[53] S. Hampshire, K.H. Jack, Densification and Transformation Mechanisms in Nitrogen Ceramics, in: Prog. Nitrogen Ceram., Springer Netherlands, Dordrecht, 1983: pp. 225–230.

[54] A. Rosenflanz, I.-W. Chen, Kinetics of phase transformations in SiAlON ceramics: I. effects of cation size, composition and temperature, J. Eur. Ceram. Soc. 19 (1999) 2325–2335.

[55] J. Weiss, Silicon Nitride Ceramics: Composition, Fabrication Parameters, and Properties, Annu. Rev. Mater. Sci. 11 (1981) 381–399.

[56] D.R. Messier, F.L. Riley, R.J. Brook, The ?/? silicon nitride phase transformation, J. Mater. Sci. 13 (1978) 1199–1205.

[57] V.. Sarin, On the α-to-β phase transformation in silicon nitride, Mater. Sci. Eng. A. 105 (1988) 151–159.

[58] F.L. Riley, Silicon Nitridation, in: Prog. Nitrogen Ceram., Springer Netherlands, Dordrecht, 1983: pp. 121–133.

[59] K.H. JACK, V – The Relationship of Phase Diagrams to Research and Development of Sialons, in: Phase Diagrams, 1978: pp. 241–285.

[60] L.J. Bowen, R.J. Weston, T.G. Carruthers, R.J. Brook, Hot-pressing and the α-β phase transformation in silicon nitride, J. Mater. Sci. 13 (1978) 341–350.

[61] L.J. Bowen, T.G. Carruthers, R.J. Brook, Hot-Pressing of Si_3N_4 with Y_2O_3 and Li_2O as Additives, J. Am. Ceram. Soc. 61 (1978) 335–359.

[62] H.F. Priest, F.C. Burns, G.L. Priest, E.C. Skaar, Oxygen Content of Alpha Silicon Nitride, J. Am. Ceram. Soc. 56 (1973) 395–395.

[63] P. Drew, M.H. Lewis, The microstructures of silicon nitride ceramics during hot-pressing transformations, J. Mater. Sci. 9 (1974).

[64] V.A. Izhevskiy, L.A. Gênova, J.C. Bressiani, Review article: RE-SiAlONa¤b- composites. Formation, thermal stability, phase relationships, reaction densification, Cerâmica. 45 (1999) 05–23.

[65] C.L. Hewett, Y.-B. Cheng, B.C. Muddle, M.B. Trigg, Thermal Stability of Calcium α-sialon Ceramics, J. Eur. Ceram. Soc. 18 (1998) 417–427.

[66] H. Mandal, D.P. Thompson, 3 Sialon Transformation in Calcium- containing -SiAlON Ceramics, J. Eur. Ceram. Soc. 19 (1999) 543–552.

[67] J.W.T. van Rutten, H.T. Hintzen, R. Metselaar, Phase formation of Ca-α-sialon by reaction sintering, J. Eur. Ceram. Soc. 16 (1996) 995–999.

[68] S.-F. Kuang, Z.-K. Huang, W.-Y. Sun, T.-S. Yen, Phase relationships in the system MgO-Si3N4-AlN, J. Mater. Sci. Lett. 9 (1990) 69–71.

[69] T. Ekström, Transient liquid phase sintering of silicon nitride, in: Proc. Int. Ceram. Conf. Austceram 90, Perth, Aust., 1990: pp. 586–591.

[70] T. Ekstrom, alpha sialons, in: Ceram. Mater. Components Engines, 1990.

[71] H.X. Li, W.Y. Sun, P.L. Wang, D.S. Yan, T.Y. Tien, The effect of GPS parameters on mechanical properties of Y—α-SiAlON ceramics, Ceram. Int. 23 (1997) 449–456.

[72] C.R. Zhou, Z.B. Yu, V.D. Krstic, Pressureless sintered self-reinforced Y-α-SiAlON ceramics, J. Eur. Ceram. Soc. 27 (2007) 437–443.

[73] Y. Cai, Z. Shen, J. Grins, S. Esmaeilzadeh, T. Höche, Self-Reinforced Nitrogen-Rich Calcium-α-SiAlON Ceramics, J. Am. Ceram. Soc. 90 (2007) 608–613.

[74] R.F. Silva, J.M. Gomes, A.S. Miranda, J.M. Vieira, Resistance of Si3N4 ceramic tools to thermal and mechanical loading in cutting of iron alloys, Wear. 148 (1991) 69–89.

[75] D.W. Richerson, P.M. Stephan, Evolution of Applications of Si_3N_4;-Based Materials, Mater. Sci. Forum. 47 (1989) 282–0.

[76] H. PENG, Spark Plasma Sintering of Si_3N_4-Based Ceramics -Sintering mechanism-Tailoring microstructure-Evaluating properties, 2004.

[77] Syalon 101 | Silicon Nitride (Si3N4) Ceramic Properties | International Syalons (Newcastle) Ltd, http://www.syalons.com/advanced-ceramic-materials/silicon-nitride-and-sialon-ceramics/syalon-101/ (accessed August 24, 2017).

[78] Syalon 050 | Silicon Nitride (Si3N4) Ceramic Properties | International Syalons (Newcastle) Ltd, http://www.syalons.com/advanced-ceramic-materials/silicon-nitride-and-sialon-ceramics/syalon-050/.

[79] J. Aucote, S.R. Foster, Performance of sialon cutting tools when machining nickel-base aerospace alloys, Mater. Sci. Technol. 2 (1986) 700–708.

[80] Alumina (Al_2O_3) Ceramic Properties | Aluminon 96, Aluminon 995, Aluminon 999 | International Syalons (Newcastle) Limited, http://www.syalons.com/advanced-ceramic-materials/alumina-ceramics/.

[81] F. Thummler, State of the Art: Engineering Ceramics, J. Eur. Ceram. Soc. 6 (1990) 139–51.

[82] N. Camuşcu, D.P. Thompson, H. Mandal, Effect of starting composition, type of rare earth sintering additive and amount of liquid phase on αa ⇆ β sialon transformation, J. Eur. Ceram. Soc. 17 (1997) 599–613.

[83] Y. Torres, D. Casellas, M. Anglada, L. Llanes, Fracture toughness evaluation of hardmetals: influence of testing procedure, Int. J. Refract. Met. Hard Mater. 19 (2001) 27–34.

[84] A.G. Evans, E.A. Charles, Fracture Toughness Determinations by Indentation, J. Am. Ceram. Soc. 59 (1976) 371–372.

[85] S. Hampshire, M.J. Pomeroy, Grain boundary glasses in silicon nitride: A review of chemistry, properties and crystallisation, J. Eur. Ceram. Soc. 32 (2012) 1925–1932.

[86] S. Stach, S. Roskosz, J. Cybo, J. Cwajna, Properties of sialon ceramics evaluated by means of multifractal, surface stereometry and quantitative fractography techniques, Mater. Charact. 60 (2009) 1151–1157.

[87] M. Liška, P. Šajgal'\ik, D. Salamon, Mechanical Properties and Microstructure of $α$-SiAlON Based Cutting Tools, in: Fractography Adv. Ceram. II, Trans Tech Publications, 2005: pp. 250–253.

[88] H. Mandal, S. Turan, A. Kara, F. Kara, Novel SiAlON Ceramics for Cutting Tool Applications, in: SiAlONs, Trans Tech Publications, 2003: pp. 193–202.

[89] H. Mandal, B. Bitterlich, K. Friederich, SiAlON-SiC-Composites for Cutting Tools, in: 11th Int. Ceram. Congr., Trans Tech Publications, 2006: pp. 1786–1791.

[90] A.S. Hakeem, J. Grins, S. Esmaeilzadeh, La–Si–O–N glasses: Part I. Extension of the glass forming region, J. Eur. Ceram. Soc. 27 (2007) 4773–4781.

[91] B.A. Ahmed, A.S. Hakeem, T. Laoui, R.M.A. Khan, M.M. Al Malki, A. Ul-Hamid, F.A. Khalid, N. Bakhsh, Effect of precursor size on the structure and mechanical properties of calcium-stabilized sialon/cubic boron nitride nanocomposites, J. Alloys Compd. 728 (2017) 836–843.

[92] C.L. Hewett, Y.-B. Cheng, B.C. Muddle, M.B. Trigg, Phase Relationships and Related Microstructural Observations in the Ca-Si-Al-O-N System, J. Am. Ceram. Soc. 81 (2005) 1781–1788.

[93] Development of a single-phase Ca-α-SiAlON ceramic from nanosized precursors using spark plasma sintering, Mater. Sci. Eng. A. 673 (2016) 243–249.

[94] M.M. Al Malki, R.M.A. Khan, A.S. Hakeem, S. Hampshire, T. Laoui, Effect of Al metal precursor on the phase formation and mechanical properties of fine-grained SiAlON ceramics prepared by spark plasma sintering, J. Eur. Ceram. Soc. 37 (2017) 1975–1983.

[95] J.D. Bolton, A.J. Gant, Microstructural Development and Sintering Kinetics in Ceramic Reinforced High Speed Steel Metal Matrix Composites, Powder Metall. 40 (1997) 143–151.

[96] Z. Ahmadi, B. Nayebi, M. Shahedi Asl, M. Ghassemi Kakroudi, Fractographical characterization of hot pressed and pressureless sintered AlN-doped ZrB2–SiC composites, Mater. Charact. 110 (2015) 77–85.

[97] I. Ahmad, H. Cao, H. Chen, H. Zhao, A. Kennedy, Y.Q. Zhu, Carbon nanotube toughened aluminium oxide nanocomposite, J. Eur. Ceram. Soc. 30 (2010) 865–873.

[98] N. Bakhsh, F.A. Khalid, A.S. Hakeem, Synthesis and characterization of pressureless sintered carbon nanotube reinforced alumina nanocomposites, Mater. Sci. Eng. A. 578 (2013) 422–429.

[99] G. Petzow, R. Telle, R. Danzer, Microstructural defects and mechanical properties of high-performance ceramics, Mater. Charact. 26 (1991) 289–302.

[100] C.A. Wood, H. Zhao, Y.-B. Cheng, Microstructural Development of Calcium alpha-SiAlON Ceramics with Elongated Grains, J. Am. Ceram. Soc. 82 (2004) 421–428.

[101] S.C. Zhang, W.G. Fahrenholtz, G.E. Hilmas, E.J. Yadlowsky, Pressureless sintering of carbon nanotube–Al2O3 composites, J. Eur. Ceram. Soc. 30 (2010) 1373–1380.

[102] W.-Y. Sun, T.-Y. Tien, T.-S. Yen, Subsolidus Phase Relationships in Part of the System Si,Al,Y/N,O: The System Si3N4AINYNAl2O3Y2O3, J. Am. Ceram. Soc. 74 (1991) 2753–2758.

[103] R.-J. Xie, N. Hirosaki, K. Sakuma, Y. Yamamoto, M. Mitomo, Eu2+-doped Ca-α-SiAlON: A yellow phosphor for white light-emitting diodes, Appl. Phys. Lett. 84 (2004) 5404–5406.

[104] J. Grins, S. Esmaeilzadeh, Z. Shen, Structures of Filled α-Si $_3$ N $_4$ -Type Ca $_{0.27}$ La $_{0.03}$ Si $_{11.38}$ Al $_{0.62}$ N $_{16}$ and LiSi $_9$ Al $_3$ O $_2$ N $_{14}$, J. Am. Ceram. Soc. 86 (2003) 727–30.

[105] S. Suzuki, T. Nasu, S. Hayama, M. Ozawa, Mechanical and Thermal Properties of beta'-Sialon Prepared by a Slip Casting Method, J. Am. Ceram. Soc. 79 (1996) 1685–1688.

[106] F. Izumi, M. Mitomo, Y. Bando, Rietveld refinements for calcium and yttrium containing ?-sialons, J. Mater. Sci. 19 (1984) 3115–3120.

[107] M.J. Pomeroy, C. Mulcahy, S. Hampshire, Independent Effects of Nitrogen Substitution for Oxygen and Yttrium Substitution for Magnesium on the Properties of Mg-Y-Si-Al-O-N Glasses, J. Am. Ceram. Soc. 86 (2003) 458–464.

[108] V.A. Gunchenko, V.N. Pavlikov, G. V. Trunov, Kinetics and mechanism of oxidation of β-sialons, Sov. Powder Metall. Met. Ceram. 27 (n.d.) 470–474.

[109] J. Persson, T. Ekström, P.O. Käll, M. Nygren, Oxidation behaviour and mechanical properties of β- and mixed α-β-sialons sintered with additions of Y2O3and Nd2O3, J. Eur. Ceram. Soc. 11 (1993) 363–373.

[110] L. Liu, R.-J. Xie, N. Hirosaki, T. Takeda, C. Zhang, J. Li, X. Sun, Photoluminescence properties of β-SiAlON:Yb $^{2+}$, a novel green-emitting phosphor for white light-emitting diodes, Sci. Technol. Adv. Mater. 12 (2011) 034404.

[111] S.-F. Kuang, Z.-K. Huang, W.-Y. Sun, T.-S. Yen, Phase relationships in the Li2O-Si3N4-AlN system and the formation of lithium-??-sialon, J. Mater. Sci. Lett. 9 (1990) 72–74.

[112] T.-S. Sheu, Microstructure and Mechanical Properties of the in situ beta-Si3N4/alpha'-SiAlON Composite, J. Am. Ceram. Soc. 77 (1994) 2345–2353.

[113] Y.B. Xie, Rong-Jun,Mamoru Mitomo, F. F. Xu, Preparation of Ca-α-sialon ceramics with compositions along the Si3N4-1/2 Ca3N2:3AlN line, Z. Met. 92 (2001) 931–936.

[114] Y. Cai, Synthesis and Characterization of Nitrogen-rich Calcium [alpha]-sialon Ceramics, Department of Physical, Inorganic and Structural Chemistry, Stockholm University, 2009. https://books.google.com.sa/books?id=65ryjwEACAAJ.

[115] F. Ye, M.J. Hoffmann, S. Holzer, Y. Zhou, M. Iwasa, Effect of the Amount of Additives

and Post-Heat Treatment on the Microstructure and Mechanical Properties of Yttrium-α-Sialon Ceramics, J. Am. Ceram. Soc. 86 (2003) 2136–2142.

[116] Z. Shen, H. Peng, M. Nygren, Formation of in-situ reinforced microstructure in α–sialon ceramics I: Stoichiometric oxygen-rich compositions, J. Mater. Res. 17 (2002) 336–342.

[117] 12013-82-0 CAS MSDS (CALCIUM NITRIDE) Melting Point Boiling Point Density CAS Chemical Properties, http://www.chemicalbook.com/ChemicalProductProperty_US_CB2672982.aspx (accessed September 24, 2017).

[118] A. Thorel '", J.Y. Laval+, D. Broussaud, High Temperature Mechanical Properties And Intergranular Structure Of Sialons, 1 (1986).

[119] S.R. Witek, G.A. Miller, M.P. Harmer, Effects of CaO on the Strength and Toughness of AIN, J. Am. Ceram. Soc. 72 (1989) 469–473.

[120] Z.-H. Xie, M. Hoffman, Y.-B. Cheng, Microstructural Tailoring and Characterization of a Calcium α-SiAlON Composition, J. Am. Ceram. Soc. 85 (2004) 812–818.

[121] Y. Zhang, Y.-B. Cheng, Grain boundary devitrification of Ca α-sialon ceramics and its relation with the fracture toughness, J. Mater. Sci. 38 (2003) 1359–1364.

[122] A. de Lofaj, F; Dorcakova, F; Kovalcik, J; Hoffmann, MJ; Lopez, The effect of lanthanides and nitrogen on microhardness of oxynitride, Kov. Mater. Mater. 41 (2003) 145–157.

[123] Y. Zhang, Y.-B. Cheng, Microstructural design of Ca α-sialon ceramics: effects of starting compositions and processing conditions, J. Eur. Ceram. Soc. 23 (2003) 1531–1541.

[124] S. Kurama, S. Kurama, M. Herrmann, H. Mandal, The effect of processing conditions, amount of additives and composition on the microstructures and mechanical properties of alpha-SiAlON ceramics, J. Eur. Ceram. Soc. 22 (2002) 109–119.

[125] Z. Yang, Q. Shang, X. Shen, L. Zhang, J. Gao, H. Wang, Effect of composition on phase assemblage, microstructure, mechanical and optical properties of Mg-doped sialon, J. Eur. Ceram. Soc. 37 (2017) 91–98.

[126] S. Kurama, G. Cigdemir, H. Mandal, M. Herrmann, Sr2+–Mg2+-Doped SiAlON Ceramics, J. Am. Ceram. Soc. 89 (2006) 714–716.

[127] M. Menon, I.-W. Chen, Reaction Densification of α′-SiAION: II, Densification Behavior, J. Am. Ceram. Soc. 78 (1995) 553–559.

[128] R.J. Sung, T. Kusunose, T. Nakayama, T. Sekino, S.-W.L.K. Niihara, Fabrication of transparent polycrystalline silicon nitride ceramic, in: Adv. Ceram. Matrix Compos. X Proc. 106th Annu. Meet. Am. Ceram. Soc. Indianapolis, Indiana, USA 2004, Ceram. Trans., 2005: p. 15.

[129] W. Yang, J. Hojo, N. Enomoto, Y. Tanaka, M. Inada, Near infrared transmittance of translucent Si3N4 sinteredceramics, Mater. Lett. 96 (2013) 155–157.

[130] B. Joshi, H.H. Lee, Y.H. Kim, Z. Fu, K. Niihara, S.W. Lee, Hot pressed translucent (Mg,Y)-α/β-Sialon ceramics, Mater. Lett. 80 (2012) 178–180.

[131] Y. Xiong, Z. Fu, H. Wang, W. Wang, J. Zhang, Q. Zhang, S.W. Lee, K. Niihara, Translucent Mg-α-Sialon Ceramics Prepared by Spark Plasma Sintering, J. Am. Ceram. Soc. 90 (2007) 1647–1649.

[132] K.-R. Lai, T.-Y. Tien, Kinetics of β-Si3N4 Grain Growth in Si3N4 Ceramics Sintered under High Nitrogen Pressure, J. Am. Ceram. Soc. 76 (1993) 91–96.

[133] C.J. Hwang, T.Y. Tien, Microstructural Development in Silicon Nitride Ceramics, in: Prep. Prop. Silicon Nitride Based Mater., Trans Tech Publications, 1991: pp. 84–109.

[134] M. Krämer, D. Wittmüss, H. Küppers, M.J. Hoffman, G. Petzow, Relations between crystal structure and growth morphology of β-Si3N4, J. Cryst. Growth. 140 (1994) 157–166.

[135] M. Kitayama, K. Hirao, M. Toriyama, S. Kanzaki, Modeling and simulation of grain growth in Si3N4—II. The α–β transformation, Acta Mater. 46 (1998) 6551–6557.

[136] M. Kitayama, K. Hirao, M. Toriyama, S. Kanzaki, Modeling and simulation of grain growth in Si3N4—I. Anisotropic Ostwald ripening, Acta Mater. 46 (1998) 6541–6550.

[137] T. Ekström, P.-O. Olsson, β-Sialon Ceramics Prepared at 1700°C by Hot Isostatic Pressing, J. Am. Ceram. Soc. 72 (1989) 1722–1724.

[138] T.-S. Sheu, Microstructure and Mechanical Properties of the in situβ-Si3N4/α′-SiAlON Composite, J. Am. Ceram. Soc. 77 (1994) 2345–2353.

[139] Z. Yang, H. Wang, X. Min, W. Wang, Z. Fu, S.W. Lee, K. Niihara, Effect of heating rate on microstructure and properties of spark plasma sintered Li-α-sialon, Ceram. Int. 37 (2011) 2175–2180.

[140] H. Peng, Z. Shen, M. Nygren, Reaction sequences occurring in dense Li-doped sialon ceramics: influence of temperature and holding time, J. Mater. Chem. 13 (2003) 2285–2289.

[141] H. Zhao, S.P. Swenser, Y.-B. Cheng, Elongated α-sialon grains in pressureless sintered sialon ceramics, J. Eur. Ceram. Soc. 18 (1998) 1053–1057.

[142] D.P. Thompson, P. Korgul, A. Hendry, The Structural Characterisation of Sialon Polytypoids, in: Prog. Nitrogen Ceram., Springer Netherlands, Dordrecht, 1983: pp. 61–74.

[143] F. Ye, C. Liu, L. Liu, Y. Zhou, Q. Meng, Sc3+–Lu3+-Doped α-SiAlONs, J. Am. Ceram. Soc. 91 (2008) 1022–1026.

[144] Y. Cai, Z. Shen, J. Grins, S. Esmaeilzadeh, T. Höche, Self-Reinforced Nitrogen-Rich Calcium–α-SiAlON Ceramics, J. Am. Ceram. Soc. 90 (2007) 608–613.

[145] R.H. Wentorf, R.C. DeVries, F.P. Bundy, Sintered Superhard Materials, Science (80-.). 208 (1980). http://science.sciencemag.org/content/208/4446/873 (accessed May 27, 2017).

[146] F. Ye, Z. Hou, H. Zhang, L. Liu, Y. Zhou, Spark plasma sintering of cBN/β-SiAlON

composites, Mater. Sci. Eng. A. 527 (2010) 4723–4726.

[147] M. Hotta, T. Goto, Effect of time on microstructure and hardness of βSiAlON–cubic boron nitride composites during spark plasma sintering, Ceram. Int. 37 (2011) 521–524.

[148] J.C. Garrett, I. Sigalas, M. Herrmann, E.J. Olivier, J.H. O'Connell, cBN reinforced Y-α-SiAlON composites, J. Eur. Ceram. Soc. 33 (2013) 2191–2198. http://linkinghub.elsevier.com/retrieve/pii/S0955221913001520 (accessed August 19, 2017).

[149] M. Hotta, Microstructural control for ultrafine-grained non-oxide structural ceramics, J. Ceram. Soc. Japan. 120 (2012) 123–130.

[150] V. Martínez, J. Echeberria, Hot Isostatic Pressing of Cubic Boron Nitride?Tungsten Carbide/Cobalt (cBN/WC/Co) Composites: Effect of cBN Particle Size and Some Processing Parameters on their Microstructure and Properties, J. Am. Ceram. Soc. 90 (2007) 415–424.

[151] J.D. Hansen, R.P. Rusin, M.-H. Teng, D.L. Johnson, Combined-Stage Sintering Model, J. Am. Ceram. Soc. 75 (1992) 1129–1135.

[152] H.M. Irshad, B.A. Ahmed, M.A. Ehsan, T.I. Khan, T. Laoui, M.R. Yousaf, A. Ibrahim, A.S. Hakeem, Investigation of the structural and mechanical properties of micro-/nano-sized Al2O3 and cBN composites prepared by spark plasma sintering, Ceram. Int. 43 (2017) 10645–10653.

[153] Z. Kesica, I. Lukic, M. Zdujic, H. Liu, D. Skala, Mechanochemically Synthesized CaO ZnO Catalyst For Biodiesel Production, Procedia Eng. 42 (2012) 1169–1178.

[154] R. Shuba, I.-W. Chen, The Effect of Powder Mixing Procedures on alpha-SiAlON, J. Am. Ceram. Soc. 89 (2006) 1110–1113.

[155] A.S. Hakeem, R.M.A. Khan, M.M. Al-Malki, F. Patel, A.I. Bakare, S. Ali, S. Hampshire, T. Laoui, Development and Processing of SiAlON Nano-Ceramics by Spark Plasma Sintering, in: 13th Int. Ceram. Congr. - Part C, Trans Tech Publications, 2014: pp. 63–69.

[156] Q. Liu, L. Gao, D.. Yan, D.. Thompson, Hard sialon ceramics reinforced with SiC nanoparticles, Mater. Sci. Eng. A. 269 (1999) 1–7.

[157] L. Liu, F. Ye, Y. Zhou, Z. Zhang, Q. Hou, Fast bonding α-SiAlON ceramics by spark plasma sintering, J. Eur. Ceram. Soc. 30 (2010) 2683–2689.

[158] W.-L. Wang, J.-Q. Bi, S.-R. Wang, K.-N. Sun, M. Du, N.-N. Long, Y.-J. Bai, Microstructure and mechanical properties of alumina ceramics reinforced by boron nitride nanotubes, J. Eur. Ceram. Soc. 31 (2011) 2277–2284.

[159] J. Zhang, R. Tu, T. Goto, Spark plasma sintering of Al2O3-cBN composites facilitated by Ni nanoparticle precipitation on cBN powder by rotary chemical vapor deposition, J. Eur. Ceram. Soc. 31 (2011) 2083–2087.

[160] D. Jianxin, A. Xing, Wear resistance of Al2O3/TiB2 ceramic cutting tools in sliding wear tests and in machining processes, J. Mater. Process. Technol. 72 (1997) 249–255.

[161] B. Smuk, M. Szutkowska, J. Walter, Alumina ceramics with partially stabilized zirconia for cutting tools, J. Mater. Process. Technol. 133 (2003) 195–198.

[162] J. Sun, L. Gao, X. Jin, Reinforcement of alumina matrix with multi-walled carbon nanotubes, Ceram. Int. 31 (2005) 893–896.

[163] Y.L. Dong, F.M. Xu, X.L. Shi, C. Zhang, Z.J. Zhang, J.M. Yang, Y. Tan, Fabrication and mechanical properties of nano-/micro-sized Al2O3/SiC composites, Mater. Sci. Eng. A. 504 (2009) 49–54.

[164] B. Bitterlich, S. Bitsch, K. Friederich, SiAlON based ceramic cutting tools, J. Eur. Ceram. Soc. 28 (2008) 989–994.

[165] H. WANG, Y.-B. CHENG, B.C. MUDDLE, L. GAO, T.S. YEN, Microstructure and mechanical properties of nanoscale SiC/Ca α-SiAlON composites, J. Mater. Sci. 32 (1997) 3263–3269.

[166] Y. Zhou, J. Vleugels, T. Laoui, O. Van der Biest, Toughening of X-sialon with Al2O3 platelets, J. Eur. Ceram. Soc. 15 (1995) 297–305.

[167] Y. Akimune, N. Hirosaki, T. Ogasawara, Mechanical properties of SiC-particle/sialon composites, J. Mater. Sci. Lett. 10 (1991) 223–226.

[168] S. Lin, Z. Chen, L. Li, C. Yang, Effect of impurities on the Raman scattering of 6H-SiC crystals, Mater. Res. 15 (2012) 833–836.

[169] X. Guo, H. Yang, X. Zhu, L. Zhang, Preparation and properties of nano-SiC-based ceramic composites containing nano-TiN, Scr. Mater. 68 (2013) 281–284.

[170] C.R. Zhou, Z.B. Yu, V.D. Krstic, Pressureless sintered self-reinforced Y-??-SiAlON ceramics, J. Eur. Ceram. Soc. 27 (2007) 437–443.

[171] A. Moradkhani, H. Baharvandi, Microstructural analysis of fracture surfaces and determination of mechanical properties of Al2O3–SiC–MgO nanocomposites, Int. J. Refract. Met. Hard Mater. 67 (2017) 40–55.

[172] B. Lawn, Microstructure and toughness, in: Fract. Brittle Solids, 2nd ed., Cambridge University Press, 1993: pp. 194–248.

[173] T. Rouxel, F. Wakai, M.E. Brito, A. Iwamoto, K. Izaki, Intragranular crack deflection and crystallographic slip in Si3N4/SiC nano-composites, J. Eur. Ceram. Soc. 11 (1993) 431–438.

[174] K. Shirato, D. Chen, M.W. Barsoum, T. El-Raghy, R.O. Ritchie, High-Temperature Cyclic Fatigue-Crack Growth in Monolithic Ti_3SiC_2 Ceramics, in: Fatigue Fract. Behav. High Temp. Mater., John Wiley & Sons, Inc., Hoboken, NJ, USA, 2013: pp. 70–75.

[175] T. Rouxel, F. Wakai, M.E. Brito, A. Iwamoto, K. Izaki, Intragranular crack deflection and

crystallographic slip in Si3N4/SiC nano-composites, J. Eur. Ceram. Soc. 11 (1993) 431–438.

[176] L. Liu, F. Ye, X. He, Y. Zhou, Synthesis of α-SiC/α-SiAlON composites by spark plasma sintering: Phase formation and microstructures development, J. Eur. Ceram. Soc. 31 (2011) 2129–2135.

[177] L. Liu, F. Ye, Y. Zhou, Microstructure and mechanical properties of the α-SiAlON/α-SiC composites: Effects of heat treatment, Ceram. Int. 37 (2011) 3737–3741.

Vitae

Name	Bilal Anjum Ahmed
Nationality	Pakistan
Date of Birth	13th December 1987
Email	banjumahmed@gmail.com
Address	House No 445, Sec C, Phase VIII, Bahria Town, Zip Code 46220, RWP, Pakistan

Academic Background

PhD Mechanical Engineering CGPA: 4.00/4.00 Jan 2015-Apr 2018
(Specialization - Materials and Manufacturing)
King Fahd University of Petroleum and Minerals (KFUPM), Dhahran, Saudi Arabia

M.S. Materials and Surface Engineering CGPA: 3.95/4.00 Sep 2011- Apr 2013
National University of Sciences and Technology (NUST), Pakistan

B.S. Mechanical Engineering CGPA: 3.39/4.00 Sep 2007- Sep 2011
National University of Sciences and Technology (NUST), Pakistan

Patents Filed

1. Abbas S Hakeem, Tahar Laoui, Bilal Ahmed, Method of making alumina silicate oxinitride and cubic boron nitride ceramic composite (20180155250).
2. Abbas S Hakeem, Tahar Laoui, Ali Ehsan, Bilal Ahmed, H. Muzammil, Structural and mechanical properties of Nano and Micro Al_2O_3-cBN composites (Ref:503462US).

Publications (Thesis Work)

1. R.M.A Khan, B.A. Ahmed, M. M. Al Malki, A. S. Hakeem, T. Laoui, Synthesis of hard and tough calcium stabilized α-sialon/SiC ceramic composites using nano-sized precursors and spark plasma sintering, Journal of Alloys and Compounds, 757, 2018, Pages 200-208.
2. B.A. Ahmed, A.S. Hakeem, T. Laoui, M. Al Malki, M.A. Ehsan, S. Ali, Low-temperature spark plasma sintering of calcium stabilized alpha sialon using nano-size aluminum nitride precursor, Int. J. Refract. Met. Hard Mater. 71, 2018, 301–306.
3. B.A. Ahmed, A. S. Hakeem, T. Laoui, R.M.A Khan, M. M. Al Malki, A. Ul-Hamid, F.A. Khalid, N. Bakhsh, Effect of precursor size on the structure and mechanical

properties of calcium-stabilized sialon/cubic boron nitride nanocomposites, Journal of Alloys and Compounds, 728, 2017, 836-843.

Publications (Other Work)

4. H. Muzammil Irshad, Bilal Ahmed, Abbas Hakeem, M Ali Ehsan, Tahar Laoui, Effect of Ni content and Al2O3 particle size on the thermal and mechanical properties of Al_2O_3/Ni composites prepared by spark plasma, International Journal of Refractory Metals and Hard Materials, Available online 24 May 2018.
5. H.M. Irshad, B.A. Ahmed, M.A. Ehsan, T.I. Khan, T. Laoui, M.R. Yousaf, A. Ibrahim, A.S. Hakeem, Investigation of the structural and mechanical properties of micro-/nano-sized Al_2O_3 and cBN composites prepared by spark plasma sintering, Ceram. Int. 43, 2017, 10645–10653.
6. Ahmad Nawaz Khan & Bilal Anjum Ahmed, Comparative study of Polyamide 6 reinforced with glass fiber and montmorillonite, Polym. Bull. 72, 2015, 1207-1216.
7. B.A. Ahmed, Synthesis of laser beam rapidly solidified novel surfaces on D2 tool steel, Key Engineering Materials, 510-511, 2012, 493-499.

Conferences

1. B.A. Ahmed, A.S. Hakeem, T. Laoui, Low Temperature Development of Calcium Sialons along the Alpha/(alpha+beta) Phase Boundary using nano-size Oxi-nitride Precursors and Spark Plasma Sintering Technique, 14th Ceramics Congress CIMTEC 2018, June 4-8, 2018, Perugia Italy.
2. Abbas Saeed Hakeem , Bilal Anjum Ahmed , Akolade Idris Bakare , Ibrahim Ahmed Ibrahim Ali, Muhammad Ehsan Ali and Tahar Laoui, Cubic Boron Nitride Reinforced Sialon Nano-Composites by Spark Plasma Sintering, 2nd World Congress and Expo on Nanotechnology and Material Science , April 04-06, 2016 at Dubai, UAE.
3. Abbas Hakeem ,Bilal Ahmed , Akolade Idris Bakare, Ibrahim Ahmed Ibrahim Ali, Tahar Laoui, Sialon nano-composites matrix reinforced by cubic boron nitride prepared by using spark plasma sintering, International Conference and Exhibition on Materials Chemistry, March 31-April 01, 2016 Valencia, Spain
4. B. Ahmed, A. Hakeem, A. Ibrahim, M. Ehsan, T. Laoui, Spark Plasma Sintering of Ca-α-Sialon Matrix reinforced with Cubic Boron Nitride Particles, The 4th Saudi International Nanotechnology Conference 2016, Dhahran KSA.